ČESKÉ VYSOKÉ UČENÍ TECHNICKÉ V PRAZE

Fakulta stavební
Katedra mechaniky

Quasicontinuum Approach Applied to Inelastic Materials

Diploma Thesis

Využití kvazikontinua při modelování nepružných materiálů

Diplomová práce

Fakulta stavební
Studijní program: SI
Studijní obor: K

Vedoucí práce: Prof. Ing. Milan Jirásek, DrSc.

Karel Mikeš

Praha 2015

Poděkování

Na tomto místě bych rád poděkoval panu Prof. Ing. Milanu Jiráskovi, DrSc., za odborné vedení, řadu cenných nápadů a užitečných připomínek.

Prohlášení

Prohlašuji, že jsem tuto diplomovou práci vypracoval samostatně pouze za odborného vedení vedoucího práce Prof. Ing. Milana Jiráska, DrSc. Dále prohlašuji, že veškeré podklady, ze kterých jsem čerpal, jsou uvedeny v seznamu použité literatury.

Datum: Podpis:

Abstrakt

Kvazikontinuální (QC) metoda je poměrně nový způsob modelování materiálů, který kombinuje přesný atomistický přístup se zjednodušením v podobě kontinua. Hlavní myšlenkou QC je snížit výpočetní nároky snížením počtu stupňů volnosti (SV) plně atomistického modelu. Za tímto účelem je ze všech atomů vybrána jen určitá podmnožina významných atomů, která reprezentuje celý systém. Tyto atomy se nazývají rep-atomy a jsou použity k aproximování SV ostatních atomů [21]. Tento postup byl původně navržen pro pravidelné atomistické mřížky, ale v této práci je použit na nepravidelné částicové struktury reprezentující homogenní materiál. Pro elastické materiály jsou představeny tři metody používající zjednodušený částicový model založené na myšlence QC. Je navržena také QC metoda pro plastické materiály, která vychází z modelu microplane [2]. Metody pro oba typy materiálů jsou implementovány v programu OOFEM [24]. Přesnost, efektivita a vlastnosti jednotlivých metod používajících myšlenku QC je vyhodnocena porovnáním výsledků s přesným čistě částicovým přístupem pro několik příkladů s různými typy materiálů.

Klíčová slova

Kvazikontinuální metoda, diskrétní částicový model, homogenizace, microplane model.

Abstract

The quasicontinuum (QC) method is a relatively new computational technique. This technique is a combination of continuum and atomistic approaches. The key idea of QC is to reduce the computational cost by reducing degrees of freedom (DOF) of the fully atomistic approach. Instead of dealing with all atoms, a small relevant subset of atoms is selected to represent the whole system. These atoms, the so-called repatoms, are used to approximate the DOF of other atoms [21]. This technique was originally proposed for regular atomistic lattices. In this work, this technique is applied to an irregular set of particles representing a homogeneous material. This thesis provides three models using a simplified discrete particle model based on the idea of QC for elastic material. Also, a QC model for plastic materials using the idea of microplanes [2] is proposed. Models for both types of materials are implemented in OOFEM [24]. Accuracy, efficiency and specific properties of all simplified models based on the idea of QC are evaluated by comparison of results with the exact pure particle approach for a number of examples with different types of materials.

Key words

Quasicontinuum method, discrete particle model, homogenization, microplane model.

Content

1 Introduction

1.1 Discrete material models

One of the most natural ways to set up a material model is to use a network of particles interacting via discrete links or beams that represent discrete microstructure of modeled material. An advantage of this approach is that the discrete models can naturally capture phenomena incurred by the material microstructure. Therefore, the discrete material models are frequently used to simulate all sorts of materials such as paper [17], textile and fibrous material [7, 36] or fiber composites [3]. And last but not least, a lot of effort was put into creating a discrete model of concrete [10, 16, 18, 27] and [28]. But on the other hand, there are two main disadvantages of particle models. At the first, the large number of particles is needed to investigate the response of large-scale physically relevant models. This results in a huge number of DOF and it makes the system of equations of these models expensive to solve. Secondly, the process of assembling of this system is also computationally expensive because all discrete connections must be visited.

Both of these disadvantages of discrete particle models can be removed by using simplified continuous models based on one of the conventional homogenization procedures. But these continuous models cannot capture localized phenomena, e.g. Bažant shows in [1] that the only valid approach to softening damage is a discrete (lattice-particle) simulation of the mesostructure of the entire structural region in which softening damage can occur.

Another way to reduce the computational cost of the discrete particle models is a combination of simplified continuous model with the exact discrete description in the parts where it is needed. But the combination of two different approaches entails that some hand shaking procedure is needed at the interface between continuous and discrete domain [9]. The quasicontinuum (QC) method is a suitable way how to combine the advantages of continuous models with the exact description of discrete particle model without additional coupling procedures.

1.2   Quasicontinuum method

The quasicontinuum (QC) method was originally proposed by Tadmor, Ortiz and Phillips [32, 35] in 1996. The original application of this computational technique was a simplification of a simulation of large atomistic lattice models described by long-range conservative interaction potentials. Since the time, QC methods have been widely used to investigate local phenomena of these lattice models with long range interactions [9] and [31]. Recently, the application of QC methods has been successfully extended to other lattices and interaction potentials. For example, the application of QC method to the structural lattice models of fibrous material with short range nearest-neighbor interactions is provided by Beex et al. with conservative [4] and non-conservative [5, 6] interaction potentials including dissipation and fiber sliding but still applied to the regular lattices only. In this work, we focused on the application of QC approach with the same types of short range interactions but applied to the irregular set of particles connected by discrete links.

An overview of applications and current directions of QC methods is provided by Miller and Tadmor in [20, 21] and [31] or in part IV in the book of the same authors [34]. And many useful materials including the software and the QC code can be found on the web page: `http://qcmethod.org/` [33].

1.3   The idea of quasicontinuum method

The main idea of the QC method is to reduce the DOF and computational demand without losing the exact atomistic description in regions where it is required. Therefore, two types of regions in the solved domain are considered. In the regions of high interest, the pure particle approach is required and all particles contribute to DOF. By contrast, in the regions of low interest, continuum assumptions can be used.

The key idea of QC method can be briefly presented in three steps:

- **Interpolation** of DOF is used in the region of low interest and the number of DOF is significantly reduced.
- **Summation** rule is applied to eliminate the requirement of visiting all particles during the assemblage of the solved system.
- **Adaptivity** provides the arbitrary changes of the region of high interest during the simulation process.

1.3.1 Interpolation

Only a small subset of particles is selected to represent the entire system. These particles, the so-called repnodes, represent the nodes of a triangular mesh that are used to interpolate the DOF of other particles in the region of low interest. The position of the node of interpolation mesh is not arbitrary, but has to coincide with one of the rep-nodes, i.e., with a particle carrying DOF. In the regions of high interest, all particles are selected as repnodes to provide the exact particle representation. This interpolation provides the significant reduction of DOF without losing the exact description in the parts of high interest. Interpolation mesh in the region of low interest can be coarse with large elements and then the reduction of DOF is significant.

1.3.2 Summation

If the so-called summation procedure is not applied, then all particles need to be visited to construct the system of governing equations and it makes the process computationally expensive. If the summation rule is used, then only one sampling particle for each interpolation triangle is used to obtain accurate solution. It makes this process faster but problems occur on the interface between regions of high and low interest. Because of the interpolation and the summation, the deformation of each interpolation element is represented by one particle. Therefore, the deformations in the regions of low interest are piecewise constant while the deformations in the regions of high interest are solved exactly. Consequently, forces of nonphysical character, so-called ghost-forces, appear on the interface [20] and [29]. This problem can be solved by the cluster summation rule presented in [15] and extended in [11]. In this case the summation of one element is done only in the clusters of given radius and all particles outside the cluster are solved exactly. Next improvement is the central summation rule introduced by Beex in [4]. In central summation only the particles that have one or more neighboring particles in a different element must be computed exactly.

In this work, irregular lattices are used, and therefore, the summation procedure is realized by a homogenization of links networks contributing to the corresponding interpolation elements. Some truss elements are selected to be solved exactly to provide the interface between exactly solved and interpolated domain and to eliminate the ghost-forces. This procedure is in more detail described in chapters 4.3 and 4.4.

1.3.3 Adaptivity

The regions of high interest can be set explicitly as constant during the entire simulation process, or can be changed as needed in each time step. Hand-shaking procedure between the regions of low and high interest is not needed. Therefore the type of region can be changed only by the addition of the repnodes before each step. New triangulation of interpolation mesh can be done but it is not necessary; see chapters 3.1 and 3.2. A suitable change of the regions of high interest is often associated with a substantial increase of accuracy and, in several specific cases, it is necessary to represent the correct physical behavior, e.g., in the crack propagation process.

1.4 Methodology

In this work, we focus on discrete particle systems with short-range elastic and inelastic interactions. Such systems are typically used in simulations of heterogeneous materials. Particles in these systems are distributed randomly and do not form regular lattices like in atomistic systems, but the idea of QC can still be used.

Three methods based on the idea of quasicontinuum are introduced and compared with the pure particle approach in 2D. Accuracy is expressed in terms of errors in displacement and strain. The number and position of repnodes are adaptively changed to achieve the optimal result.

The simulation algorithm is composed of the following steps:

- Generation of particles and of connecting links
- Selection of repnodes and interpolation elements
- Application of a simplification rule
- Computation in OOFEM
- Post processing of results and error evaluation

The procedures and details of all individual steps are described in the following chapters.

2 Generating particles and connecting them by links

In the first step, the input geometry of the particle system is generated; it is specified by the position of all particles in the system and by the information which particles are connected. This process depends on the type of represented material.

2.1 Homogeneous material with uniform distribution of particles

For this type of material, at the first, the required number of particles is generated in the solved 2D domain. Then all pairs of particles satisfying an appropriate rule are connected by a link.

2.1.1 Generating particles

The following rules are applied to obtain the required properties of the generated system of particles representing the required material.

- The total number of particles in the solved domain, N_P

- The minimal distance between each two particles, R_P

- The maximal number of all generations, C_tot

- The maximal number of generations until a newly generated particle is accepted, C_gen

The position of each particle is generated randomly. The minimal distance between each two particles R_P is checked in all iterations. If the distance between a newly generated particle and one of existing particles is smaller than R_P, then the newly generated particle is not accepted. New particles are generated until the required number of particles or the maximal number of iterations is reached.

Distance checking is the most time consuming part of this process. If the minimal distance criterion must be evaluated for all existing particles, computational cost grows unacceptably with the number of particles N_p; see Fig. 3 (dashed black). Therefore, a quadtree structure is used to make the distance checking faster.

2.1.2 Quadtree structure

The solved domain is bounded by a rectangular region, which is recursively subdivided into four quadrants several times. The number of subdivisions depends on the number of particles placed inside. In general, the level of subdivision is different for

each quadrant and subquadrant to provide the maximal number of particles in the final quadrant lower than a prescribed value. An example of this unequal division can be seen in *Fig. 1*.
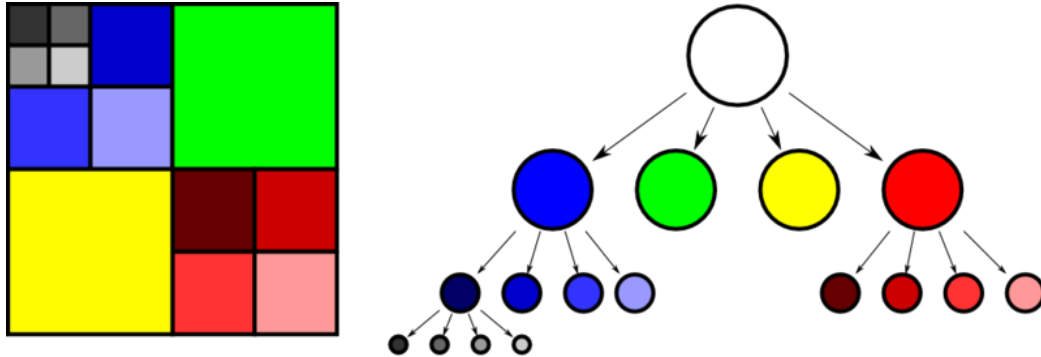
Fig. 1 Example of quadtree structure. Taken over from: WIKIPEDIA. Avalible at:
`https://upload.wikimedia.org/wikipedia/de/a/a7/Quadtree.png.`

But in our case the distribution of particles is uniform and the number of particles in the final quadrants for a sufficiently filled domain is almost the same, because it can be affected by the shape of the solved domain only. Hence, we can consider the same level of division for all quadrants. After all particles are generated, lists of particles placed in each quadrant are created for all final quadrants. Then only the necessary neighboring quadrants are scanned during distance checking; see *Fig. 2*.

Numerical tests showed that this method becomes efficient for systems with at least a few thousands of particles. Fig. 3 shows the dependence of time effort on the final number of particles in 2D solved domain. The curve for generating particles with using the full distance checking procedure, where all newly generated particles are tested with all existing particles, is plotted by black dashed line. The curves obtained by using quadtree structure with two, three and four levels of subdivision are plotted by black, blue and red solid line respectively. It takes some time to sort particles in to subdivided quadrants. Hence, it is not surprising that for a small number of particles (less than a few thousands) the procedures using higher level of subdivision are slower and the full distance checking procedure is the fastest. But with an increasing number of particles the pains taken by the subdividing is outweighed by faster distance checking and the order of procedures start to turn over. For a higher number of particles (more than ten thousands) the time effort of full distance checking procedure increases exponentially and for the instance the generating of 25 000 particles was not finished even in

two hours simulation. By contrast, the dependence of procedures using quadtree structure seems to be linear; see Fig. 3. It is because for pretty filled domain the number of particles that needs to be checked for a newly generated particle remains almost constant.
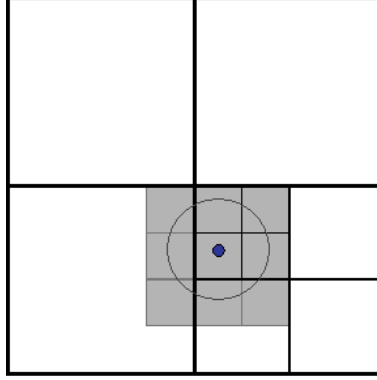
Fig. 2 Example of neighboring quadrants in quadtree structure.

It is noteworthy that, for all examples used in Fig. 3, the dominant stopping criterion was the criterion of maximal number of generation until one newly generated particle is accepted ($C_\text{gen} = 10^4$). Therefore the numbers of particles in several sets (with the same or the different distance checking procedure) generated with the same parameters are not exactly the same and the values of time effort have a random character. But the main features can still be well observed. To obtain exactly the same behavior for all procedures with the same geometry without the influence of randomness, the same sequences of random numbers must be used for all simulations. Then the time effort of different methods generating the same set of particles is obtained, but it is not our main purpose.

The whole process of generating particles can also be realized very effectively with different generating procedures. For instance, the generating procedure can use the Latin Hypercube Sampling or Delaunay triangulations [22] or can be based on the genetic algorithms or Monte Carlo methods [8]. In all cases, the parallelization can be used to reach a significant reduction of computational demands. However the search for the best generating algorithm is not the original purpose of this work and non-parallel algorithm using the quadtree structure turned out to be fully sufficient for generating particles in 2D. Also in 3D, an analogous algorithm using octree structure can be used.

Only the squares are replaced by cubes and each cube is subdivided into eight sub-cubes.
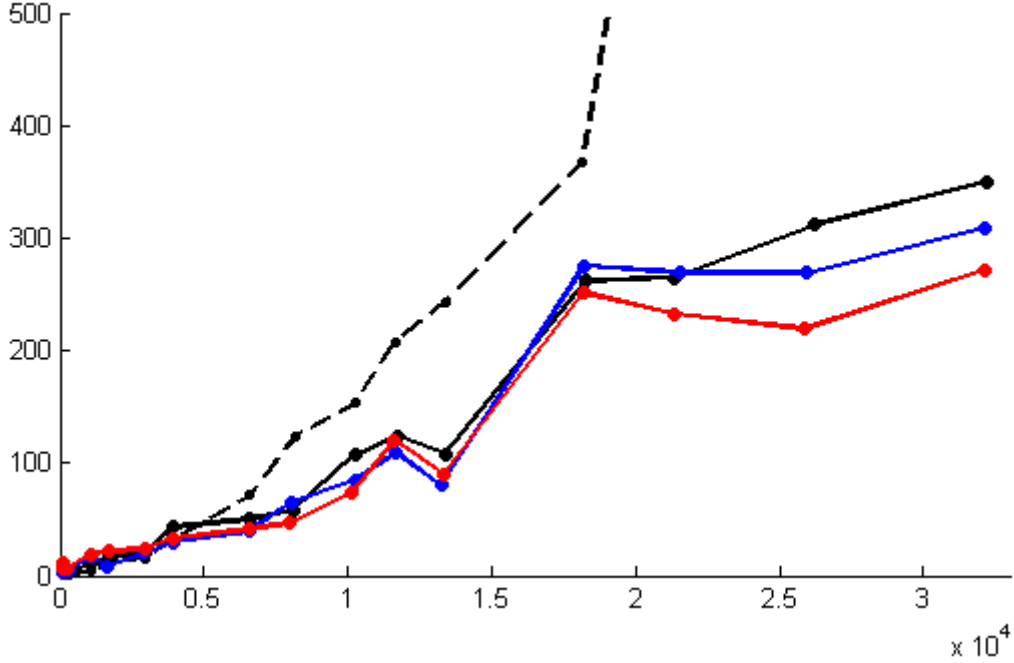
Fig. 3 The dependence of time effort on the final number of particles for generating particles with full distance checking procedure (dashed black), procedure using quadtree with two (solid black), three (blue) and four (red) levels of subdivision.

2.1.3 Boundary conditions

Boundary conditions of a point support are realized through the use of 6 regular nodes to prevent local effects; see *Fig. 4*. Only one node in the middle is subjected to the appropriate boundary condition.

2.1.4 Connecting by links

Finally, each two particles satisfying an appropriate rule are connected by a link. Only a short-distance interaction model is considered. The connecting rule depends on the type of material.

For an isotropic material, a circle rule can be applied, i.e., each two particles whose distance is less than a prescribed distance R_t are connected by a link. The prescribed radius is selected in the form $R_t = kR_P$. In 2D, factor k should be selected from the range $\langle 1.8, 2.0 \rangle$ to obtain the optimal truss element density; see *Fig. 4* (top). Prob-

lems can occur in examples with $R_t < 1.8R_P$ because the link connection can be too loose, which can lead to a kinematic mechanism; see *Fig. 4* (bottom).
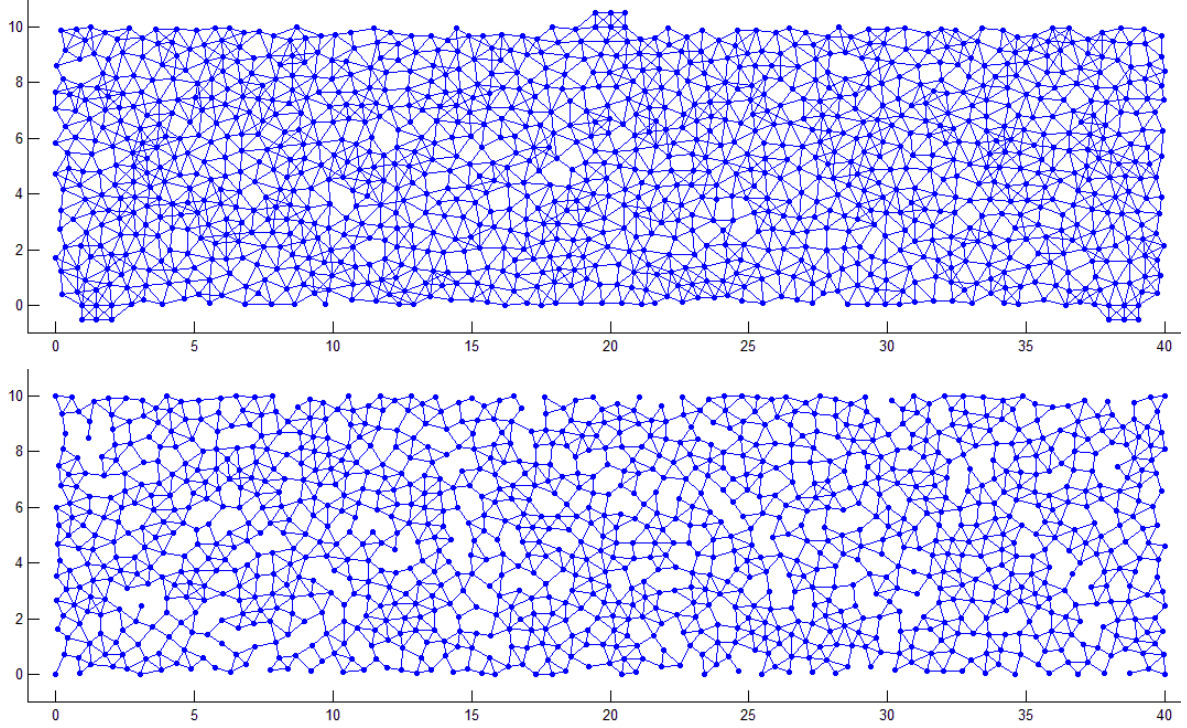
Fig. 4 Particles connected by links (circle rule). Optimal set for $R_P = 0.5$; $R_t = 1.9R_P$ (top), unsuitable set with mechanisms for $R_P = 0.5$; $R_t = 1.6R_P$ (bottom).
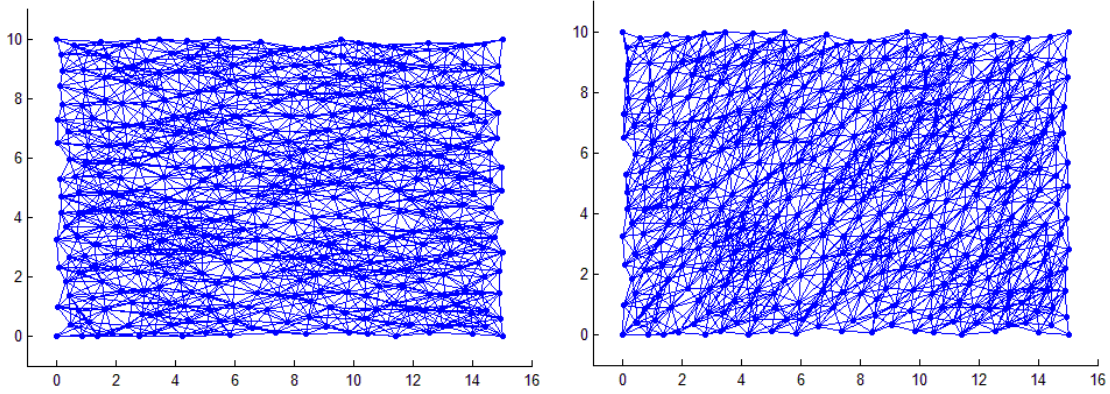
Fig. 5 Particles connected by links (elliptic rule) for $a = 2R_t$, $b = 1R_t$, $\varphi = 0$ (left) and $a = 2R_t$, $b = 1R_t$, $\varphi = \pi/4$ (right).

For an orthotropic material, an elliptic rule can be applied. Each particle is considered as the center of one ellipse. Then all particles lying in the same ellipse are connected by links to the particle in the centre. The ellipse is defined by the length of the horizontal axis a and vertical axis b and can also be rotated by an angle φ (defined

counterclockwise). The different lengths of axes lead to the orthotropic properties; see *Fig. 5*.

2.2   Materials with fibrous structure

Fibrous materials are formed by long yarns. This structure is typical for example for textile, paper or fiber-concrete. The structure of fibrous material cannot be represented by the random sets of particles used in the previous chapter because long fibers are not created if this type of random set of particles is used. To generate the fibrous structure of material, a reverse process is used. At the first, long fibers are generated and then particles are created in the position of fiber intersections.

2.2.1   Generating line segments

At the first, the required number of long fibers is generated. Then particles are placed into the position of all fiber intersections in the solved 2D domain. The fibers are represented as line segments with random length with uniform distribution from $L_{\min}$ to $L_{\max}$. The position of each line segment is given by the position of its center and by the rotation angle. The positions of the centers are randomly generated with uniform distribution and minimal distance R_P. The procedure for generating particles from part 2.1 is used here; see grey dots in *Fig. 6*. The distribution of rotation angle can be set as uniform; see *Fig. 9* and *Fig. 8* or some directions can be preferred; see *Fig. 7*.

2.2.2   Creating particles and links

In the next step, the intersections of all particles are computed. If the centers are generated only in the solved domain then the concentration of intersections in border areas is lower than in the middle of solved domain. To ensure the same density of intersections in the whole solved domain, the centers of the line segment must be generated not only in the solved domain but in surrounding area as well. The optimal size of outer area, where the centers are generated is $L_{\max}/2$; see *Fig. 6*. Finally, all particles lying on the same line segment are subsequently connected by links one after another. Therefore each particle is contained maximally in the four links because of the origin of intersection.
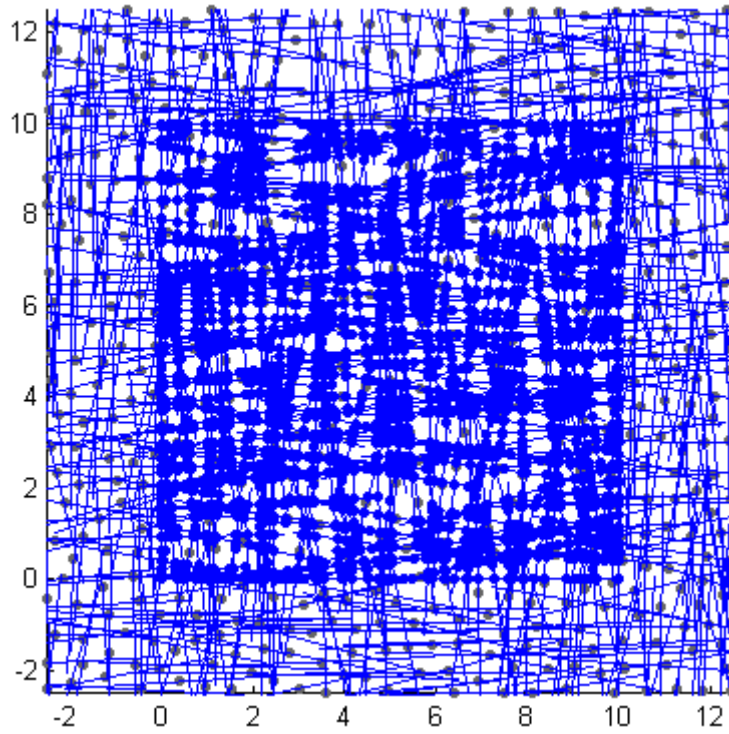
Fig. 6 Randomly generated centers (grey) of line segment with preferred orthogonal orientation and intersections (blue) computed only in solved domain 10x10.
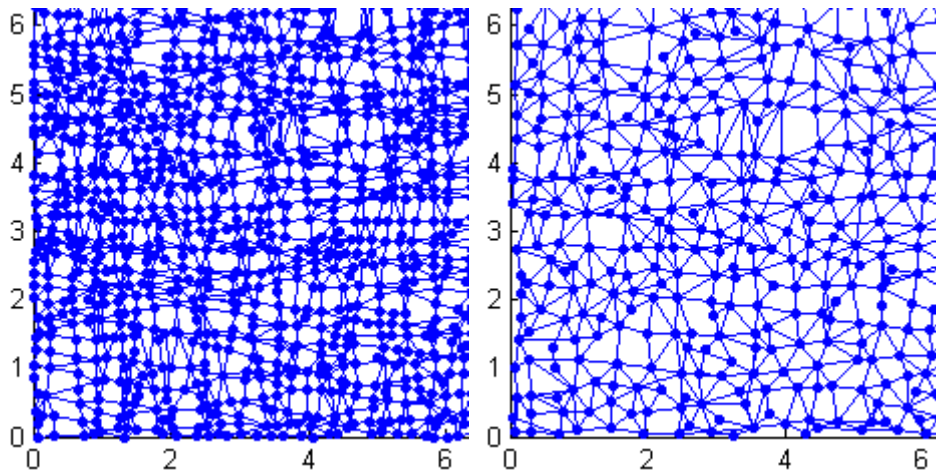
Fig. 7 Example of the particles connected by links obtained from the same set of line segments with $R_P = 0.5$ and preferred orthogonal orientation with two different connecting radii $R_c = 0.25R_P$ (left) and $R_c = 0.50R_P$ (right).

2.2.3 Consolidation of too close particles

Particles created in the previous step are mainly located in clusters; see *Fig. 6*. And many places are empty. To ensure a good distribution of particles in the whole solved domain a consolidation procedure is necessary. Therefore the value of connection radius R_c is set and all particles in this radius are consolidated into one particle. The position of this new particle is computed as an average of all consolidated particles. The

link connections remain unchanged. Therefore, one consolidated particle can be connected by more than four links and fibers are not straight.

For one set of generated line segments, several sets of particles and links can be created by setting the different connecting radius R_c; see *Fig. 7*. This radius should be set no less than $R_c \geq 0.5R_P$ to ensure the uniform distribution of particles after connection. Higher value of R_P provides a better distribution but at the same time reduces the number of particles and breaks the continuity of fibers especially if they are located only in preferred directions. For the uniform orientation of fibers, the value of $R_c \geq 2.0R_P$ can still be used; see *Fig. 8*.

The process of particle consolidation is realized in the loop through all particles. The realization of this loop should be repeated until no consolidation is possible to ensure that no pair of particles is closer than the connecting radius. Because after finishing one loop, it can happen that two newly created particles are in connecting radius. But the distance checking is time consuming process, even if the quadtree structure is used, and one realization of consolidating loop is enough to eliminate the problematic clusters of particles, therefore this loop is realized just once.
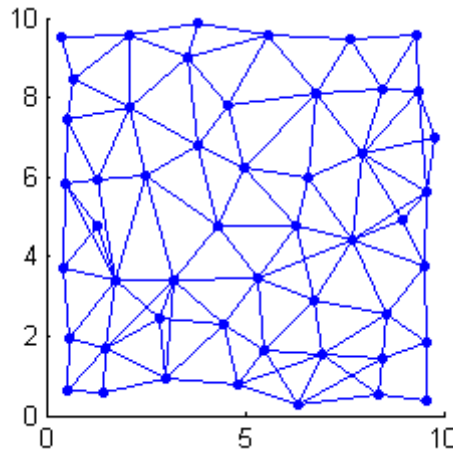
Fig. 8 Particles connected by links generated for fibrous material with uniform distribution of orientation of line segments for $R_P = 0.5$ and connecting radius $R_c = 2.5R_P$.

2.2.4 Removing of useless particles and links

Sometimes, it can happen, especially near the boundary, that some particles are not connected by any link or connected only with one link. Such particles with independent DOF are useless and attached links are useless too. Thus they are removed. Also the removing process is realized in the loop through all particles. And this loop should be, again, repeated until any removing is possible because after finishing the loop new

particles connected by only one link can appear (in previous loop connected also by any removed link).

The boundary conditions are realized in the same way as for the homogenous material with a uniform distribution of particles in part 2.1.

An example of final particles connected by links with uniform rotation of fibers is shown in *Fig. 9*. The position of particles is well-distributed and the structure of long fibers is clearly visible in each direction; see *Fig. 9*. For comparison, an example of real structure of nanotextile is taken over from [14] and depicted in *Fig. 10*.
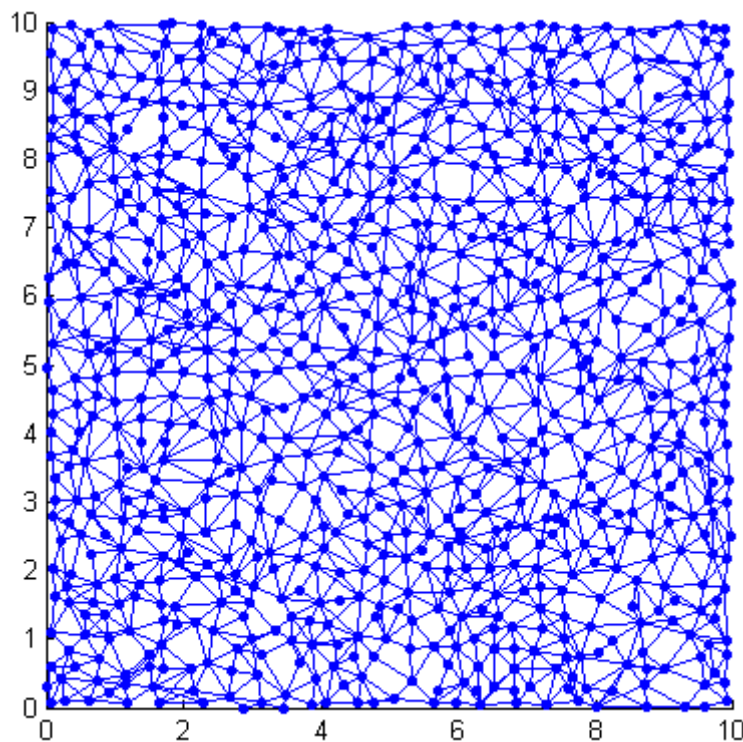
Fig. 9 Particles connected by links generated for fibrous material with uniform distribution of orientation of line segments for $R_P = 0.5$ and connecting radius $R_c = 0.5 R_P$.

2.2.5 Input with exact geometry of real material

Another way, how to obtain the input geometry, is analyze the real microstructure of material. For example, an algorithm converting the image of real nanofibers (such as *Fig. 10*) into 3D model is used in [26].
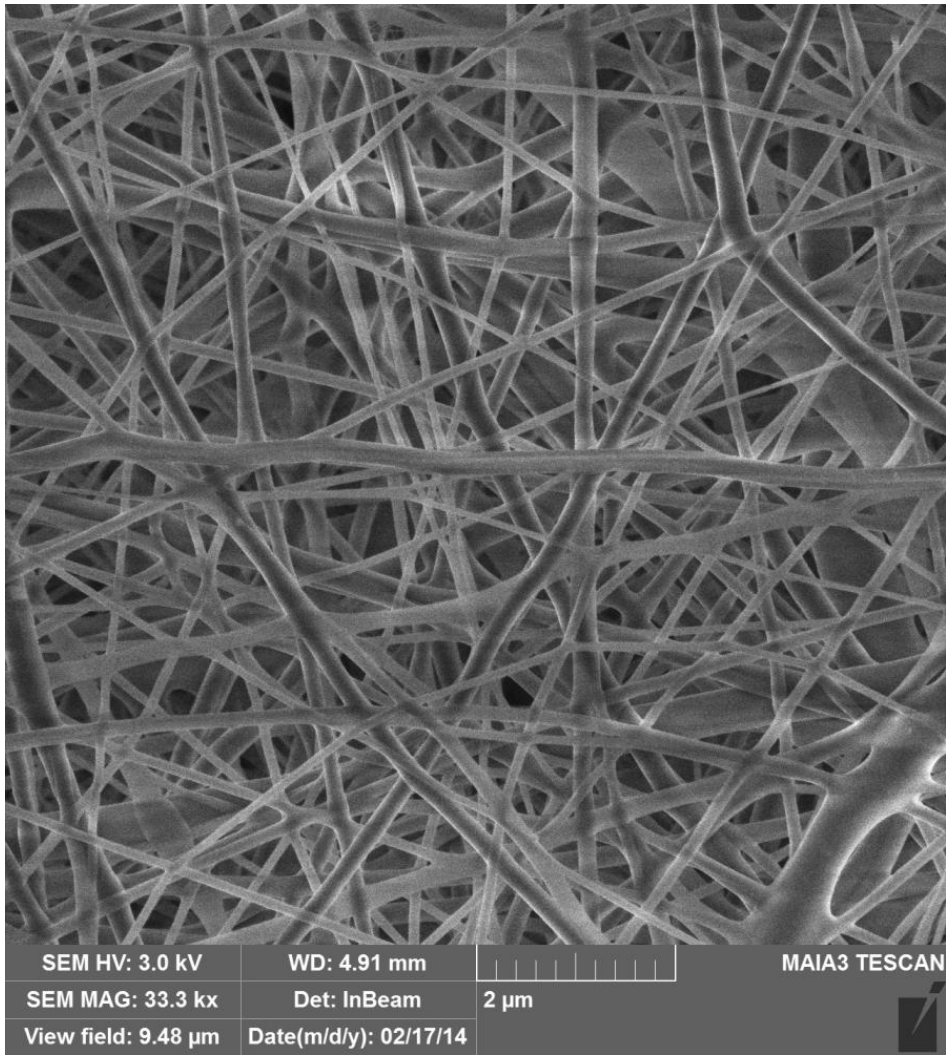
Fig. 10 Example of real structure of nanotextile, taken over from [14].

3 Selection of repnodes and interpolation elements

In the QC approach, most of the DOF are approximated. For that purpose, a sufficient subset of particles is selected as repnodes. There are two reasons why particles can be selected as a repnode. The first one is if the particle is situated in a region of high interest. All such particles are selected as repnodes to represent the exact particle behavior in this region. But also in a region of low interest, a sufficient number of repnodes are needed to represent the simplification of this region. These repnodes form interpolation elements and their position depends on the type of triangulation of interpolation mesh. Two ways how to create an interpolation mesh with added repnodes in a region of high interest are described below. The basic triangulation is done by the T3D mesh generator [25] in both of them.

3.1 Addition of repnodes without densification of interpolation mesh (MESH1)

In this case, the optimal 2D triangulation with a prescribed density is done by T3D in the whole solved domain. Then all newly created nodes of the mesh are shifted to the position of the nearest particles and these particles are labeled as repnodes. Sometimes, two or more nodes of one mesh element happen to be shifted to the same position, which leads to degeneration of a triangular element to a line or a point. Such degenerated elements are detected and removed. After that, all nodes in the region of high interest that do not have the repnode status yet are labeled as repnodes.

This process allows creating an interpolation mesh with a predefined density with the nodes in the position of particles and repnodes in the region of high interest which do not affect the mesh; see Fig. 11

3.2 Addition of repnodes with densification of interpolation mesh (MESH2)

In this case, the reverse order is used. At first, all particles in regions of high interest are selected as repnodes. Then all existing repnodes are considered as nodes of the initial 2D mesh and the triangulation is finished by T3D in the whole domain. The sizes of mesh elements are affected by the position of existing mesh nodes (repnodes) and continuously change from the minimal value (distance between particles in the region of

high interest) to the maximal one (prescribed value in the region of low interest). All newly created nodes of the mesh are shifted to the position of the nearest particle and this particle is labeled as a repnode. Mesh elements degenerated to a line or a point are detected and removed.

This process allows creating an interpolation mesh with the nodes in the position of particles with variable density affected by the position of repnodes in the region of high interest; see *Fig. 12*.
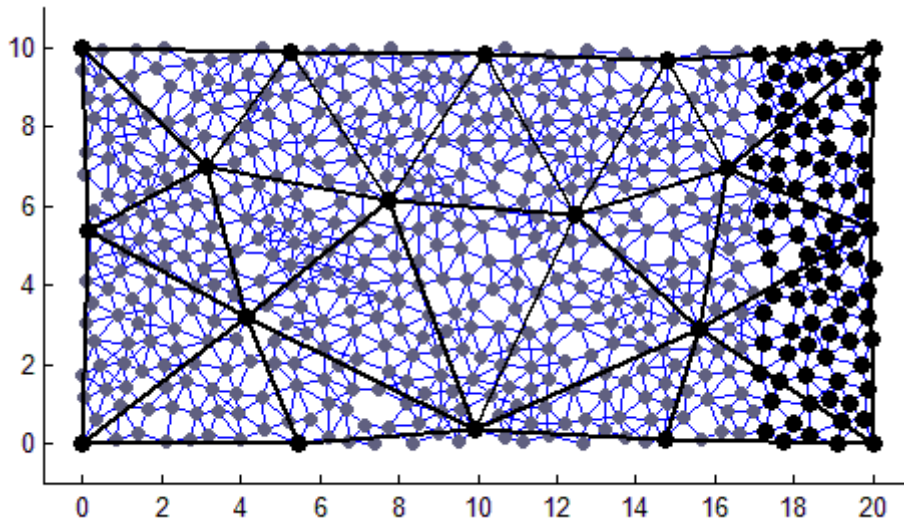
Fig. 11 Interpolation mesh with constant density. Repnodes and interpolation elements (black), hanging nodes (grey) and truss elements (blue).
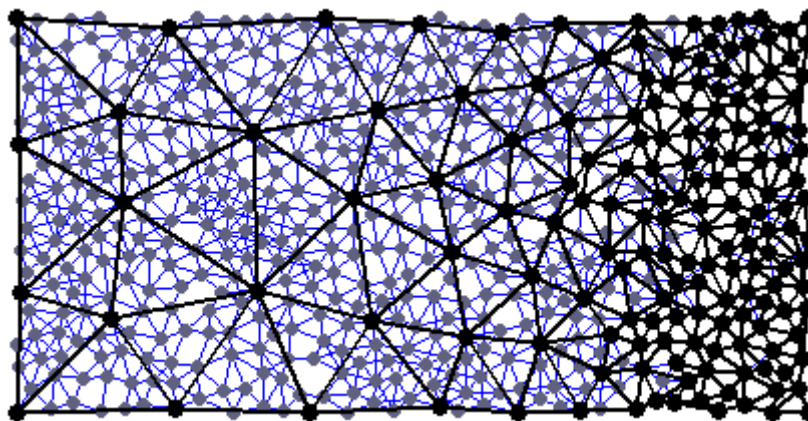
Fig. 12 Interpolation mesh with variable density. Repnodes and interpolation elements (black), hanging nodes (grey) and truss elements (blue).

3.3   Boundary conditions

If any of the boundary condition is realized through the use of 6 extra nodes, then all these nodes are labeled as repnodes. But interpolation elements formed by these nodes are not taken into account because they are located outside the solved domain.

3.4   Modeling of cracks

A crack can be modeled as a notch with a finite width or as a sharp spike. But in both cases it is required to include the information about crack into the input geometry. And the mesh generator is restricted to respect the crack. But it is also possible to realize the interpolation mesh independently of the crack geometry. For that purpose, an idea of doubled elements is used. This idea stems from the extended finite elements (XFEM) [23], where doubled DOF are used in elements with a crack.

In our case, the doubled elements are used in the following way:

- The initial crack is modeled as a segment connecting two points
- The mesh generator is not affected by the crack
- Then elements intersecting the crack are detected and doubled
- One of the double elements is connected on the left side and the other on the right side of the crack and then labeled as left or right
- The hanging nodes are also labeled as left or right according to their position with respect to the crack.
- Left hanging nodes can be interpolated by the left elements only, and vice versa
- An area near the crack tip is included in the area of high interest and realized with repnodes and truss elements, therefore interpolation elements are not needed here

This process of crack modeling is more convenient because it does not need the generation of a mesh with a special shape and the crack can propagate arbitrarily without remeshing and the exact behavior around the crack tip can still be captured by adding repnodes. Crack propagation can then be realized by breaking a bar near the crack tip.

4 Application of simplifying rule

From the previous two chapters, we know how to generate and describe the input geometry of the problem and now it is finally time to apply some simplifying rule based on the idea of QC. In this chapter, four models using different levels of simplification are presented.

4.1 Pure particle model (M1)

This model does not use any simplification. Only particles and links are used as an input for this model. Repnodes and interpolation elements are not needed. Every single particle represents a node with two independent DOF (vertical and horizontal displacement) and the links are described by 1D truss elements. Consequently, all links are taken in to account explicitly and connections contribute to the stiffness matrix.

This model can be considered as the exact model and results obtained by using this model are used as a reference solution for other simplified models. Nevertheless, the results of this "exact" model are not totally exact because depend on the position of particles which is generated randomly in the first step. The results are not the same if two different set of representing particles are generated for one input geometry. It is because the particles are generated with uniform distribution from the global point of view but not in all scales. In some parts, the density of particles can be a little higher or lower than average value, which makes these parts stiffer or weaker. This behavior does not have negative influence on global results. But if the solution computed only on one set of particles is used as a reference solution then the error values for other simplified models can be significantly affected by the distribution of particles. Therefore, it is necessary to compare the results of simplified model with exact solution for several random generations and not just for one. The average error from several generations can be used as an objective error indicator of simplified models.

4.2 Hanging nodes model (M2)

The first way how to use QC idea to simplify the pure particle models is by using approximation of DOF of particles not labeled as repnodes. This particles are called hanging nodes because their DOF are not independent but they are hanged on appropri-

ate repnodes. For that purpose, the interpolation elements formed just by the repnodes are used. For all hanging nodes the relevant interpolation element is found. It is either the element in which the hanging node is located or the nearest element if the hanging node is not located in any interpolation elements; see *Fig. 13*. The displacement of each hanging nodes is given by the displacements of the vertices of its selected interpolation element. Consequently, DOF of all hanging nodes are interpolated (or extrapolated) by the DOF of repnodes.
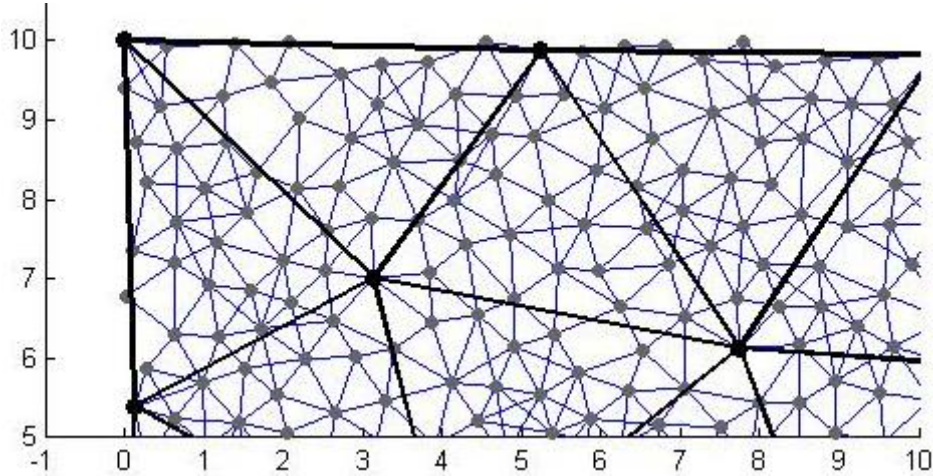
Fig. 13 Example of hanging nodes (grey) located outside of interpolation elements.

All nodes (particles) connected with truss elements contribute to the stiffness matrix but only the repnodes have independent DOF. The repnodes with two DOF (vertical and horizontal displacement) represent the nodes of an interpolation mesh. The Interpolation mesh is realized by 2D plane triangle elements. Zero thickness is assigned to these elements and thus they do not contribute to the global stiffness matrix. These elements are used only to approximate displacements of nodes not selected as repnodes.

In OOFEM implementation, the nodes carrying DOF (repnodes) are modeled as regular nodes. The nodes with interpolated DOF (hanging nodes) are realized with a special type of node. For this type of node, the subset of interpolation elements can be specified. Then the nearest interpolation elements is found only prom this subset and not from all interpolation elements. This allows to distinguish overlap elements along the crack.

The truss connection is realized in the same way as for model M1. In the region of high interest, all nodes are repnodes. Therefore, no hanging nodes with interpolated

22

DOF are there. And description of this region is exact as well as for model M1 using pure particle approach.

4.2.1 Linear interpolation

Linear interpolation (extrapolation) rule is used.

$$u = \frac{1}{A} \sum_{i=1}^{3} A_i u_i \tag{1}$$

where u is an interpolated quantity, u_i is the value in i^{th} node of the interpolation element, A is an area of this element and A_i is i^{th} area coordinate of interpolated point.

4.3 General homogenization model (M3)

In this model, 2D plane elements are used to replace the stiffness represented by 1D truss elements in the region of low interest. Thereby, a substantial number of truss elements can be removed and number of DOF is significantly reduced.

Material properties of 2D plane elements are identified by the homogenization of all 1D truss elements. There are several ways how to identify material parameters which depend on the type of materials. Homogenization process is described in more detail in subchapters 4.3.1 - 4.3.6. Obtained parameters are set the same for all 2D elements.

Geometry of interpolation elements are used for plane elements. The interpolation elements with zero stiffness are replaced by the plane elements with stiffness obtained in homogenization process. Plane strain or plane stress 2D elements can be used but the corresponding homogenization process must be considered.

Then hanging nodes with interpolated DOF are removed and truss elements connecting them can be removed too. It leads to the significant reduction of DOF. But it must be done carefully.

The truss elements connecting two hanging nodes (in the same or in two different elements) can be removed because their stiffness is represented by 2D elements. Truss elements connecting one repnode and one hanging node laying in the same 2D element can be removed too because their stiffness is still captured.

A problem occurs if a bar goes through an edge of 2D element and connects one hanging node with one repnode. It can happen if 2D elements are too small or on the

interface between region of low and high interest; see *Fig. 14*. Such truss elements cannot be removed because their stiffness is not covered by 2D elements. In these cases, such hanging nodes are not removed and such truss elements remain too.
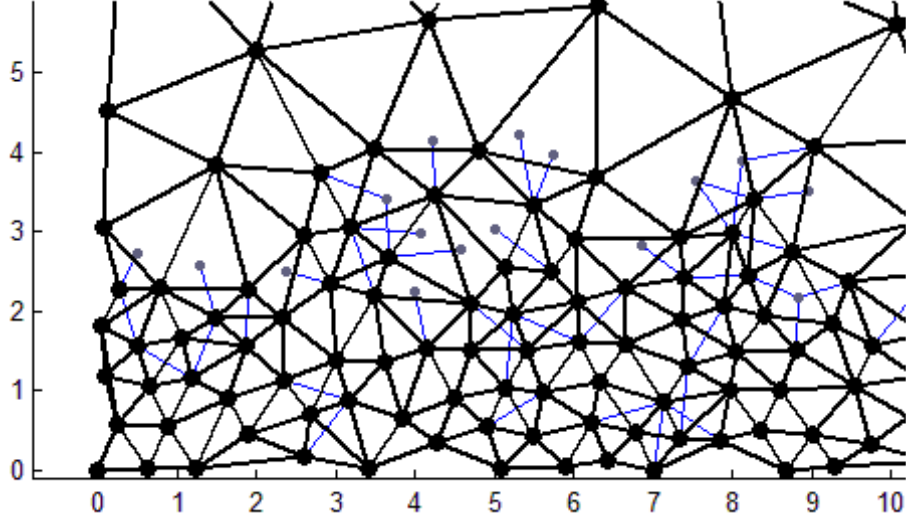
Fig. 14 Example of truss elements (blue) and hanging nodes (grey) remaining on the interface.

4.3.1 Assemblage of global stiffness matrix

The global stiffness matrix is assembled from the contribution of all links. Global stiffness tensor is defined in [30] as

$$\boldsymbol{D}_e = \frac{1}{V} \sum_{i=1}^{N_t} L_i E_{t_i} A_i (\boldsymbol{N}_i \otimes \boldsymbol{N}_i) \tag{2}$$

where $\boldsymbol{N} = \boldsymbol{n} \otimes \boldsymbol{n}$ and $\boldsymbol{n}$ is a unit vector of characteristic direction of the link. E_t is its Young's modulus, A is the cross-section area and L is the length of the link. V is the volume of solved domain. Then final stiffness tensor is evaluated in the loop through all N_t links in solved domain. The symmetry of computed tensor is guaranteed by $\boldsymbol{n} \otimes \boldsymbol{n} \otimes \boldsymbol{n} \otimes \boldsymbol{n}$.

Generally in 3D, the stiffness tensor has 81 components because of dimension 3x3x3x3. But because of symmetry, only 21 components are independent and stiffness tensor can be represented by the symmetric stiffness matrix 6x6. In 2D, three lines and three columns related to the third direction can be removed. Then stiffness in 2D can be represented by symmetric stiffness matrix 3x3 with 6 independent components

$$D_c = \begin{pmatrix} a & b & c \\ b & d & e \\ c & e & f \end{pmatrix} \tag{3}$$

This matrix is obtained by using the right components from the global stiffness tensor computed according to (2). Although the geometry of particles and links is generated for isotropic material the computed stiffness matrix corresponds to the generally anisotropic material because of influence of randomness.

4.3.2 Approximation of stiffness matrix

For the homogenized material, the computed stiffness matrix D_c can be used exactly as a material stiffness matrix but in some cases it is more convenient to approximate computed matrix by some matrix with specific properties.

Approximated matrix D_a is found in an apriory given form. The components of D_a are identified by minimizing the error in terms of the norm of the difference between D_a and D_c.

Two ways how to calculate the norm of the difference between computed matrix and approximated matrix are used.

At the first the norm using eigenvectors of D_a is denoted $\|\cdot\|_A$ and defined as

$$\|D_c - D_a\|_A^2 = \sum_{i=1}^{3} v_i (D_c - D_a) v_i^T \tag{4}$$

where v_i is i^{th} eigenvector of matrix D_a.

Then the norm using square of the components of the difference matrix $D_a - D_c$ is denoted $\|\cdot\|_B$ and defined as

$$\|D_c - D_a\|_B^2 = \sum_{i=1}^{3} \sum_{j=1}^{3} \left(w_{ij} \left(D_{c,ij} - D_{a,ij} \right) \right)^2 \tag{5}$$

where $D_{a,ij}$ is the component of D_a on the ith row and i^{th} column, and w_{ij} is the component of weight matrix W defined as

$$W = \begin{pmatrix} 1 & 1 & 2 \\ 1 & 1 & 2 \\ 2 & 2 & 4 \end{pmatrix}. \tag{6}$$

The weight matrix W appears because of matrix representation of stiffness tensor. If the norm is computed directly from the stiffness tensor D_e

$$\|\boldsymbol{D}_e\|^2 = \boldsymbol{D}_{ijkl}\,\boldsymbol{D}_{ijkl} \tag{7}$$

then some summands appear more often than others. That is why the corresponding weights are necessary to obtain the correct norm by using the stiffness matrix instead of stiffness tensor.

In the next three subsections, it is shown how the computed matrix $\boldsymbol{D}_c$ can be approximated by isotropic or orthotropic stiffness matrix. In the following two subsections we assume that the material of the elements is isotropic. The definition of theoretical stiffness matrix of isotropic material in 2D is different for plane stress and plane strain.

4.3.3 Homogenization by isotropic stiffness matrix for plane stress

The 2D stiffness matrix for plane stress is defined as

$$\boldsymbol{D}_{iso,stre} = \frac{E}{(1+\nu)(1-2\nu)}\begin{pmatrix} 1-\nu & \nu & 0 \\ \nu & 1-\nu & 0 \\ 0 & 0 & \dfrac{1-2\nu}{2} \end{pmatrix} \tag{8}$$

where E is Young's modulus and ν is Poisson's ratio of the material. These two parameters are identified by minimizing the approximation error.

4.3.3.1 Results for norm $\|\cdot\|_A$

If the approximate matrix is set $\boldsymbol{D}_a = \boldsymbol{D}_{iso,stre}$ and the first matrix norm is used then the error can be expressed as a function of E and ν

$$f(E,\nu) = \left(k_1 - \frac{2E}{(1+\nu)(1-2\nu)}\right)^2 + \left(k_2 - \frac{2E}{1+\nu}\right)^2 + \left(k_3 - \frac{E}{2(1+\nu)}\right)^2 \tag{9}$$

where

$$k_1 = a + 2b + d \tag{10}$$
$$k_2 = a - 2b + d \tag{11}$$
$$k_3 = f \tag{12}$$

where $a, b, \dots, f$ are constant components of computed stiffness matrix $\boldsymbol{D}_c$.

To be able to find the minimum analytically, it is convenient to do the following substitution

$$\lambda = \frac{E\nu}{(1+\nu)(1-2\nu)} \qquad\qquad E = \frac{\mu(3\lambda + 2\mu)}{\lambda + \mu} \tag{13}$$

$$\mu = \frac{E}{2(1+v)} \qquad\qquad v = \frac{\lambda}{2(\lambda+\mu)} \qquad (14)$$

and substitute Lamé's parameters λ and μ instead of E and v into the function (9). After the substitution, the objective function

$$f(\lambda,\mu) = (k_1 - 4\lambda - 4\mu)^2 + (k_2 - 4\mu)^2 + (k_3 - \mu)^2 \qquad (15)$$

is quadratic with the respect to the both variables. By standard minimizing we obtain a unique solution

$$\lambda = \frac{1}{68}(17k_1 - 16k_2 - 4k_3) \qquad (16)$$

$$\mu = \frac{1}{17}(4k_2 + k_3) \qquad (17)$$

or

$$E = \frac{(35a + 134b + 35d - 4f)(4a - 8b + 4d + f)}{289(a + 2b + d)} \qquad (18)$$

$$v = \frac{a + 66b + d - 4f}{34(a + 2b + d)} \qquad (19)$$

4.3.3.2 Results for norm $\|\cdot\|_B$

In this case, approximate matrix is still set $\boldsymbol{D}_a = \boldsymbol{D}_{iso,stre}$ but the second matrix norm is used. Then the error can be expressed as a function of E and v

$$\begin{aligned} f(E,v) = {}&\left(a - \frac{E(1-v)}{(1+v)(1-2v)}\right)^2 + 2\left(b - \frac{Ev}{(1+v)(1-2v)}\right)^2 \\ &+ \left(d - \frac{E(1-v)}{(1+v)(1-2v)}\right)^2 + 16\left(f - \frac{E}{2(1+v)}\right)^2. \end{aligned} \qquad (20)$$

To be able to find the minimum analytically, it is convenient to do the following substitution

$$\alpha = \frac{v}{1-2v} \qquad\qquad E = \beta + \frac{\alpha\beta}{1+2\alpha} \qquad (21)$$

$$\beta = \frac{E}{1+v} \qquad\qquad v = \frac{\alpha}{1+2\alpha} \qquad (22)$$

and substitute parameters α and β instead of E and v into the function (20). After the substitution, the objective function

$$f(\alpha,\beta) = (a - \alpha\beta - \beta)^2 + 2(b - \alpha\beta)^2 + (d - \alpha\beta - \beta)^2 + 4(2f - \beta)^2 \qquad (23)$$

is quadratic with the respect to the both variables. By standard minimizing we obtain a unique solution

$$\alpha = \frac{2(a + 3b + d - 4f)}{a - 2b + d + 16f} \tag{24}$$

$$\beta = \frac{1}{10}(a - 2b + d + 16f) \tag{25}$$

or

$$E = \frac{(7a + 16b + 7d - 8f)(a - 2b + d + 16f)}{50(a + 2b + d)} \tag{26}$$

$$v = \frac{2(a + 3b + d - 4f)}{5(a + 2b + d)}. \tag{27}$$

4.3.4   Homogenization by isotropic stiffness matrix for plane strain

The 2D stiffness matrix for plane stress is defined as

$$\boldsymbol{D}_{iso,stra} = \frac{E}{1 - v^2} \begin{pmatrix} 1 & v & 0 \\ v & 1 & 0 \\ 0 & 0 & \frac{1 - v}{2} \end{pmatrix} \tag{28}$$

and approximate matrix is set $\boldsymbol{D}_a = \boldsymbol{D}_{iso,stre}$.

4.3.4.1   Results for norm $\|\cdot\|_A$

If the approximate matrix is set $\boldsymbol{D}_a = \boldsymbol{D}_{iso,stra}$ and the first matrix norm is used then the error can be expressed as a function of E and v

$$f(E, v) = \left(k_1 - \frac{2E}{1 - v}\right)^2 + \left(k_2 - \frac{2E}{1 + v}\right)^2 + \left(k_3 - \frac{E}{2(1 + v)}\right)^2. \tag{29}$$

To be able to find the minimum analytically, it is convenient to do the following substitution

$$\gamma = \frac{2E}{1 - v} \qquad\qquad E = \frac{\alpha - 4\mu}{\alpha + 4\mu} \tag{30}$$

$$\mu = \frac{E}{2(1 + v)} \qquad\qquad v = \frac{4\alpha\mu}{\alpha + 4\mu} \tag{31}$$

and substitute parameters γ and μ instead of E and v into the function (32). After the substitution, the objective function

$$f(\gamma, \mu) = (k_1 - \gamma)^2 + (k_2 - 4\mu)^2 + (k_3 - \mu)^2 \tag{32}$$

is quadratic with the respect to the both variables. By standard minimizing we obtain a unique solution

$$\gamma = k_1 \tag{33}$$

$$\mu = \frac{1}{17}(4k_2 + k_3) \tag{34}$$

or

$$E = 4(a + 2b + d)\frac{(4a - 8b + 4d + f)}{33a + 2b + 33d + 4f} \tag{35}$$

$$v = \frac{a + 66b + d - 4f}{33a + 2b + 33d + 4f}. \tag{36}$$

4.3.4.2 Results for norm $\|\cdot\|_B$

In this case, approximate matrix is still set $\boldsymbol{D}_a = \boldsymbol{D}_{iso,stra}$ but the second matrix norm is used. Then the error can be expressed as a function of E and v

$$f(E,v) = \left(a - \frac{E}{1 - v^2}\right)^2 + 2\left(b - \frac{Ev}{1 - v^2}\right)^2 + \left(d - \frac{E}{1 - v^2}\right)^2 \\ + 16\left(f - \frac{E}{2(1 + v)}\right)^2. \tag{37}$$

To be able to find the minimum analytically, it is convenient to do the following substitution

$$\alpha = \frac{v}{1 - v} \qquad\qquad E = \beta + \frac{\alpha\beta}{1 + \alpha} \tag{38}$$

$$\beta = \frac{E}{1 + v} \qquad\qquad v = \frac{\alpha}{1 + \alpha} \tag{39}$$

and substitute parameters α and β instead of E and v into the function (37). After the substitution, the objective function

$$f(\alpha,\beta) = (a - \alpha\beta - \beta)^2 + 2(b - \alpha\beta)^2 + (d - \alpha\beta - \beta)^2 + 4(2f - \beta)^2 \tag{40}$$

is quadratic with the respect to the both variables. By standard minimizing we obtain a unique solution

$$\alpha = \frac{2(a + 3b + d - 4f)}{a - 2b + d + 16f} \tag{41}$$

$$\beta = \frac{1}{10}(a - 2b + d + 16f) \tag{42}$$

or

$$E = \frac{(a + 2b + d)(a - 2b + d + 16f)}{2(3a + 4b + 3d + 8f)} \tag{43}$$

$$v = \frac{2(a + 3b + d - 4f)}{3a + 4b + 3d + 8f}. \tag{44}$$

29

4.3.5 Homogenization by orthotropic stiffness matrix

In this case a concept of orthotropic material is accepted. The matrix of 2D orthotropic material with the respect to the axes of orthotropy is defined as

$$\boldsymbol{D}_{orth} = \begin{pmatrix} E_x(1 - \nu_{yz}\nu_{zy})/\delta & E_y(\nu_{xy} - \nu_{xz}\nu_{zy})/\delta & 0 \\ E_y(\nu_{xy} - \nu_{xz}\nu_{zy})/\delta & E_y(1 - \nu_{xz}\nu_{zx})/\delta & 0 \\ 0 & 0 & G_{xy} \end{pmatrix} \qquad (45)$$

where

$$\delta = 1 - (\nu_{xy}\nu_{yx} + \nu_{yy}\nu_{yy} + \nu_{zx}\nu_{xz}) - (\nu_{xy}\nu_{yz}\nu_{zx} + \nu_{yx}\nu_{zy}\nu_{xz}) \qquad (46)$$

where E_i is Young's modulus in the ith direction, G_{xy} is the shear modulus in xy plane, ν_{ij} major Poisson's ratio, and ν_{ji} minor Poisson's ratio. In 2D, there are only six independent material parameters, because symmetry conditions yield [23]

$$\nu_{xy}E_y = \nu_{yx}E_x, \qquad (47)$$

$$\nu_{yz}E_z = \nu_{zy}E_y, \qquad (48)$$

$$\nu_{zx}E_x = \nu_{xz}E_z. \qquad (49)$$

The orientation of the axes of orthotropy can be arbitrary and must be identified too. The minimization must be realized numerically [19], with the respect to all seven parameters (six parameters of 2D orthotropic material and the angle of the axes rotation). Numerical minimization is time expensive if it must be realized for all elements. Therefore this type of stiffness matrix is acceptable only for the general homogenization model M3. For model M4 with individual homogenization (described thereinafter), it is more effective to use exact anisotropic stiffness matrix.

4.3.6 Homogenization by exact anisotropic stiffness matrix

In this case, the material of the elements is considered to be generally anisotropic and the full computed stiffness matrix $\boldsymbol{D}_s$ defined in (3) is used as the material stiffness matrix. Identification procedure is not needed because all 6 component of computed stiffness matrix are entered in the OOFEM input.

4.4 Individual homogenization model (M4)

This model stems from model M3 and tries to improve the following deficiencies:

- In model M3, stiffness matrix of 2D element is obtained by the contribution of all truss elements but then parts of some truss elements remain in some 2D ele-

ments. If element is small the error caused by the twice considered parts of truss elements can be significant.

- Model M3 assume that material properties are the same in all points of material.

This model removes these deficiencies by identifying material parameters individually for each element. For that purpose the stiffness matrix must be assembled for all elements.

Then the homogenization of stiffness matrix for each element is realized by one of the procedures described in 4.3.3 - 4.3.6. The material can be again considered as isotropic, orthotropic or generally anisotropic. For computation of local parameters of material, it makes sense to consider orthotropic or anisotropic material even if resulting material behavior is isotropic. Because for small elements, an exclusion of the contribution of one truss element can result in a significant failure of isotropy.

4.4.1 Assemblage of local stiffness matrix for all interpolation elements

The stiffness matrix is assembled individually for all 2D elements. The stiffness matrix of each element is assembled only from the contributions of the parts of the links which are really situated inside the element. But at the same time, some links (for which it is necessary) remain in input file as 1D truss elements and do not contribute to the stiffness matrix of any 2D element.

The loop through all links is realized and the contribution of every link is computed according to the following rules which depend on the type of ends of the link.

Repnode – repnode

- Link is realized by 1D truss element
- This link does not contribute to the stiffness matrix of any 2D elements

Hanging node – hanging node

If one or both of the ends of the link are situated outside of interpolation element

- This link is realized by 1D truss element
- Both hanging nodes remain in input file
- This link does not contribute to the stiffness matrix of any 2D elements

If both of the ends of the link are situated in the same element

- The stiffness contribution of this link is computed according to (2)
- The entire contribution of this link is assembled to this element

If both of the ends of the link are situated in the different elements

- The stiffness contribution of this link is computed according to (2)
- All elements which this links goes through are detected
- The stiffness contribution is distributed to all the detected element according to the length of the part of the link inside each element

Repnode – hanging node

If both of the ends of the link are situated in the same element

- The stiffness contribution of this link is computed according to (2)
- All contribution is assembled to this element

If both of the ends of the link are situated in the different elements

- Link is realized by 1D truss element
- Hanging node remains in input file
- This link does not contribute to the stiffness matrix of any 2D elements

4.4.2 Modeling of cracks

If the crack is modeled by the overlap elements then the same rules can be used. It is only necessary to do extra decision on which side of the crack the link is situated. And according to this decision the stiffness contribution is assigned to the correct one of the overlap elements.

4.4.3 Computational effort

OOFEM input file for model M4 is almost the same as for M3 with only one exception. In M4 input file there are more types of materials with different parameters for plane elements. And also numerical tests show that computation with M4 is slightly slower than with M3 because M4 has to deal with more materials. But this difference is negligible. But set-up process of identifying material parameters is measurably slower for M4. This difference depends on the type of homogenization.

Both models M3 and M4 are several times faster than M1 and M2 even if the time of set-up process is involved.

5 Post processing of results and error evaluation

After choosing one of the simplified models, numerical simulations are performed using the open-source finite element code OOFEM [24]. OOFEM computes the displacement values for repnodes and hanging nodes, the strain and stress values for 1D truss elements and 2D plane elements. Then some post processing procedures are required to evaluate error of chosen model and to plot computed results.

5.1 Error evaluation

For M3 and M4 we obtain the continuous results in the region of low interest represented by 2D elements. For each element, there are constant stress and strain and linear displacement, if triangular 2D elements with linear approximation are used. By contrast for M1 and M2, the values of obtained result are in the discrete position of particles or links. There are two ways how to compare continuous results with discrete values. The first one is to make continuous values from the discrete result by computing average on the area of each element. But this comparing does not lead to the good error prediction because a lot of information is lost by averaging. The second one and more convenient way is to recalculate the needed discrete values from the continuous results.

At the first the values of displacements are computed in the position of all nodes which are not used in M3 and M4 as repnode or hanging node. Displacements inside of the elements are interpolated according to (1). Extrapolation outside of the elements is not needed because all nodes outside are treated as hanging nodes and displacements are computed explicitly. In the next step the strain is computed from the displacement for all links which are not considered as truss elements and computed explicitly. Finally the stress is computed from the strain. Now for M3 and M4, the corresponding values for all particles and truss elements are available to be compared with M1.

The error for i^{th} model $e_{x,i}$ is computed by comparing the corresponding values x_i (displacement, stress or strain) with the results x_1 of M1. As it is noted above the error values depend on the position of generated particles. Therefore the error is evaluated as an average for P randomly generated sets of particles and links.

Absolute error is defined as

$$e_{x,i} = \frac{1}{P} \sum_{j=1}^{P} \left| x_{i,j} - x_{1,j} \right| \tag{50}$$

and relative error as

$$\bar{e}_{x,i} = \frac{1}{P} \sum_{j=1}^{P} \frac{\left| x_{i,j} - x_{1,j} \right|}{\left| x_{i,j} \right|} \tag{51}$$

where $x_{i,j}$ is monitored value computed with i^{th} model for j^{th} generation of particles and P is the total number of iterations.

Frequently, it happens that for some particles or links the real value $x_{i,j}$ is close to zero, e. g. the displacement near the supported particles or the strain in the truss element perpendicular to the load direction. Then the value of relative error is extremely high even if the absolute error is small. Consequently it is more convenient to use absolute error divided by some characteristic value instead of relative error.

To be able to compare individual models, it is useful to define some global indicator of error.

$$E_{tot,x,i}^{2} = \sum_{i=1}^{T} e_{x,i}{}^{2} \tag{52}$$

or

$$E_{max,x,i} = \max_{i}\left(e_{x,i} \right). \tag{53}$$

Here, T is the total number of nodes respectively bars if error is evaluated in displacement or stress or strain.

5.2 Visualization of the results and errors

The results and errors are represented by the values in discrete points. It is convenient for computing but less comfortable for visualization. Naturally, it is possible to depict some color points into the place with error, color lines instead of stress and strain or resized vectors instead of displacement. But because of our experience with continuously looking world around us, it is more pleasurable to see a full-filled color plot.

For that purpose, a regular square grid is used and the plotted values are converted. The plotted value of each cell in the grid is computed as an average of all values placed inside the cell. If the cell is empty then its value is interpolated as an average of

the values of neighboring cells. The size of the grid in each direction is selected close to the minimal distance of two particles R_P to ensure that the maximal number of values in one cell is not too high and simultaneously to minimize the number of empty cells.

6 Material representation

6.1 Elastic materials

6.1.1 Elastic truss elements

If the link connection is considered as purely elastic then all links are realized by elastic bars and the stiffness of the truss elements is defined as

$$k = \frac{EA_t}{L} \tag{54}$$

where L is the bar length (corresponding to the distance of connected particles) and EA_t is the cross-section stiffness of the bar which is the same for all bars and its value is set to represent the global behavior of real material.
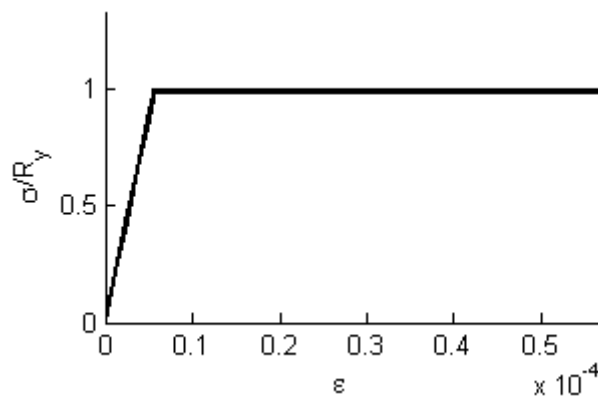
6.1.2 Elastic continuous elements

Material of 2D elastic elements is represented by the 6x6 stiffness matrix obtained by using one of the homogenization procedures described in section 4.3.

6.2 Plasticity

For quasicontinuous simulations of plastic materials, the description of both the plastic truss elements and the 2D plastic material is needed.
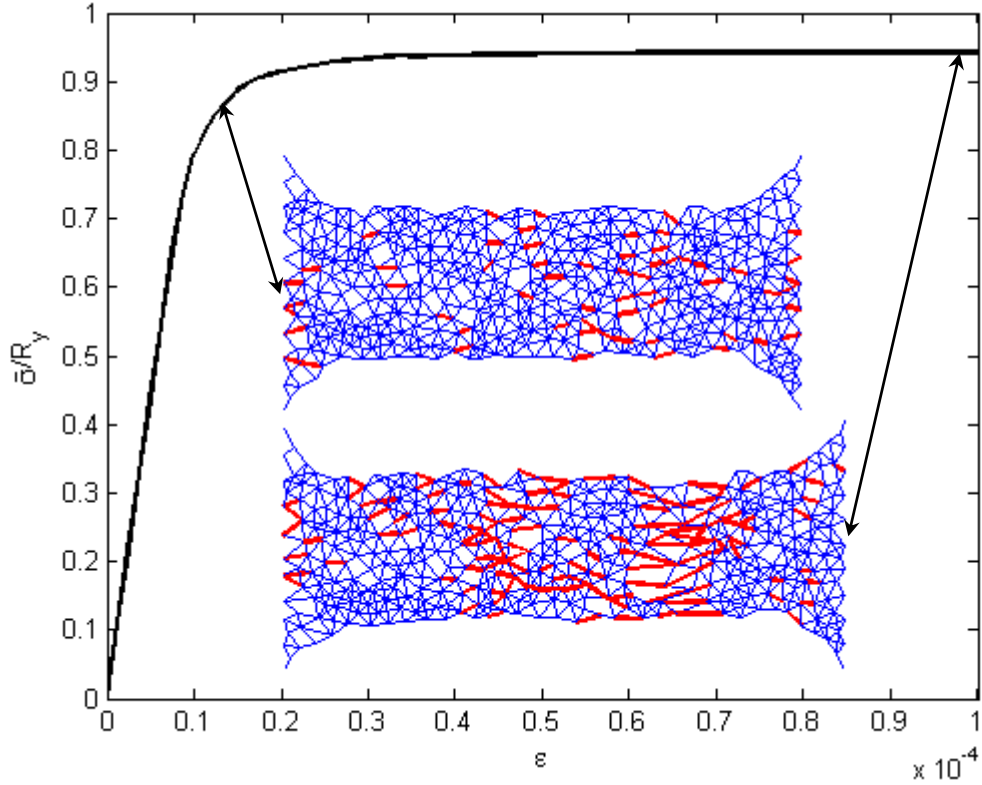
6.2.1 Plastic truss elements

Material of bars is considered to be perfectly elasto-plastic; see *Fig. 15*.The plastic limit is considered only in tension and characterized by the value of maximal uniaxial yield stress R_y. Elastic stiffness E_t and the area of bar cross-section A_t are the same as for elastic computation.

6.2.2 Uniform tension test of an example with plastic truss elements

An example formed from randomly generated particles with $R_P = 0.5$ connected by plastic truss elements is submitted to the uniform tension test. The dimensions of this example are 20x10. In addition, a significant narrow region is realized in the middle, see *Fig. 16*, to avoid a high number of truss elements in plastic state starting from the loaded particles along the vertical boundaries.

Fig. 16 Stress-strain diagram (black) of discrete particle model with plastic truss elements. Two examples of deformed truss elements (blue) with marked truss elements in plastic state (red) in different loading steps.

Material parameters are the following:

$$E_t = 1000, \qquad A_t = R_P, \qquad R_y = 0.01. \qquad (55)$$

The specific physical units are not used but one can consider MPa and mm. In 2D, all quantities are relative to the thickness of the specimen hence the area has the same unit as the length.

Equivalent strain ε is evaluated as

38

$$\varepsilon = \frac{u_x}{L_1} \tag{56}$$

where u_x is prescribed displacement in the loading (horizontal) direction and $L_1 = 20$ is the length of the specimen in this direction.

Equivalent stress $\bar{\sigma}$ is evaluated as

$$\bar{\sigma} = \frac{\sum F_i}{L_2 R_y} \tag{57}$$

where $\sum F_i$ is sum of all reaction on loaded side and $L_2 = 6$ is the width in the narrow region.

Stress-strain diagram of above defined equivalent values is depicted in *Fig. 16*. It can be observed that initial response is linear, as long as all bars remain in an elastic state. When some bars (mainly oriented in loading direction) get into the plastic state the linearity is lost. During next loading, the number of bars in plastic state is still increasing and the response is less and less stiff until plastic mechanism is formed; see examples in *Fig. 16*.

6.2.3 Microplane model

The description of the 2D material with plastic properties is based on the idea of microplanes. The definition of such models can be found in chapter 25 in the book [12]. The essential idea of microplane models is to characterize the constitutive law in terms of stress and strain vectors instead of second-order tensors. The relation between the stress and strain vectors is used on planes with various orientations, so-called microplanes. The macroscopic stress and strain tensors are obtained by a summation of all these vectors under the assumption of static or kinematic constraint. All possible spatial orientations of microplanes are considered. The orientation of each microplane is defined by its unit normal $\boldsymbol{n}$. In our case the kinematic constraint is used. Then the strain vector ε^n on the microplane is the projection of strain tensor $\boldsymbol{\varepsilon}$.

$$\varepsilon_i^n = \varepsilon_{ij} n_j. \tag{58}$$

Then the normal strain on the microplane is

$$\varepsilon_N = n_i \varepsilon_i^n = n_i \varepsilon_{ij} n_j = N_{ij} \varepsilon_{ij} \tag{59}$$

where $N_{ij} = n_i n_j$.

The microplane model from [2] with only the normal strain on microplanes is used. The shear strain on microplanes is not considered.

In 2D, all possible orientations of normal microplane vectors form a unit semi-circle and each microplane can be defined by an angle $\alpha \in \langle -\frac{\pi}{2}, \frac{\pi}{2} \rangle$; see *Fig. 17*. The microplanes with $\alpha = -\frac{\pi}{2}$ and $\alpha = \frac{\pi}{2}$ are equivalent.
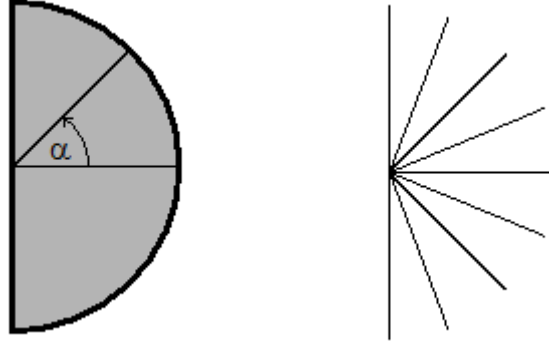
Fig. 17 All possible orientations of microplane normal vectors (left). Example of finite number of microplanes used in numerical integration (right).

The components of normal vectors are

$$n_1 = \cos \alpha, \tag{60}$$
$$n_2 = \sin \alpha.$$

Each microplane can be in elastic or plastic state. For monotonous loading process, we can assume that if one microplane gets in to the plastic state then this microplane is never unloaded back to the elastic state. Then the conditions are the following:

The microplane is in elastic state if

$$\varepsilon_N E_N < S_0 \tag{61}$$

or in plastic state if

$$\varepsilon_N E_N \geq S_0 \tag{62}$$

where E_N it Young's modulus on the micro level and S_0 is maximal yield stress. It is assumed that the microplanes can only get into the plastic state in tension and not in compression.

Then the stress σ_N on the microplane is defined as

$$\sigma_N = \varepsilon_N E_N \quad \text{for microplanes in elastic state}$$
$$\sigma_N = S_0 \qquad \text{for microplanes in plastic state}$$
(63)

For the value of macroscopic stress, the integral formula is obtained from the weak form of the equilibrium of the stresses on the micro and macro levels

$$\sigma_{ij} = \frac{2}{\pi} \int_{\Omega} \sigma_N N_{ij} \, d\Omega$$
(64)

where the integration is taken over all possible orientation of microplanes represented by the surface of unit semicircle. The factor $\frac{2}{\pi}$ is the inverse value of the volume of the integration domain in 2D.

In numerical computation, the Gaussian integration is used to approximate the integral formula. Integration is replaced by the summation with tabular weights and only a finite number of microplanes is used; see *Fig. 17*.

6.2.4 Semi-analytic study of 2D microplane model

If macroscopic stress tensor is given in each time step then the macroscopic response of microplane element is obtained by using kinematic constraint (59), yield conditions (61)-(63) and macroscopic stress, the integral formula (64).

But now, let us assume that the 2D microplane element is loaded by fixed rate of principal stresses

$$\sigma_{22} = k_\sigma \, \sigma_{11}$$
(65)

where $k_\sigma \in \langle 0,1 \rangle$ is given stress ratio.

The simulation is controlled by the linearly increasing strain ε_{11}. Then the ratio of principal strains is not constant during the plastic process. The second component of principal strain can be written as

$$\varepsilon_{22} = k_\varepsilon \, \varepsilon_{11}$$
(66)

where k_ε it unknown strain ratio changing during the loading process.

Then the normal strain on the microplane can be expressed from kinematic constraint (59) as

$$\varepsilon_N = \varepsilon_{11} \cos^2(\alpha) + k_\varepsilon \, \varepsilon_{11} \sin^2(\alpha).$$
(67)

41

Then the yield condition is

$$\cos^2(\alpha) + k_\varepsilon \, \sin^2(\alpha) \geq \frac{S_0}{E_N \varepsilon_{11}}. \tag{68}$$

For a current load level, represented by ε_{11}, this condition divides the integration domain into elastic and plastic part; see *Fig. 18*. The microplanes with $\alpha \in \langle -\alpha_c, \alpha_c \rangle$ get into the plastic state and the rest of integration domain remain elastic. It is also visible that the firts microplane that gets into the plastic state has the normal angle $\alpha = 0$, which corresponds to the microplane perpendicular to the direction of loading.
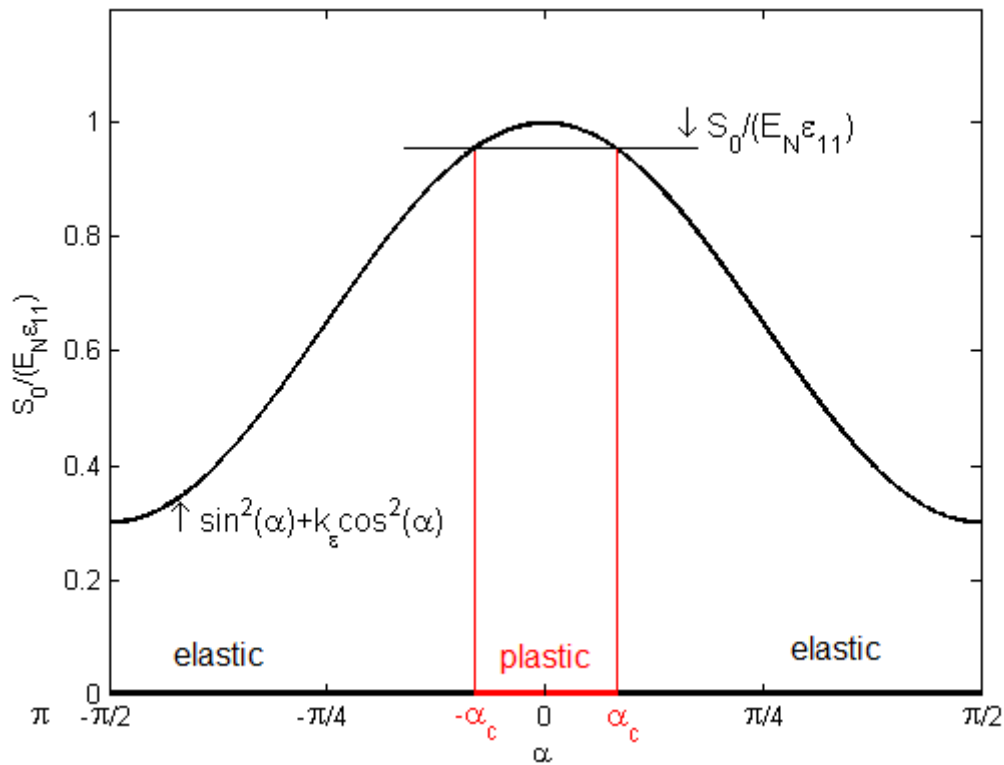
Fig. 18 Example of yield condition dividing integration domain into elastic part (black) and plastic part (red).

The symmetry of yield condition function results in the symmetry of integration domains. The integrated functions that appear in the integral formula (64) for σ_{ij} are either all even if $i = j$ ($\sin^2 \alpha$, $\cos^2 \alpha$, $\sin^4 \alpha$, $\cos^4 \alpha$, $\sin^2 \alpha \cos^2 \alpha$) or all odd if $i \neq j$ ($\sin \alpha \cos \alpha$, $\sin^3 \alpha \cos \alpha$, $\sin \alpha \cos^3 \alpha$). Therefore only one half of integration domain can be considered, because the integral from an even function taken over a symmetric interval is equal to the double integral taken over one half of the symmetric domain.

The half-length integration domain can be divided by the critical angle α_c into elastic and plastic part, see *Fig. 18*, defined as

$$\Omega_{el} = \langle \alpha_c, \frac{\pi}{2} \rangle,$$
$$\Omega_{pl} = \langle 0, \alpha_c \rangle. \tag{69}$$

This symmetry also result in no shear stress, if the element is loaded by the combination of principal stresses, because the integral from an odd function taken over a symmetric interval is always zero and it automatically ensures that

$$\sigma_{12} = 0. \tag{70}$$

The nonzero components of macroscopic stress tensor with consideration of new integration domains are

$$\sigma_{11} = \frac{4}{\pi} \int_0^{\alpha_c} S_0 \cos^2(\alpha) \, d\alpha + \frac{4}{\pi} \int_{\alpha_c}^{\pi/2} \left(\varepsilon_{11} \cos^4(\alpha) + k_\varepsilon(t)\varepsilon_{11} \cos^2(\alpha) \sin^2(\alpha) \right) d\alpha \tag{71}$$

and

$$\sigma_{22} = \frac{4}{\pi} \int_0^{\alpha_c} S_0 \sin^2(\alpha) \, d\alpha + \frac{4}{\pi} \int_{\alpha_c}^{\pi/2} \left(\varepsilon_{11} \cos^2(\alpha) \sin^2(\alpha) + k_\varepsilon(t)\varepsilon_{11} \sin^4(\alpha) \right) d\alpha. \tag{72}$$

In this case, the critical angle α_c depends on the unknown strain ratio k_ε and can be expressed from the yield condition as

$$\alpha_c(k_\varepsilon) = \arcsin \sqrt{\frac{\frac{S_0}{E_N \varepsilon_{11}} - 1}{k_\varepsilon - 1}}. \tag{73}$$

Then σ_{11} and σ_{22} are functions of k_ε. After integration we obtain

$$\sigma_{11}(k_\varepsilon) = \frac{2S_0}{\pi}(\alpha_c + \sin \alpha_c \cos \alpha_c) +$$
$$+ \frac{E_N \varepsilon_{11}}{8\pi} \left(6\pi - 12\alpha_c - 8\sin(2\alpha_c) - \sin(4\alpha_c) + k_\varepsilon(2\pi - 4\alpha_c - \sin(4\alpha_c)) \right) \tag{74}$$

and

$$\sigma_{22}(k_\varepsilon) = \frac{2S_0}{\pi}(\alpha_c - \sin \alpha_c \cos \alpha_c) +$$
$$+ \frac{E_N \varepsilon_{11}}{8\pi} \left(2\pi - 4\alpha_c - \sin(4\alpha_c) + k_\varepsilon(6\pi - 12\alpha_c + 8\sin(2\alpha_c) - \sin(4\alpha_c)) \right) \tag{75}$$

Finally, the unknown ratio k_ε is obtained as a solution of

$$\frac{\sigma_{22}(k_\varepsilon)}{\sigma_{11}(k_\varepsilon)} - k_\sigma = 0. \tag{76}$$

The final solution can only be considered as semi-analytic because the equation (76) must be solved numerically in all loading steps with the condition

$$\alpha_c(k_\varepsilon) = \arcsin\sqrt{\frac{\frac{S_0}{E_N\varepsilon_{11}} - 1}{k_\varepsilon - 1}} \in \langle 0, \frac{\pi}{2} \rangle. \tag{77}$$

Newton-Raphson method is used to find the root of eq. (76). If the first step is solved, the next solution step is very fast because the wanted k_ε changes continuously and the value from the previous step is used as a starting point in each next step.

The semi-analytic solution is compared with a numerical computation using a Gaussian integration with finite number of microplanes.

6.2.5 Uniform tension test of microplane element

A comparative example is uniform tension test where the prescribed stress ratio is

$$k_\sigma = 0. \tag{78}$$

One triangular element is loaded by the strain ε_{11} so that only σ_{11} appears. The semi-analytic solution of searched strain ratio K_ε and the critical angle α_c in all loading steps are plotted in *Fig. 19* and *Fig. 20*. Theoretically, the value of K_ε resp. α_c goes to 0 resp. $\pi/2$ if loading strain ε_{11} goes to the infinity. It corresponds to the fact that in the limit plastic state all microplanes are yielding. It can be seen that the approach to these values is slow. In real simulation, some microplanes still remain in elastic state and some transversal contraction can be observed even if an arbitrarily high finite value of prescribed strain is reached.

The stress-strain diagrams are compared in *Fig. 21*. The solution obtained by the semi-analytic procedure is plotted by thick black curve. The solutions obtained by computation in OOFEM using Gaussian integration with 5 (green), 10 (blue) and 100 (red) microplanes are depicted in the same plot. The solution with 100 microplanes is almost perfectly identical with semi-analytic solution and can be considered as exact. The solutions with low number of microplanes are visibly piecewise linear because the plastic
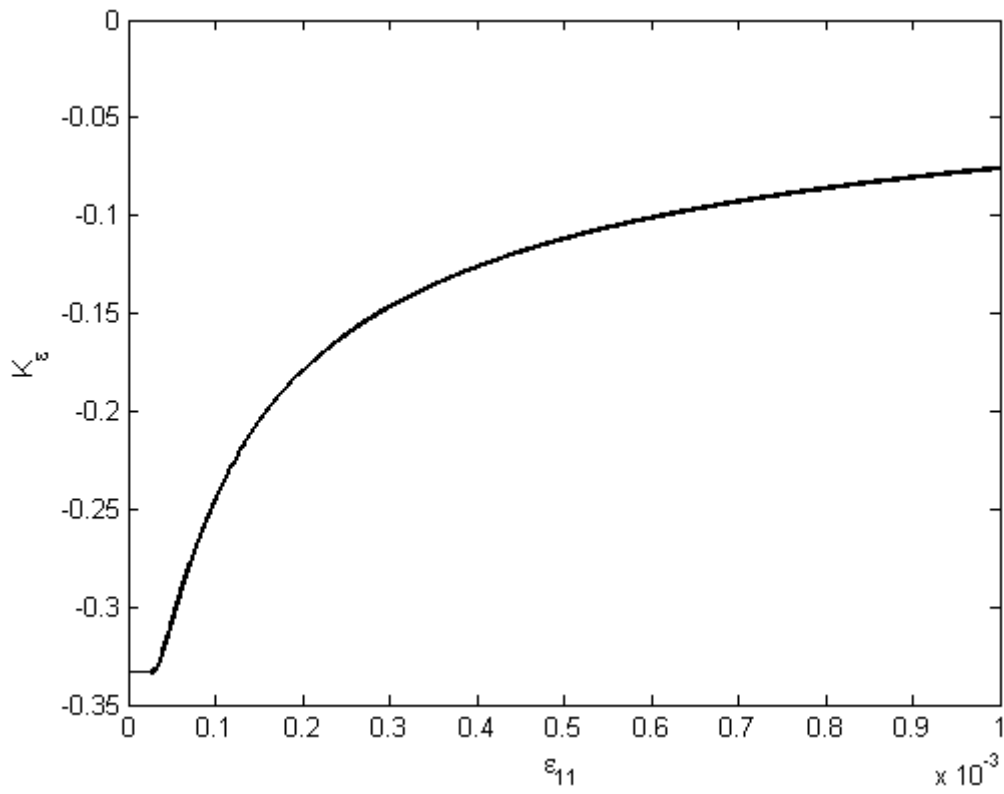
Fig. 19 Dependence of strain ratio K_ε on the prescribed strain ε_{11}.
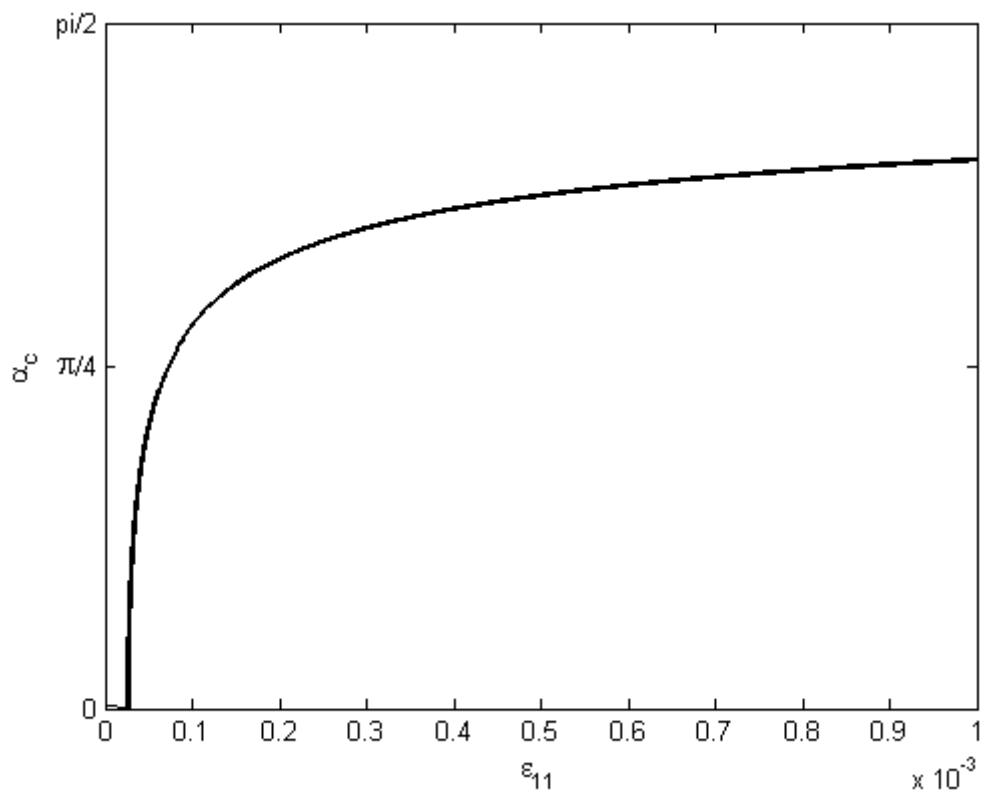

Fig. 20 Dependence of the critical angle α_c on the prescribed strain ε_{11}.

domain cannot expand continuously between angles of two neighboring microplanes. But the solution for 10 microplanes can still be considered as quite a good approximation because the value of final stress approaches to the maximal yield stress S_0. But this is not true for the solution with 5 microplanes, where only 3 of 5 microplanes can get into the plastic state and therefore this low number of microplanes cannot capture the final value of yield stress exactly.
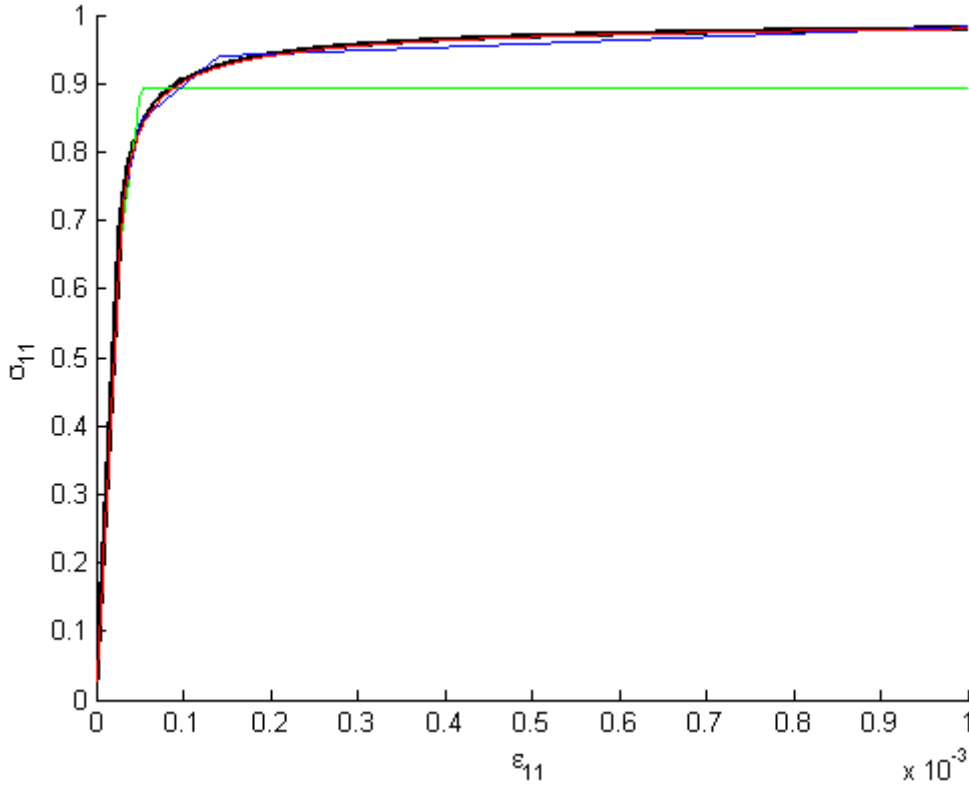

Fig. 21 Stress-strain diagram of microplane element in uniform tension test obtained by semi-analytic solution (black) and by numerical integration using 5(green), 10 (blue) and 100 (red) microplanes.

6.2.6 Comparison of plastic particle model and microplane model

The shape of stress-strain diagram is the same for the microplane 2D element and for the particle model with plastic links; compare *Fig. 16* and *Fig. 21*. For both, there are two significant points. The first one is the beginning of plastic process that corresponds to the stress state when the first microplane resp. bar gets into the plastic state. And the second one is the reach of the final yield stress when all microplanes are in plastic state or the trusses form a plastic mechanism.

For microplane model, these points can be investigated analytically. From eq. (68) for $\alpha = 0$, the first point corresponds to the moment when the maximal principal strain reaches the critical value S_0/E_N. And from eq. (75) and (76) for $\alpha = \pi/2$, the second point corresponds to the moment when one of the normal stresses reaches the critical value S_0. Graphical representation of initial and final yield surfaces in the plane of principal stresses is depicted in *Fig. 22*. It can be observed, that for the loading trajectory with $k_\sigma = 1.0$ the initial and final point are the same. This type of loading corresponds to the increasing positive hydrostatic stress and in this special case, all microplanes get into the plastic state at the same time.
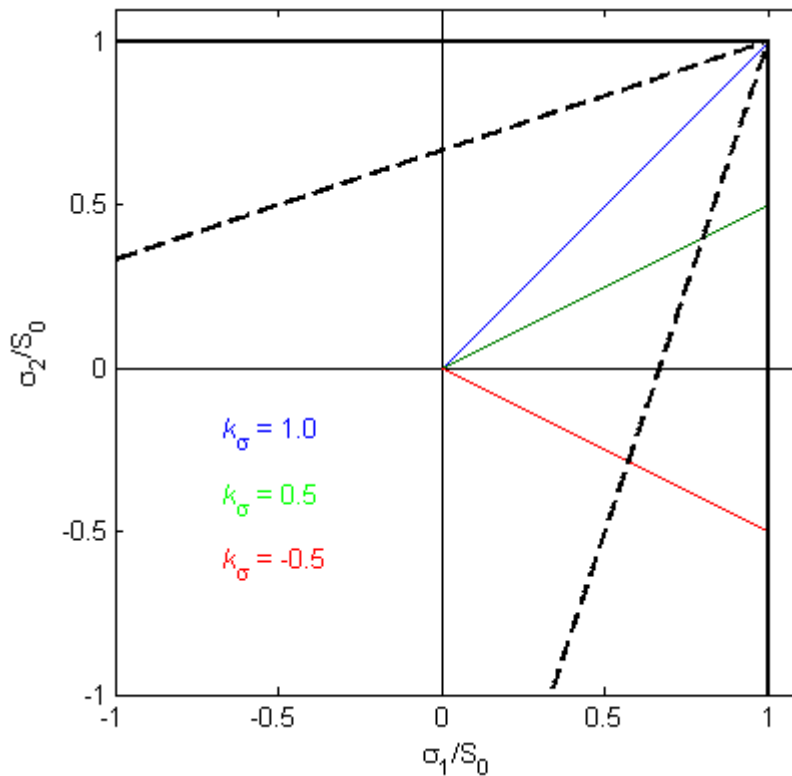
Fig. 22 Initial yield surface (dashed black) final yield surface (solid black) and examples of loading trajectories for $k_\sigma = 1.0$ (blue), $k_\sigma = 0.5$ (green) and $k_\sigma = -0.5$ (red).

For particle model, these points cannot be predicted exactly because they depend on the random position of particles. But the microplane model is equivalent to the particle modes with the uniform distribution of truss elements. Therefore one can expect that these points of both models will correspond if the particles are well distributed. Thus particle and microplane model can be considered as equivalent if they have the same value of the initial elastic stiffness and the final yield stress. The properties of microplane models are described by E_N and S_0, by contrast the description of particle

model is realized with E_t and R_y. To fit equivalent microplane and particle model, the relations between these two sets of parameters are needed. These relations can be obtained by comparison of virtual work of microplane element and the set of truss elements. The relation between Young's moduli E_N on the microplane and macro level can be written as

$$E_N = \frac{\pi}{2} E \qquad (79)$$

where macroscopic Young's modulus E is evaluated from E_t by one of the homogenization procedures for isotropic material described in 4.3.3 and 4.3.4.

The relation between maximal yield values S_0 on microplane and R_y on bar level is the following

$$S_0 = \frac{1}{V} \sum_{i=1}^{N_t} L_i R_{y_i} A_i {n_1}_i{}^2 \qquad (80)$$

where A is the cross-section area and L is the length of the link. V is the volume of microplane element, N_t is the number of truss elements in this element and $n_{1_i} = \cos \alpha_i$ is the first component of the unit normal of the link.

Simulations of an example with plastic links and equivalent microplane model are presented in section 7.6.

6.3 Other types of materials

Both elastic and inelastic material models have been presented. So far, inelastic model deals only with plasticity but can be easily extended to other types of materials.

6.3.1 Extension of particle model

The material properties of particle model are mainly given by the link connection, which is realized by 1D truss elements. Therefore a required extension of particle model can be realized using a suitable material of bars (truss elements) with a required constitutive law.

Another way how to change material properties of the particle model is to change the distribution of particles. But one should keep in mind that the distribution of particles represents, at the first, the microstructure of random material. Therefore it is better not to realize the representation of a different material type by the change of par-

ticle distribution if there is no reason resulting from the change of material microstructure.

6.3.2 Extension of continuum models

The extension of continuum models is realized via microplane model. The most important advantage of models based on the idea of microplane is the definition of the constitutive law on level of the microplane. Therefore these types of material models can be easily extended. Quite a number of material phenomena such as plastic softening, hardening, damage etc. can be simply defined on the microplane, and macroscopic response is obtained using a corresponding integration formula. The definition of material properties on the level of microplanes provides a good physical agreement with the original discrete model, where these properties are also represented by link connections among particles.

So far the microplane model has been considered as isotropic but also the anisotropy properties can be simply added by consideration of a different number of microplanes in different directions. This is realized by adding a corresponding weight function, which provides a required distribution of microplanes, into the integral formula.

7 Results

7.1 Direct tension example

The first tested example is a square with dimensions 10x10 submitted to the direct tension. Particles are generated with parameter $R_P = 0.25$. The material is considered as isotropic and the circle rule is used, $R_t = 1.9R_P$. Four sets of particles are generated and average number of particles in one set is $N_P = 1100$. Along both vertical sides, 21 particles are placed periodically with prescribed boundary conditions. The particles on the left side are fixed in both directions and particles on the right side have prescribed displacement $u = 0.002$ in horizontal direction and at the same time they are fixed in vertical direction. An example of one set of these particles is depicted in *Fig. 23*. Strain distribution for all sets of particles is computed by M1. Theoretically, the strain should be constant in the middle part of solved domain but the fluctuation caused by random position of particles can be observed; see *Fig. 24*. The error is evaluated for all sets of particles to eliminate the influence of this randomness.
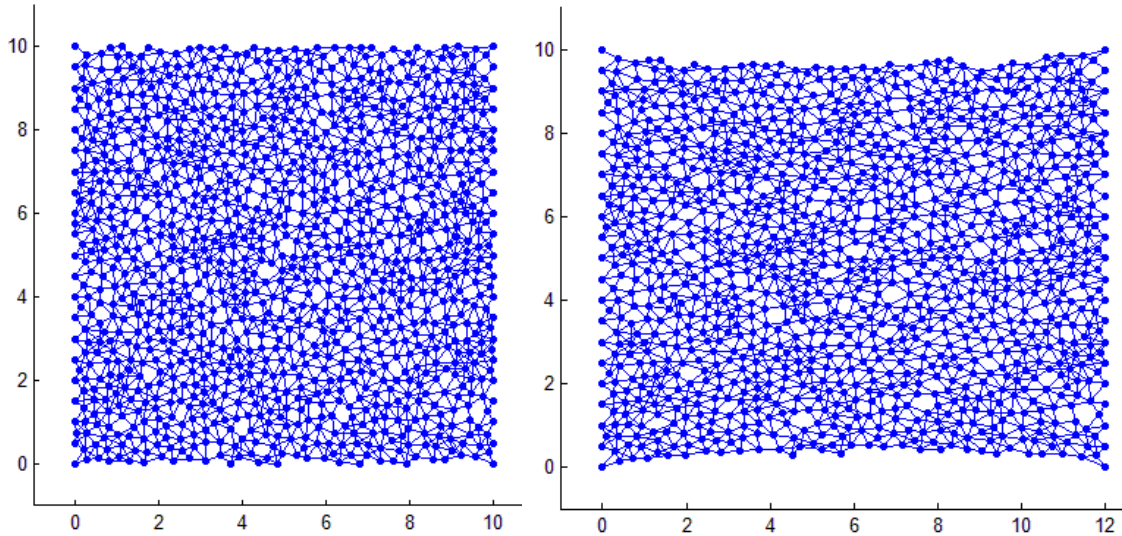
Fig. 23 Example of particles connected by links before (left) and after deformation (right). Deformation scale = 1000.

7.1.1 Simple mesh

At the first, only a simple interpolation mesh is used; see *Fig. 25*. Each set of particles (a)-(d) is computed by each simplifying model M1-M4. The results are summarized in *Table 1*. Computed time effort consists of both the time consumed by
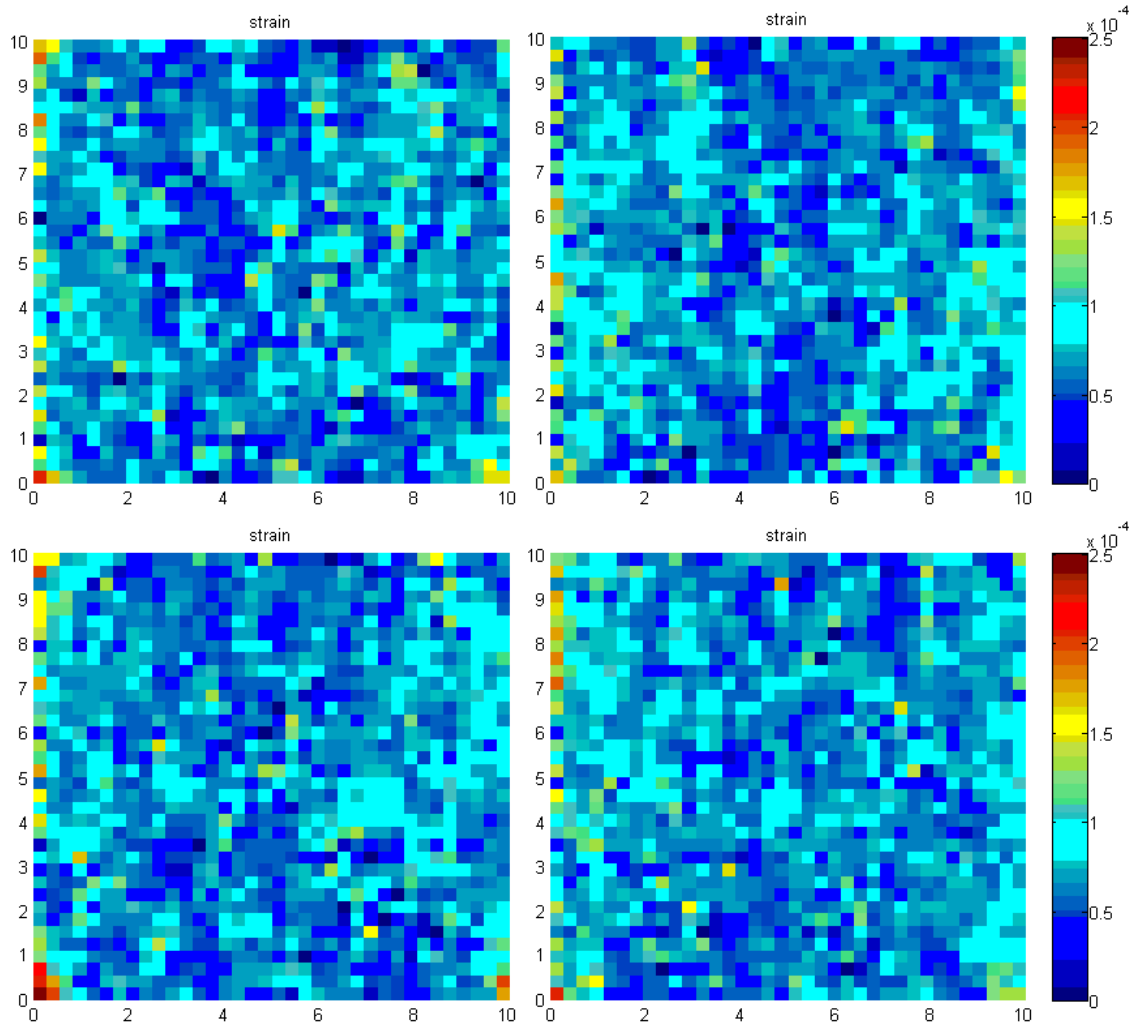
Fig. 24 Strain distribution for all sets of particles computed by M1.
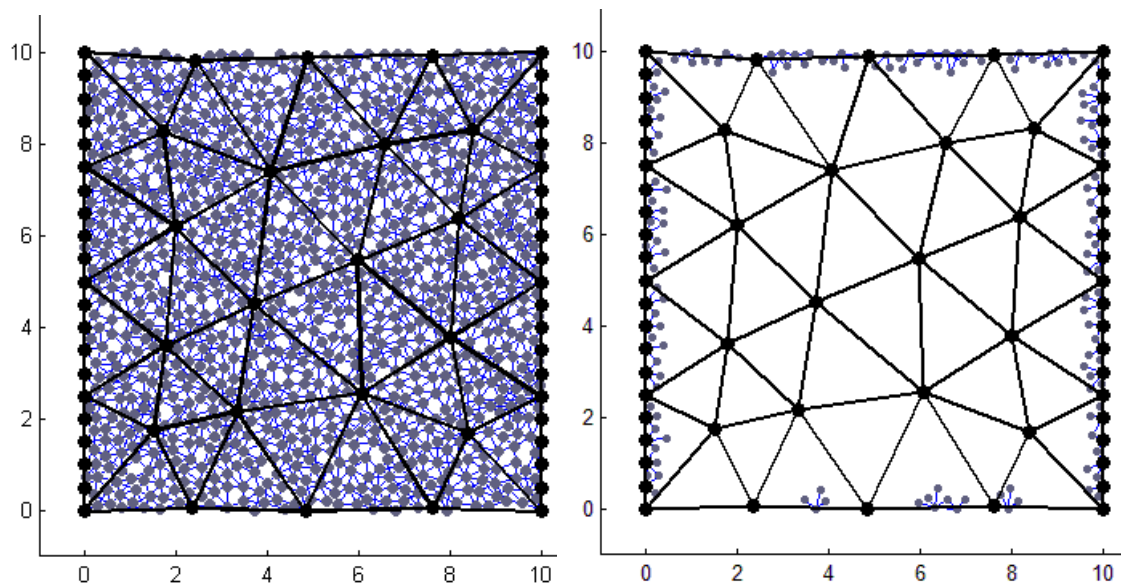

Fig. 25 Interpolation mesh with all hanging nodes(grey) used by M2 (left) and only with

some remaining hanging nodes used by M3 and M4 (right).

preparing input data of simplified model and the time of computation in OOFEM. Time consumed by generating input geometry (particles, links and elements) is not included. Global error indicator is evaluated according (52). The average of all sets of particles is computed in the last row. Absolute stress error of M2-M4 with respect to the M1 is evaluated and divided by the characteristic deformation 0.0002. This error is higher near the boundary, where the fixed boundary conditions are applied; see *Fig. 26*. It is because single fixed particles tend to be pulled out. Interpolation elements are not able to capture this behavior. That is why the region of high interest is realized along the boundary in the next step.
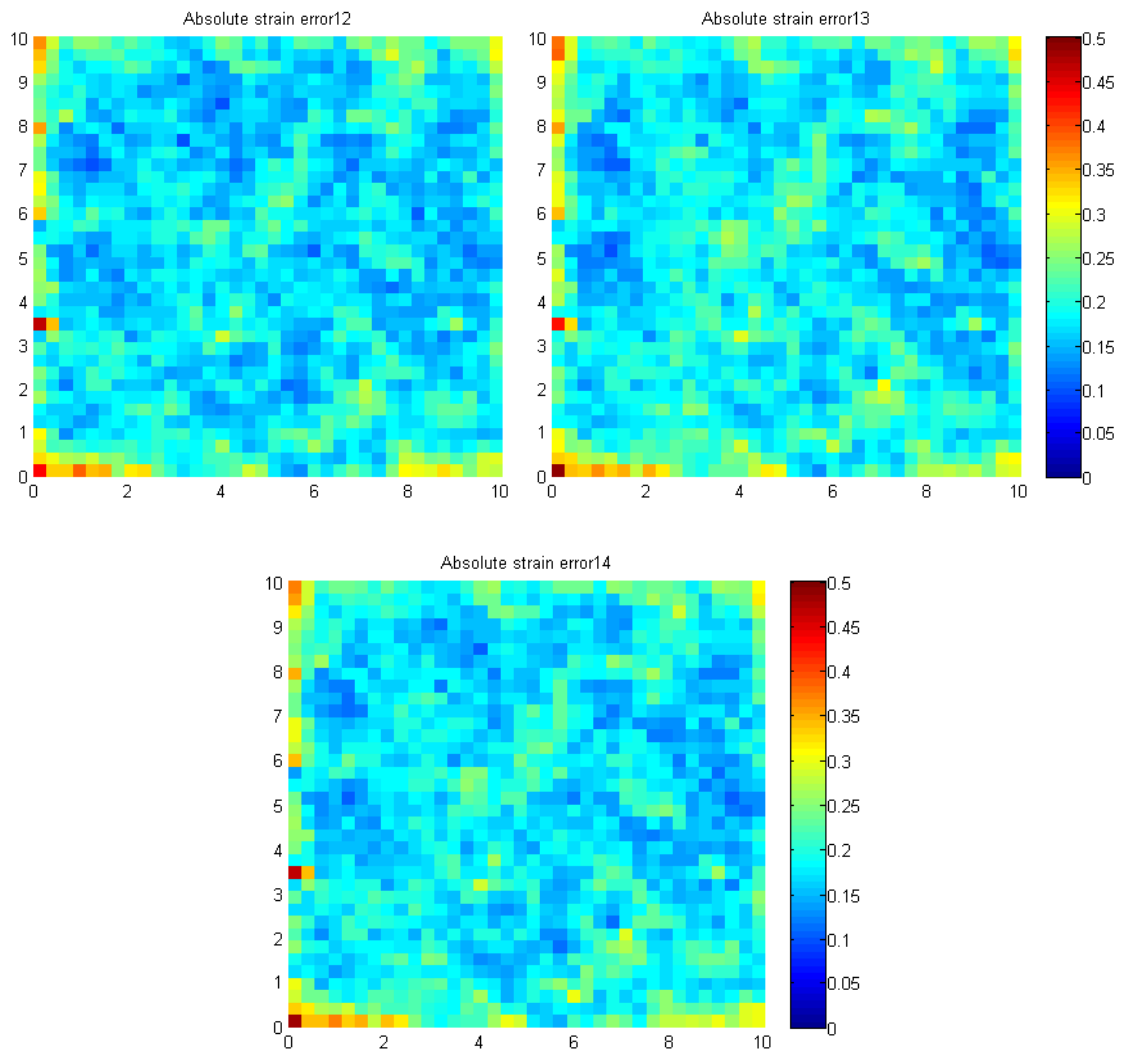
Fig. 26 Absolute strain error divided by characteristic deformation for M2 (left),
M3 (right) and M4 (bottom).

	Time effort (s)				Strain error indicator (10^{-3})		
	M1	M2	M3	M4	M2	M3	M4
(a)	4.27	5.48	0.68	1.24	2.71	2.78	2.76
(b)	4.29	5.79	0.63	1.05	2.67	2.78	2.73
(c)	3.99	5.49	0.60	1.02	2.70	2.81	2.76
(d)	4.30	5.46	0.70	1.34	2.74	2.83	2.78
Avg	**4.21**	**5.55**	**0.65**	**1.16**	**2.71**	**2.80**	**2.76**

Table 1. Comparison of time effort and error indicator in direct tension.

It is noteworthy that model M2 with hanging nodes is not faster than exact M1. Even if the number of independent DOF is reduced, current numerical implementation is unable to compute M2 faster. It is because a renumbering algorithm that makes direct solver faster works fine for M1 matrix but not for M2. Also, the structure of matrix with hanging nodes is not convenient for iterative solvers. For some examples with really simple interpolation mesh and with at least ten thousand of particles, M2 is faster than M1. But to be effective in general, suitable renumbering algorithm needs to be developed.

7.1.2 Selection of region of high interest

The problematic parts along the boundaries are selected as the thin regions of high interest and all particles are considered as repnodes here, but the interpolation mesh is not affected according to MESH1 procedure; see *Fig. 27 (bottom left)*. The results for this mesh are summarized in *Table 2*. The decrease of error indicators is less than 10%. The error is reduced along the boundary, but some high error still remains in the corners; see *Fig. 27*. This indicates that more repnodes are needed to represent realistic behavior.

	Time effort (s)				Strain error indicator (10^{-3})		
	M1	M2	M3	M4	M2	M3	M4
(a)	4.52	5.54	1.05	1.53	2.53	2.77	2.58
(b)	4.12	6.05	1.32	1.37	2.43	2.78	2.49
(c)	5.24	5.70	1.02	1.40	2.48	2.80	2.55
(d)	4.41	5.61	1.09	1.71	2.52	2.81	2.57
Avg	**4.57**	**5.73**	**1.12**	**1.50**	**2.49**	**2.79**	**2.55**

Table 2. Comparison of time effort and error indicator in direct tension with added repnodes.
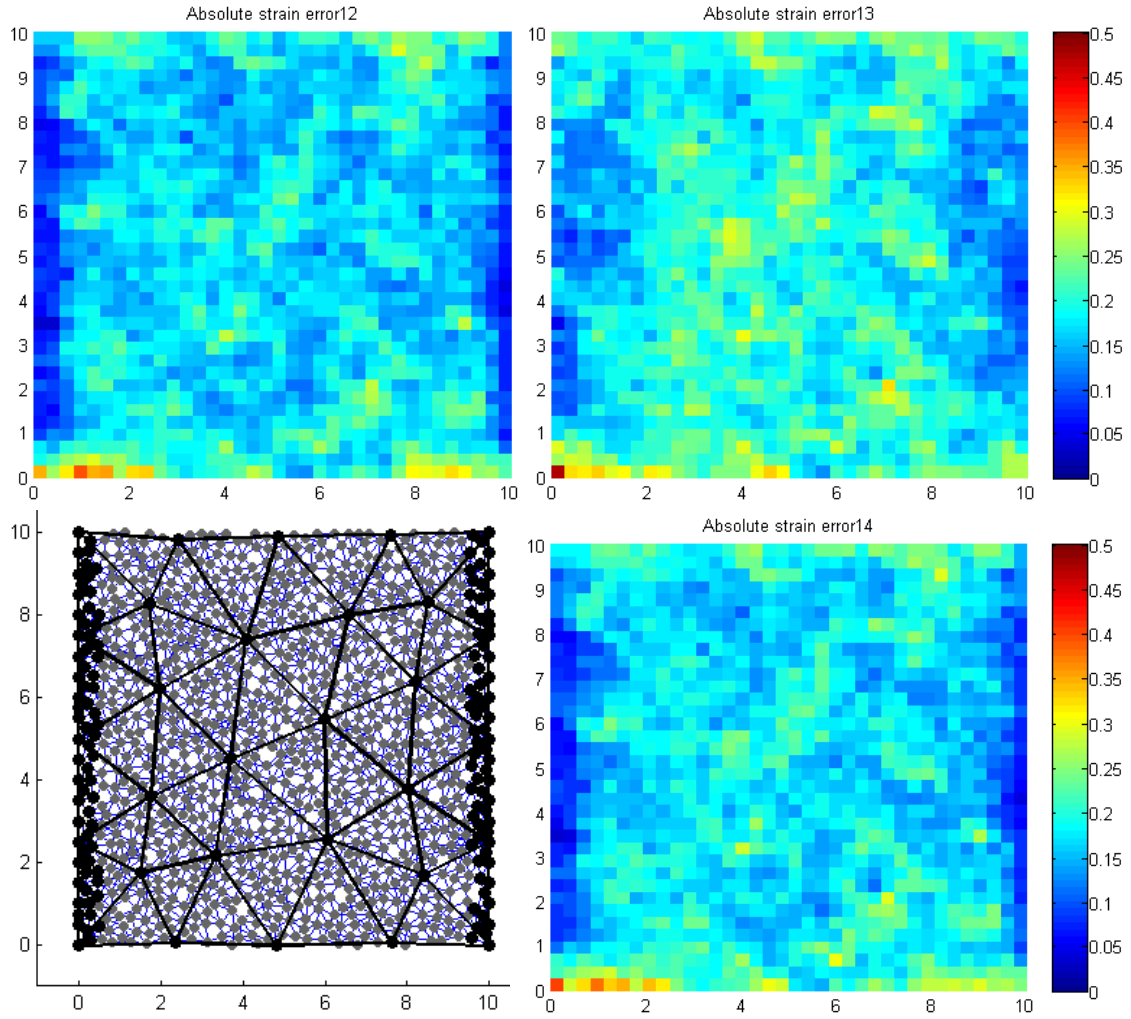
Fig. 27 Absolute strain error divided by characteristic deformation for M2 (top left), M3 (top right) and M4 (bottom right) computed with added repnodes (bottom left).

7.2 Three-point bending test

The next tested example is a beam with the dimensions 40x10 tested in a three-point bending test. Particles are generated with distance parameter $R_P = 0.5$. The material is considered as isotropic and the circle rule is used, $R_t = 1.9R_P$. Four sets of particles are generated and average number of particle in one set is $N_P = 1107$. Boundary conditions are realized using six regular nodes. The test is controlled by the displacement $u = 0.002$. *Fig. 28* shows example of generated particles and links. The fluctuation of the strain is not as significant as in the direct tension test and the distribution of strain is given mainly by the geometry of the test; see *Fig. 29*.
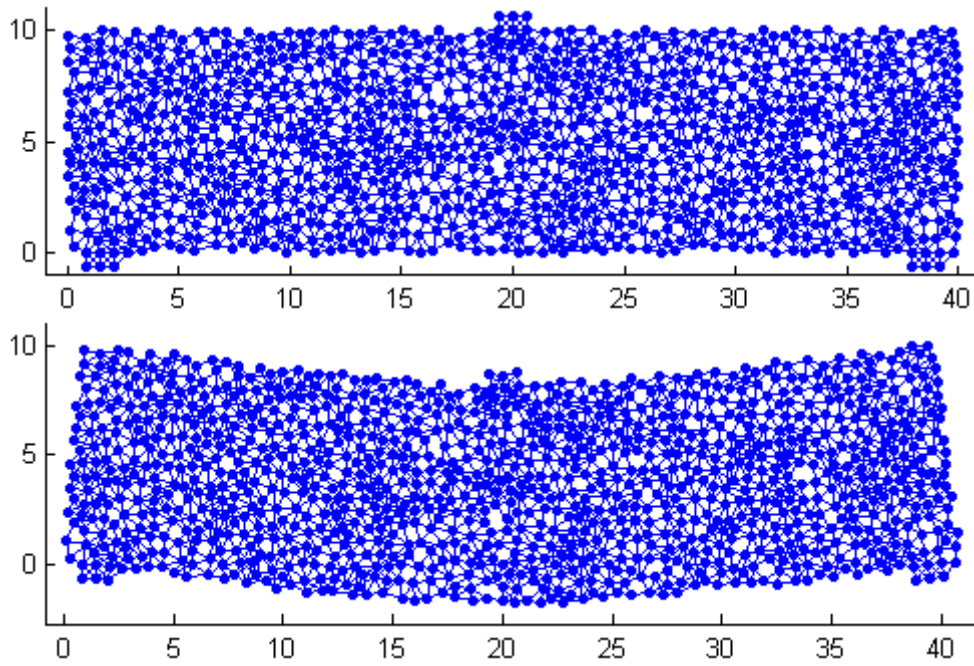
Fig. 28 Example of particles connected by links before (top) and after deformation (bottom). Deformation scale = 1000.
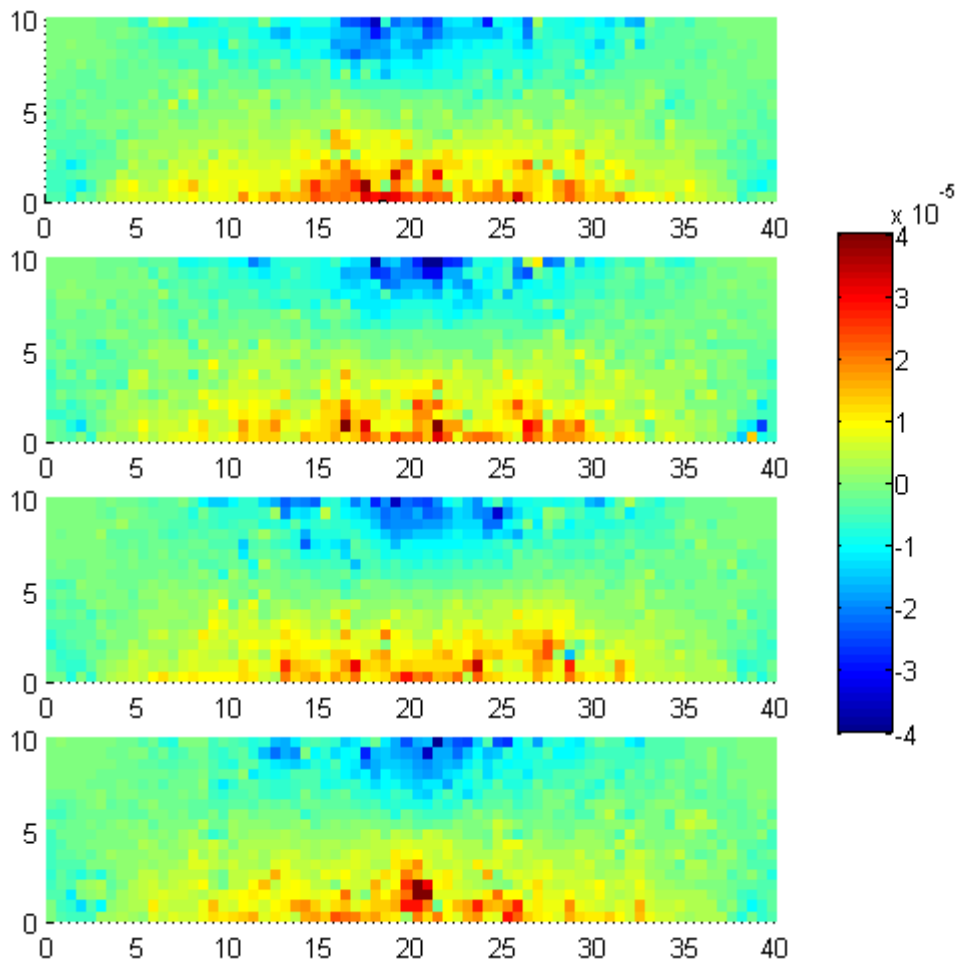

Fig. 29 Strain distribution for all sets of particles computed by M1.

7.2.1   Simple mesh

If the simple mesh from *Fig. 30* is used, then the error in the middle area is significant; see *Fig. 31*. Results are summarized in *Table 3*. Noteworthy is that the error indicator for set of particles marked as (b) is significantly higher than for other sets. It is caused by a small vacancy that occurred in the structure of (b) particles near the right support. This event cannot be captured by linear interpolation elements and repnodes are needed to achieve better description.
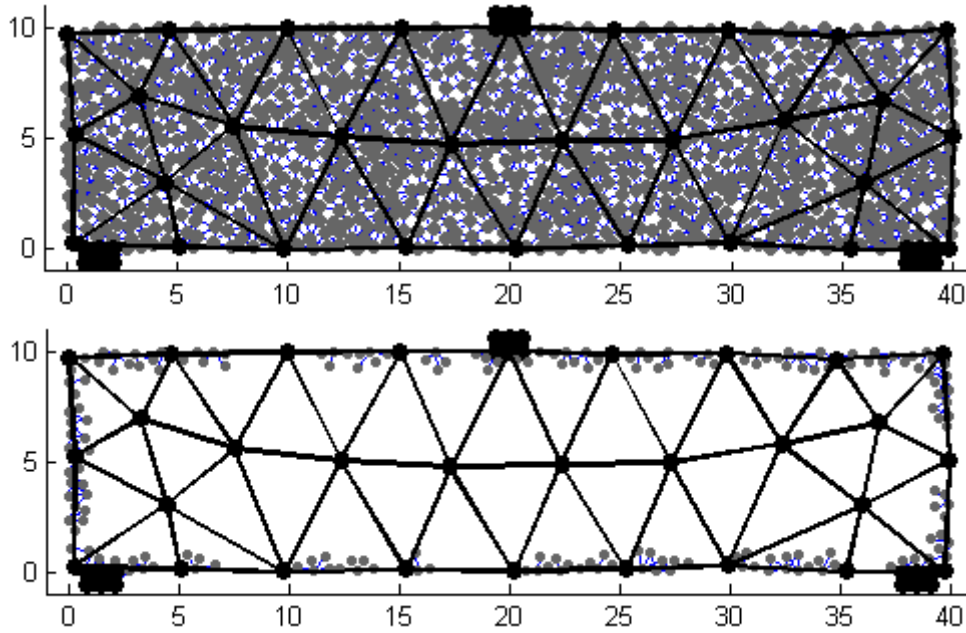
Fig. 30 Interpolation mesh with all hanging nodes(grey) used by M2 (left) and only with some remaining used by M3 and M4 (right).

	Time effort (s)				Error indicator (10^{-4})		
	M1	M2	M3	M4	M2	M3	M4
(a)	4.70	6.36	0.85	1.34	5.8575	6.0125	5.9900
(b)	4.49	6.05	0.94	1.34	8.9761	9.2865	9.1957
(c)	4.47	6.27	0.78	1.24	6.0233	6.3616	6.3545
(d)	4.99	5.81	0.87	1.28	5.9599	6.0299	6.0008
Avg	**4.66**	**6.12**	**0.86**	**1.30**	**6.8318**	**7.0574**	**7.0148**

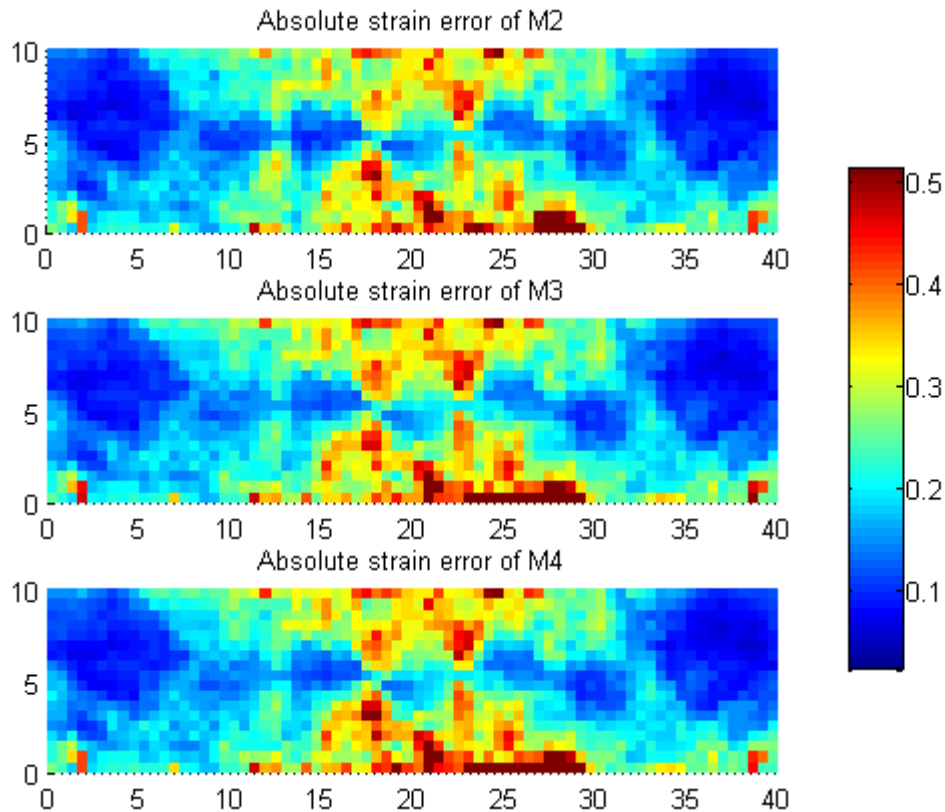*Table 3. Comparison of time effort and error indicator in bending test.*

Fig. 31 Absolute strain error divided by characteristic deformation.

7.2.2 Selection of region of high interest

The region of high interest is realized in the middle part, and repnodes are added; see *Fig. 33*. Results for this mesh are summarized in *Table 4*. For M2 and M3, the error is reduced significantly in terms of error indicator. The error indicator of M2 is reduced too, but it is two times higher than for M2 or M4, even if all three indicators are almost the same for the simple mesh. Problem is in the interface between repnodes and interpolation elements. In M3, the stiffness of large elements with repnodes inside (realized by MESH1 procedure) is overestimated. It is because 1D truss eelements connecting repnodes are evaluated explicitly, and at the same time, the stiffness of 2D is set the same as for other elements without repnodes. Thus it is better to use MESH2 procedure for M3 and generate smaller elements near the interface or eliminate this absence by using M4 instead of M3.

The error indicator of all models for set of particles (b) is still significantly higher than for other sets, and as well, the error near the supports can be observed; see *Fig. 32*.
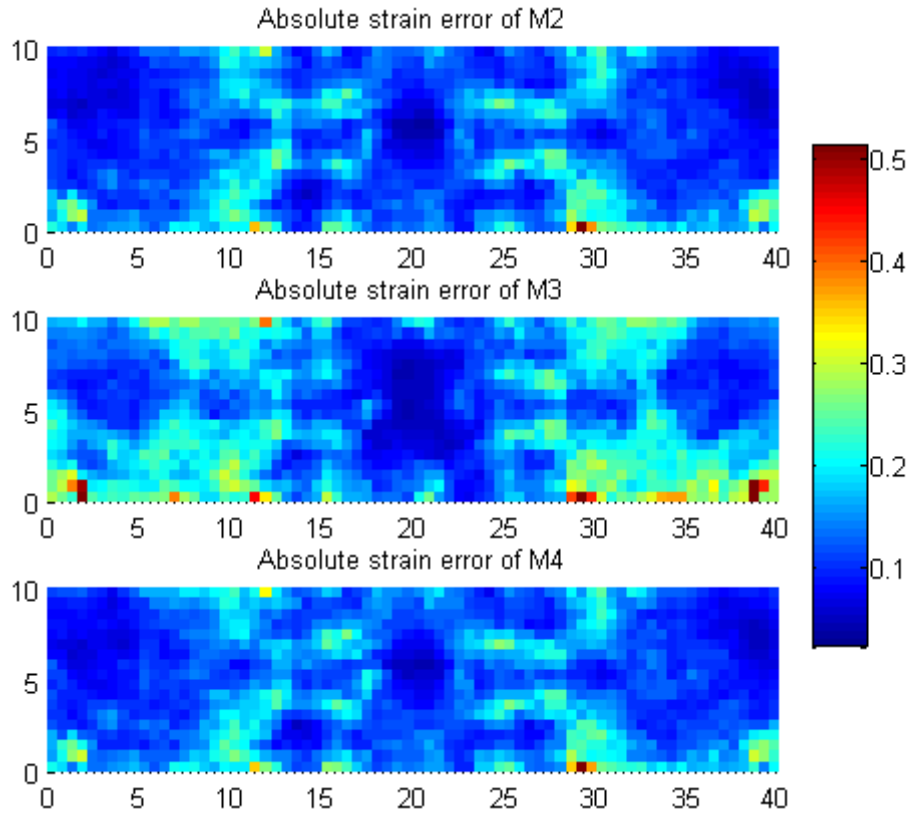
*Fig. 32 Absolute strain error computed with added repnodes and divided
by characteristic deformation.*

	Time effort (s)				Strain error indicator (10^{-4})		
	M1	M2	M3	M4	M2	M3	M4
(a)	5.45	6.22	2.68	3.35	3.3166	4.7318	3.4249
(b)	4.84	6.20	2.83	3.63	3.3121	4.7032	3.3226
(c)	4.96	5.94	2.59	2.85	3.6414	5.2364	3.9179
(d)	5.17	5.88	2.69	2.70	3.3045	4.8031	3.3166
Avg	**5.11**	**6.06**	**2.70**	**3.13**	**3.3937**	**4.8686**	**3.4955**

Table 4. Comparison of time effort and error indicator in bending test with added repnodes.
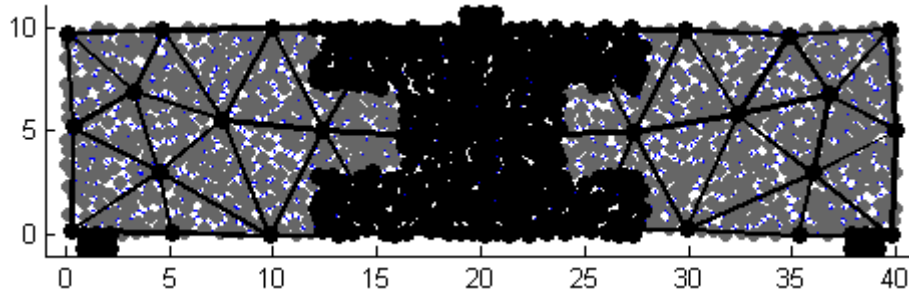
Fig. 33 Interpolation mesh with added repnodes

7.2.3 Second region of high interest

The second region of interest is realized to be able to capture exact behavior in the surrounding of supports, and furthermore, the size of interpolation elements is changed to one half; see *Fig. 34*. Results are summarized in *Table 5*. Again, the error indicators of M2 and M4 decrease much more significantly than for M3. Also the error near the supports vanishes for M2 and M4 only; see *Fig. 35*. M3 seems to be unsuitable for this mesh because it cannot capture the behavior of interface, even if the interpolation elements are smaller.
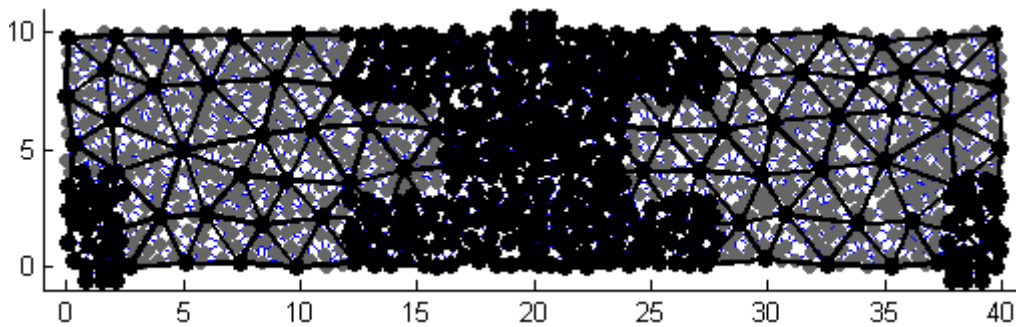

Fig. 34 Interpolation mesh with repnodes added in two regions of high interest.

	Time effort (s)				Strain error indicator (10^{-4})		
	M1	M2	M3	M4	M2	M3	M4
(a)	5.80	6.89	3.81	4.04	1.9225	3.3317	1.9662
(b)	5.54	6.62	3.43	4.55	2.1107	3.6208	2.1684
(c)	5.41	6.26	3.63	3.94	2.1218	3.6111	2.1746
(d)	5.92	7.60	3.48	4.17	2.1545	3.7403	2.2145
Avg	**5.67**	**6.84**	**3.59**	**4.18**	**2.0774**	**3.5760**	**2.1309**

Table 5. Comparison of time effort and error indicator in bending test with added repnodes.
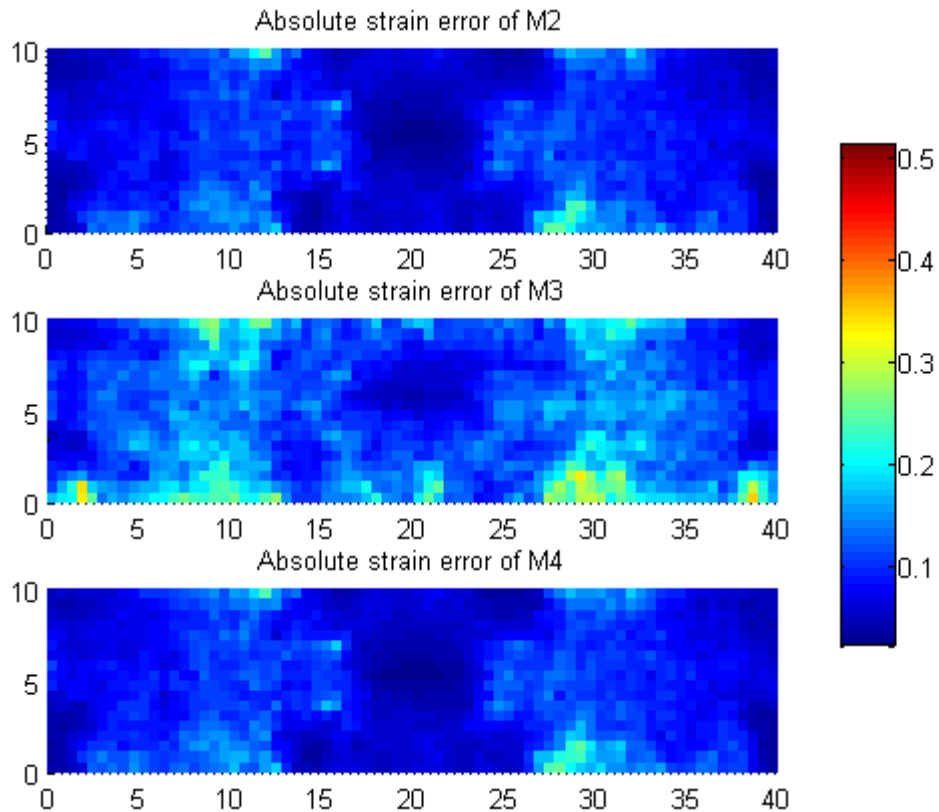
Fig. 35 Absolute strain error computed with added repnodes and divided by characteristic deformation.

7.3   Three-point bending test - beam with a notch

The last example is the same three-point bending test, but now with an initial notch. The sets of particles are the same, only the truss elements intersecting the crack are removed; see *Fig. 37*. Stress and strain are concentrated near the crack tip; see *Fig. 36*. The region of high interest covers the surrounding of crack tip; see *Fig. 38*. Results are summarized in *Table 6*. M2 and M4 provide almost the same and accurate approximation but M4 is dramatically faster. M3 is the fastest but at the price of the higher error; see *Fig. 39*.
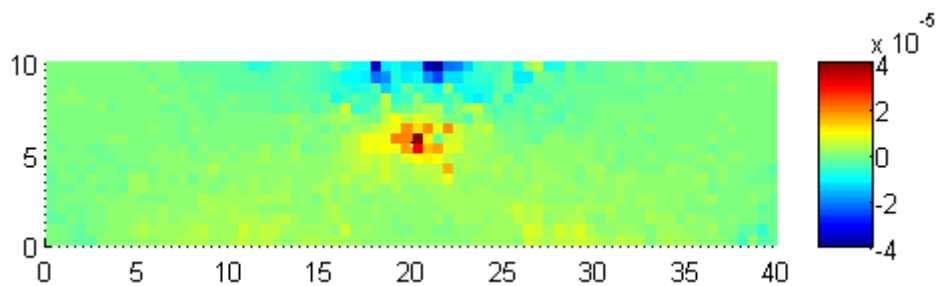

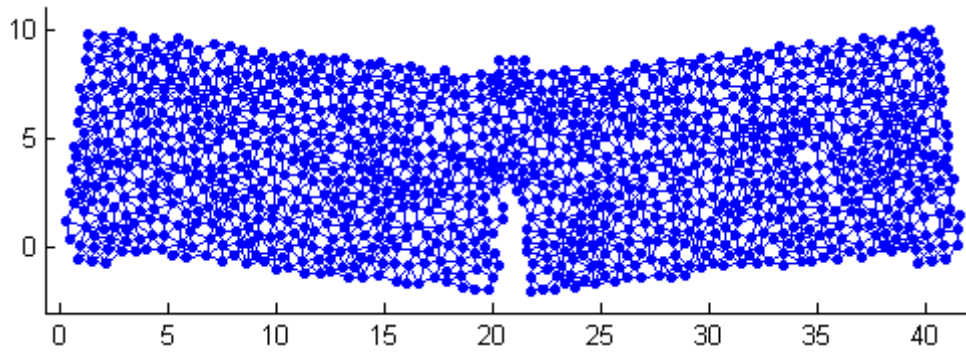*Fig. 36 Typical strain distribution computed by M1.*

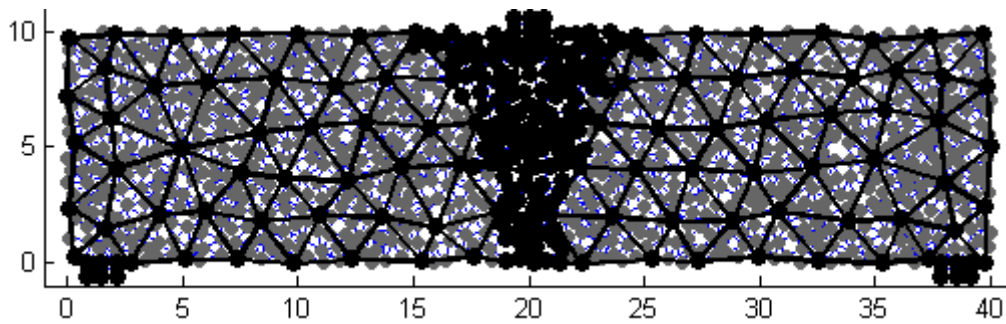*Fig. 37 Beam with the initial notch deformed in three-point bending test.*

Fig. 38 Interpolation mesh with added repnodes.

	Time effort (s)				Strain error indicator (10^{-4})		
	M1	M2	M3	M4	M2	M3	M4
(a)	4.79	6.36	1.96	2.57	1.4199	1.9336	1.4731
(b)	4.04	5.73	1.59	2.79	1.3568	2.1562	1.3817
(c)	4.77	5.94	1.60	2.66	1.5392	2.1989	1.5915
(d)	4.23	5.80	1.47	2.27	1.1340	2.1636	1.1996
Avg	**4.46**	**5.96**	**1.66**	**2.57**	**1.3704**	**2.1157**	**1.4188**

Table 6. Comparison of time effort and error indicator in bending test with crack.
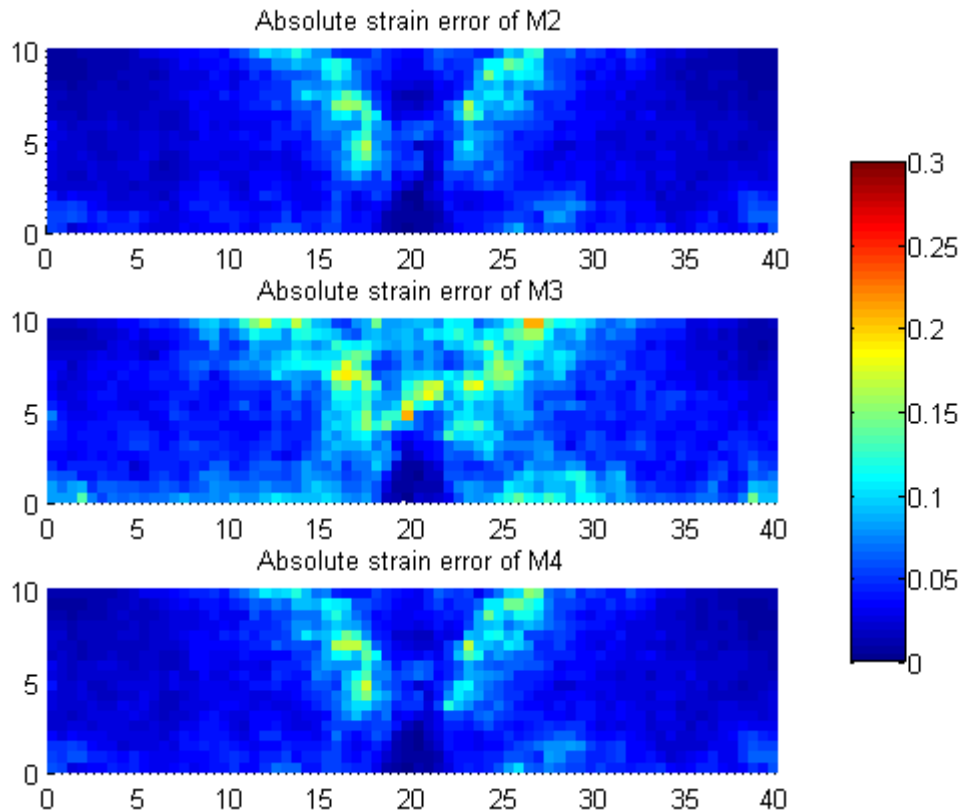
*Fig. 39 Absolute strain error computed with added repnodes and divided
by characteristic deformation.*

7.4 Uniform tension test of anisotropic material

All so far presented examples show different geometry but for isotropic materials only. The next few examples in this subchapter show a simulation of anisotropic materials represented by the set of particles and links generated using the elliptic rule described in 2.1.4.

7.4.1 Orthotropic material stiffer in vertical direction

The first isotropic example is a square with the dimensions 10x10 submitted to uniform tension test. Along both vertical sides, 21 particles are placed periodically with prescribed boundary conditions. The particles on the left side are fixed in horizontal direction and particles on the right side have a prescribed horizontal displacement $u = 0.002$. Only the bottom corners are fixed in vertical direction.

Again, four sets of particles with uniform distribution are generated with the same parameter $R_P = 0.25$ to eliminate the influence of randomness. The material is considered as orthotropic and the elliptic rule is used. The parameters of elliptic rule are

$$a = 1.0R_t, \qquad b = 1.5R_t, \qquad \varphi = 0$$

where $R_t = 1.9R_P$. Thus particles are connected in the ellipses with major axis in vertical direction. Consequently, this example is stiffer in the direction perpendicular to the direction of loading. Therefore only the minimal transverse contraction can be observed on deformed particles; see *Fig. 40*. Strain distribution seems to have almost constant character and only some fluctuation caused by the influence of randomness can be observed; see *Fig. 41 (right)*. Problems with high concentration of the strain near the particles with prescribed boundary conditions are reduced in this case because the vertical orientation of connection links dominates and loaded particles are also mutually connected in this direction. Therefore no extra repnodes are needed; see *Fig. 41 (left)*.
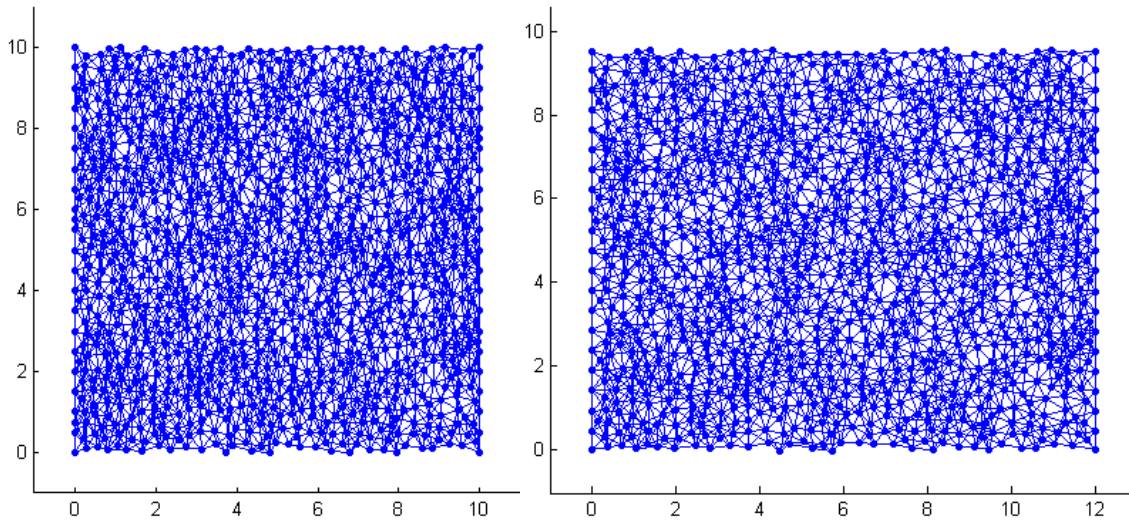
Fig. 40 Example of particles connected by links before (left) and after deformation (right). Deformation scale = 1000.

To be able to capture the influence of anisotropy, the model M4 is used with both isotropic (M4iso) and generally anisotropic stiffness matrix (M4aniso or M5). The accuracy of all models is compared in *Table 7* and absolute strain error is depicted in *Fig. 42*. Error indicator of M4aniso is naturally essentially better than of M4iso and reaches almost the same accuracy as M2 but with dramatically lower time effort. The results of M3 and M4iso, both using isotropic assumption, are less accurate but still applicable because the influence of anisotropy is not too much significant in this example.
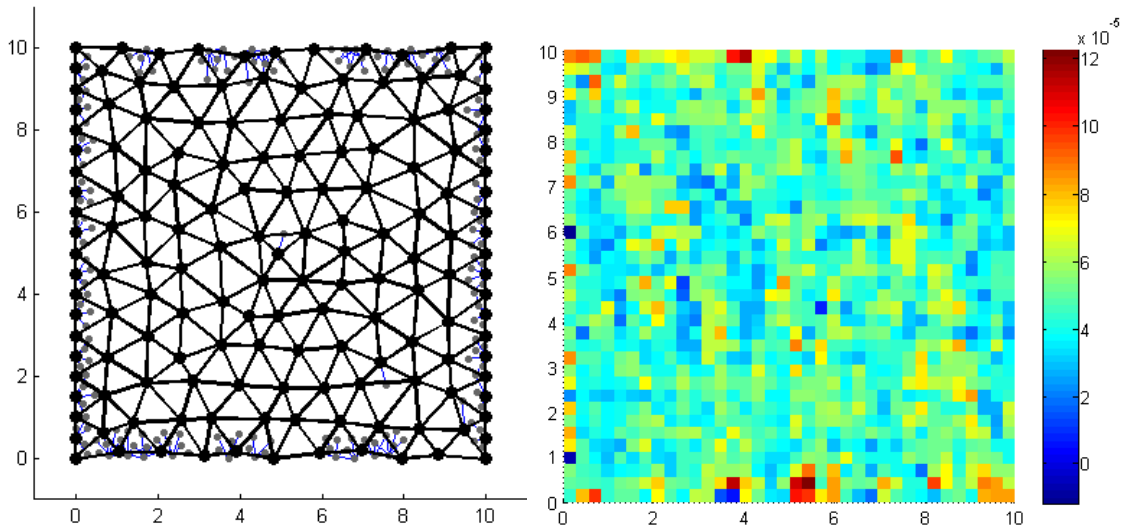
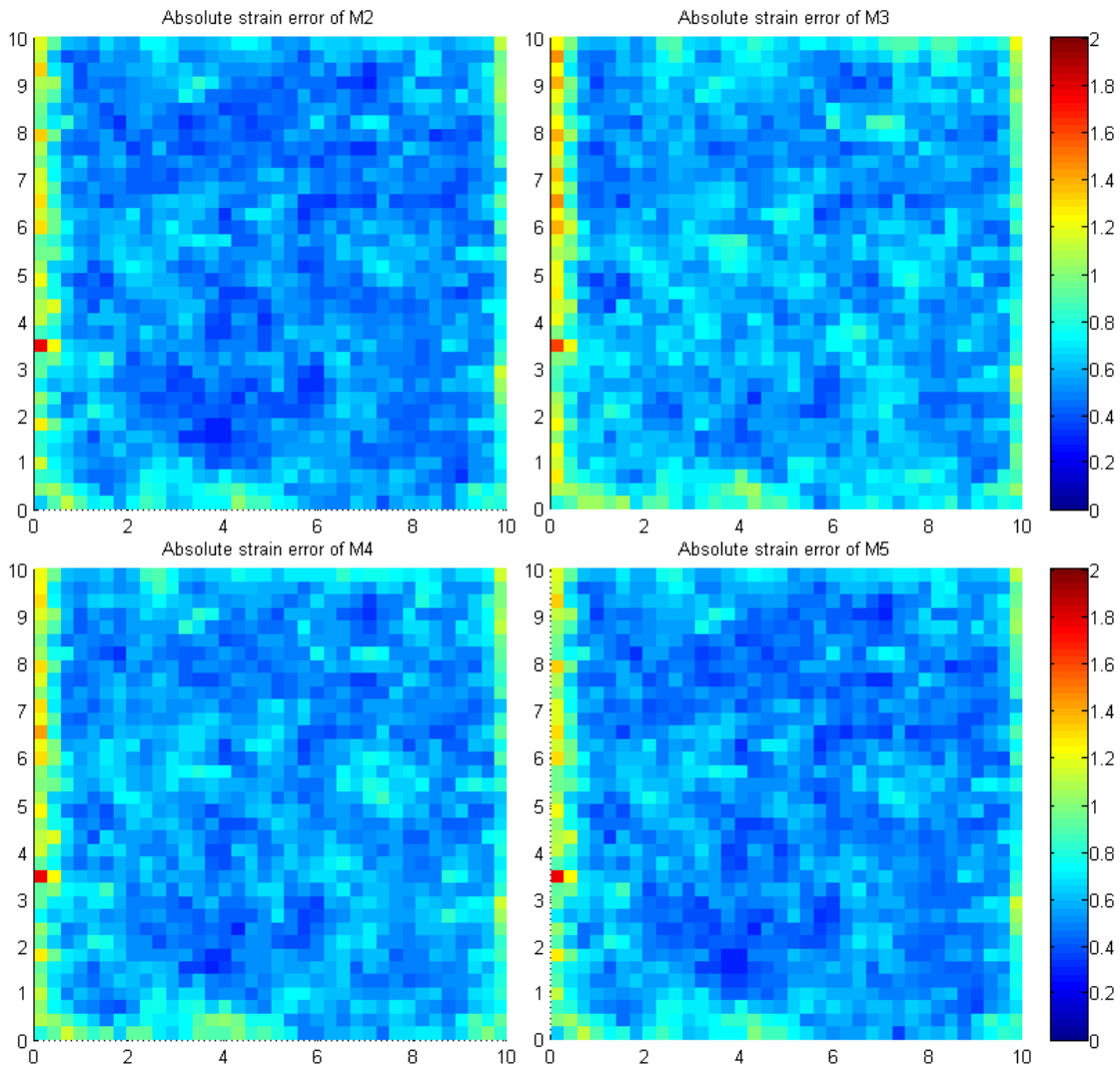*Fig. 41 Interpolation mesh (left) and strain distribution computed by M1 (right).*

Fig. 42 Absolute strain error divided by characteristic deformation

computed for all models.

	Time effort (s)					Strain error indicator (10^{-3})			
	M1	M2	M3	M4iso	M4aniso	M2	M3	M4iso	M4aniso
(a)	15.64	56.98	4.24	9.86	9.71	2.28	2.44	2.41	2.29
(b)	15.31	56.94	3.29	8.74	9.03	2.30	2.54	2.40	2.31
(c)	15.46	57.98	2.85	9.16	9.41	2.22	2.45	2.33	2.24
(d)	15.95	57.81	3.72	10.04	10.06	2.35	2.61	2.47	2.37
Avg	**15.59**	**57.43**	**3.52**	**9.45**	**9.55**	**2.29**	**2.51**	**2.40**	**2.30**

Table 7. Comparison of time effort and error indicator.

7.4.2 Orthotropic material stiffer in horizontal direction

In this example, the same four sets of particles and boundary conditions are used. The material is again considered as orthotropic and the elliptic rule is used. But the parameters of elliptic rule are different

$$a = 1.7R_t, \qquad b = 1.0R_t, \qquad \varphi = 0$$

where $R_t = 1.9R_P$. It means that the major axis of connected ellipse is oriented in the horizontal direction, i.e., direction of loading. The length of major axis increases from $1.5R_t$ to $1.7R_t$. Consequently, more significant influence of anisotropy is expected. Because the links starting the particles with prescribed boundary conditions are connected mainly in the direction of loading, the large variation of the deformation near the boundaries is expected. Therefore these parts are chosen as an area of high interest and repnodes are added. See *Fig. 43*.
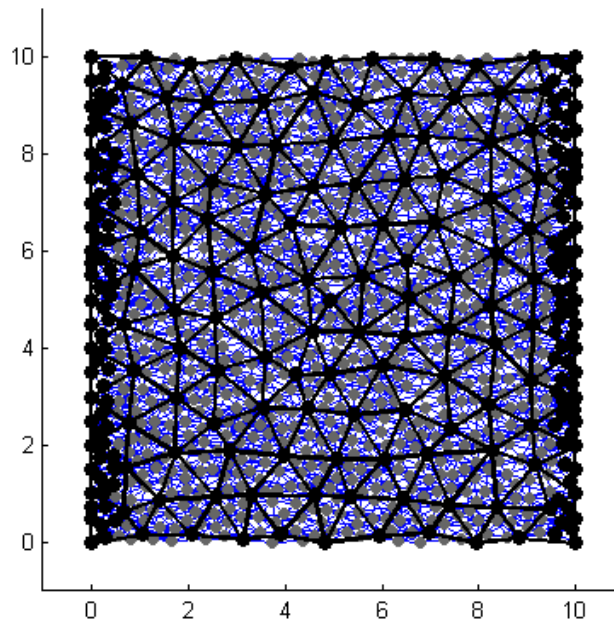

*Fig. 43 Interpolation mesh with added repnodes.*

Significantly stiffer response in the direction of loading causes a huge transversal contraction in vertical direction. But this phenomenon is not captured by the models M3 and M4iso with isotropic assumption. See the deformed particles in *Fig. 44*. An influence of ability to capture this phenomenon on the accuracy of individual models is clearly visible in the figures of displacement error; see *Fig. 46*. The displacement errors of M2 and M4aniso are almost negligible. By contrast, the displacement errors of isotropic models M3 and M4iso are increasing with the horizontal coordinates. The value of displacement error is lower near the bottom corners for all models because the displacements are fixed there.
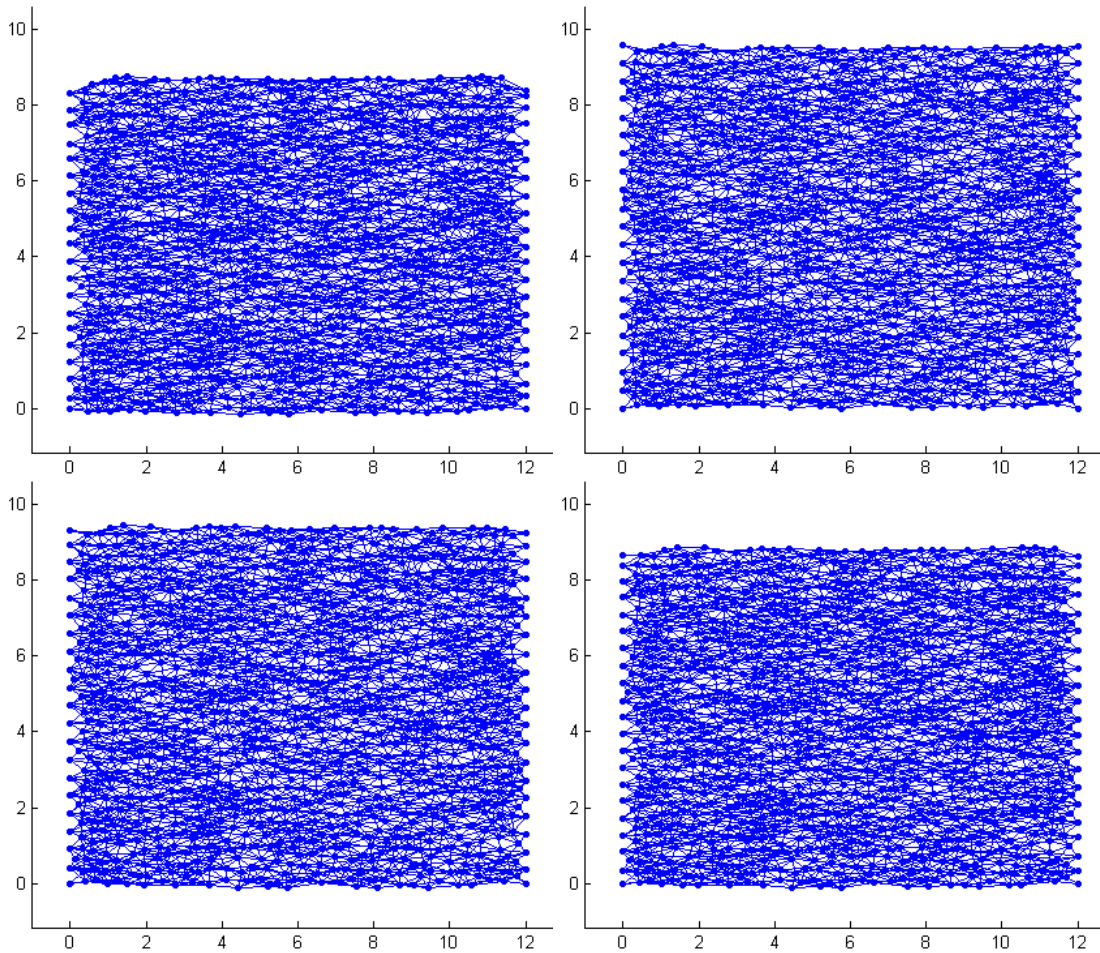
Fig. 44 Deformed particles computed by M1 (top left), M3 (top right), M4iso (bottom left) and M4aniso (bottom right). Deformation scale = 1000.

Fig. 45 shows the strain error of all models. Time effort is summarized in *Table 9*. Time consumption of M4 is almost the same for the isotropic and anisotropic stiffness. Global error indicators are evaluated in both the displacement and the strain and summarized in *Table 8*. Several times higher values of the displacement indicators show obviously that the isotropic models M3 and M4iso are not suitable for this type of material.
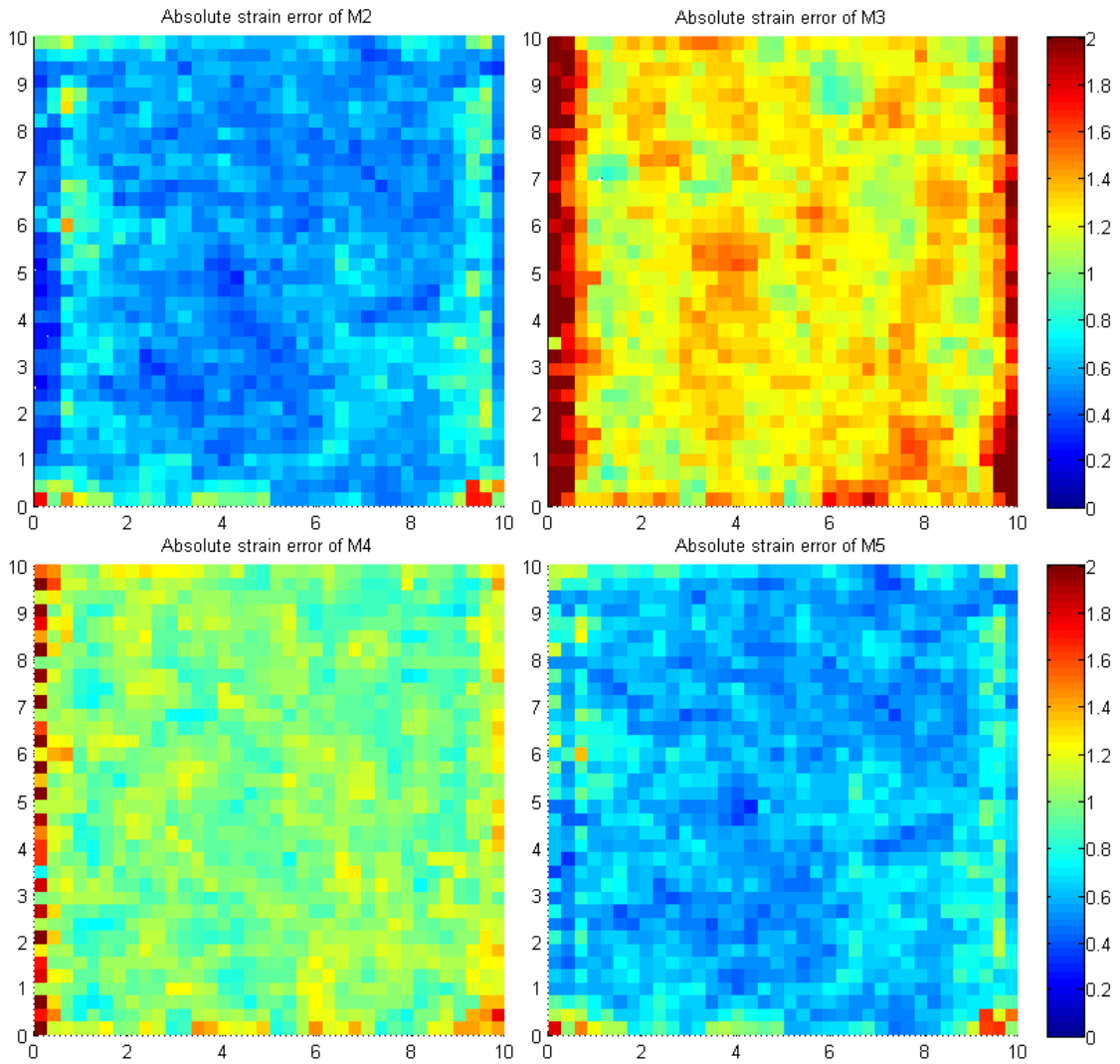
Fig. 45 Absolute strain error divided by characteristic deformation computed for all models.
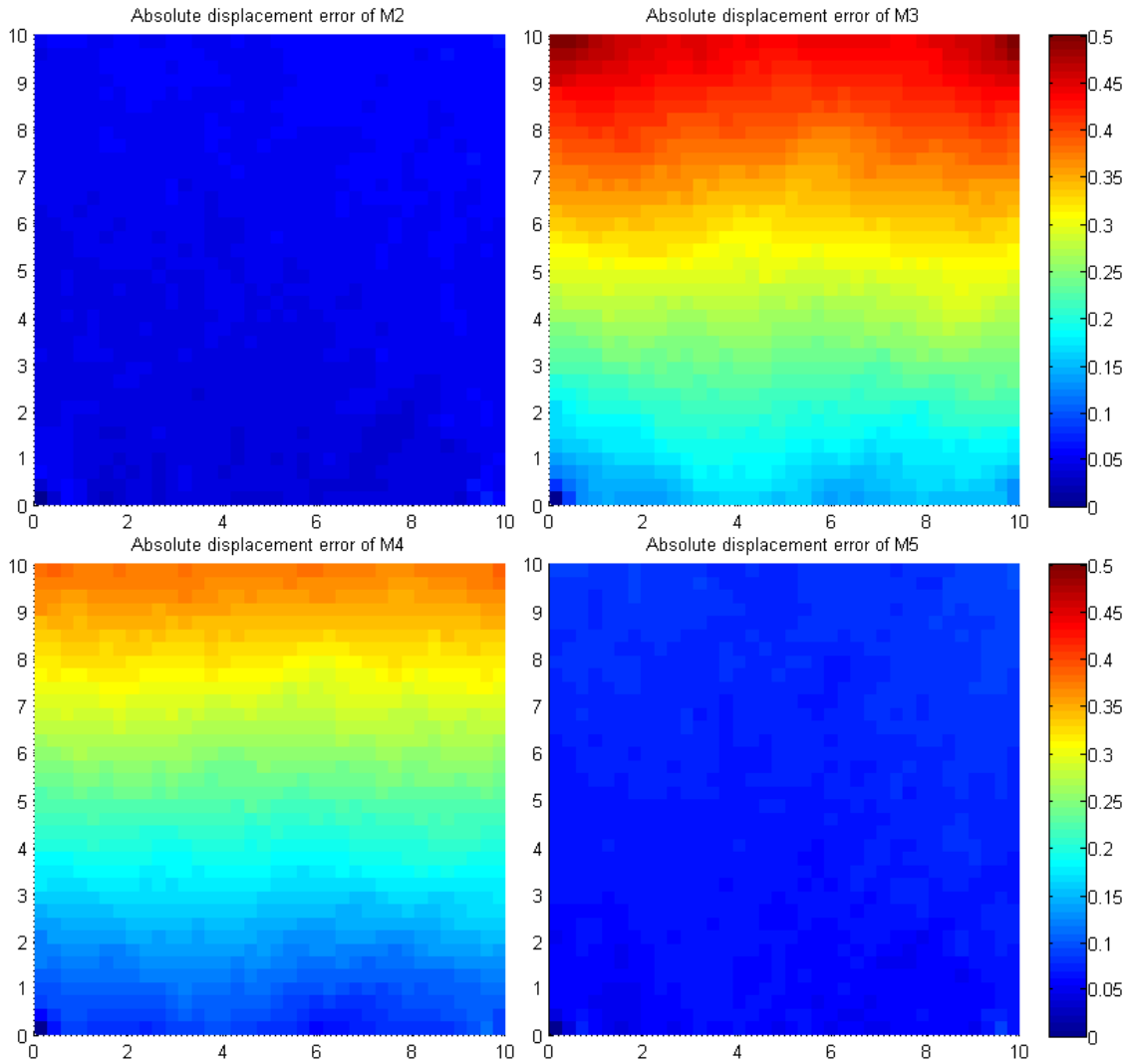
Fig. 46 Absolute displacement error divided by value of prescribed displacement computed for all models.

	Strain error indicator (10^{-3})				Displacement error indicator (10^{-3})			
	M2	M3	M4iso	M4aniso	M2	M3	M4iso	M4aniso
(a)	2.45	4.89	3.85	2.56	1.60	17.39	13.43	2.64
(b)	2.34	5.15	3.78	2.44	1.09	18.48	13.91	1.92
(c)	2.54	5.07	3.93	2.67	7.22	25.96	20.89	9.37
(d)	2.33	5.20	3.85	2.47	3.62	22.75	17.93	5.41
Avg	**2.42**	**5.08**	**3.85**	**2.53**	**3.38**	**21.14**	**16.54**	**4.83**

Table 8. Comparison of error indicator in terms of strain and displacement.

	Time effort (s)				
	M1	M2	M3	M4iso	M4aniso
(a)	17.58	62.03	7.21	15.34	15.63
(b)	17.09	60.74	6.15	13.99	14.24
(c)	17.43	60.43	6.21	14.99	15.20
(d)	17.47	62.39	6.88	16.15	16.02
Avg	**17.40**	**61.40**	**6.61**	**15.12**	**15.27**

Table 9. Comparison of time effort.

7.5 Material with variable orientation of orthotrophy

For this example four sets of particles with uniform distribution and $R_P = 0.25$ have been generated in a rectangular domain with dimensions 20x10. The links are generated with the elliptic rule with parameters

$$a = 2.0R_t, \qquad b = 1.0R_t, \qquad \varphi(x) = \frac{x}{L_x}\frac{\pi}{2}$$

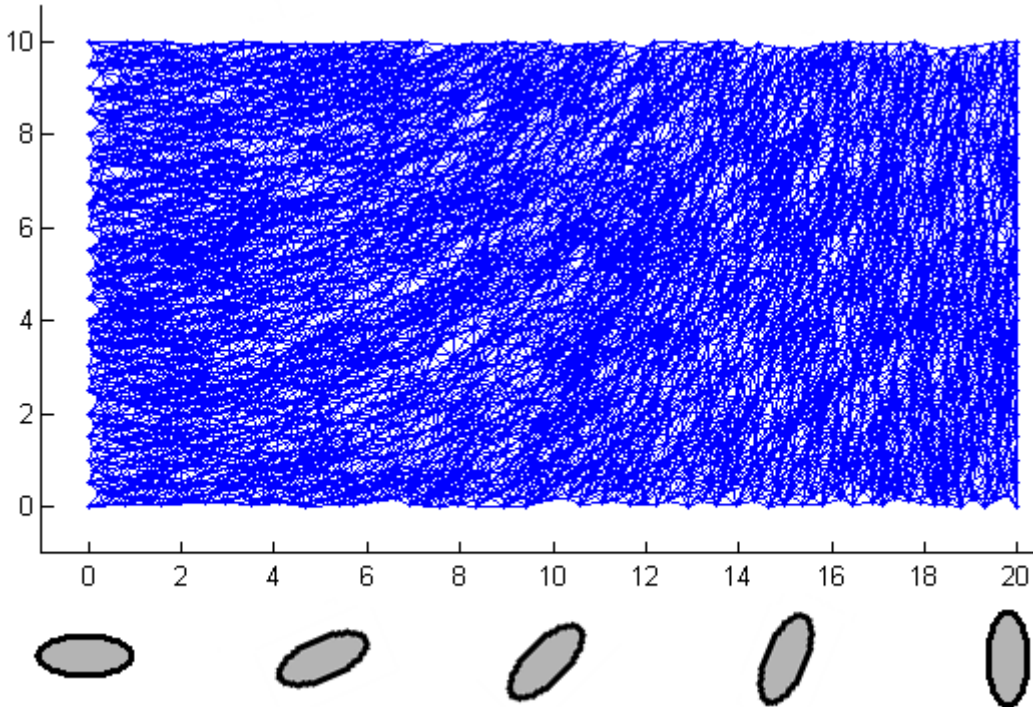where $R_t = 1.9R_P$ and L_x is the dimension of solved domain in x-direction.

Fig. 47 Example of the anisotropic material of bone with denoted continuous change of orientation.

Thus particles are connected in the ellipses whose orientation continuously changes with the horizontal coordinate from $\varphi = 0$ to $\varphi = \frac{\pi}{2}$. An example of this set of truss elements with denoted ellipse orientation is depicted in *Fig. 47*. This input geometry represents the type of anisotropic material which is typical for bones [13] because the orientation is changing during the growth.

In this case, only the left bottom corner is fixed in vertical direction. It allows the whole right side to slide down when the vertical displacement is applied; see *Fig. 48*. This sliding is caused by the orientation of anisotropy and naturally cannot be captured by the isotropic models M3 and M4iso; see the displacement error in *Fig. 51*. The change of the orientation also causes that the strain and stress distribution is not constant but increases from left to right as the material becomes stiffer in the loading direction; see *Fig. 49*. In the figure of strain distribution, high values of the strain in the links starting in the particles with the prescribed boundary conditions can be observed on the left side only, because the density of links is higher near the right boundary and strain value of one plotted grid is computed as an average of all contributing links. So repnodes are added along both of the boundaries; see *Fig. 50*.
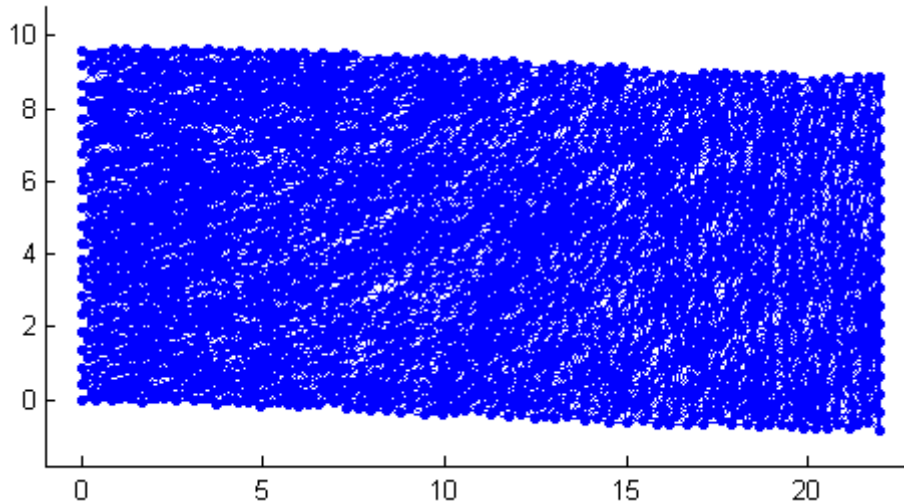
Fig. 48 Deformed particles computed with M1.

Global error indicators are evaluated in both the displacement; see *Fig. 51* and the strain; see *Fig. 52* and summarized in *Table 11*. Computational time and total time effort (including the process of generating input data of simplified model and the time of computation) are measured and summarized in *Table 10*.
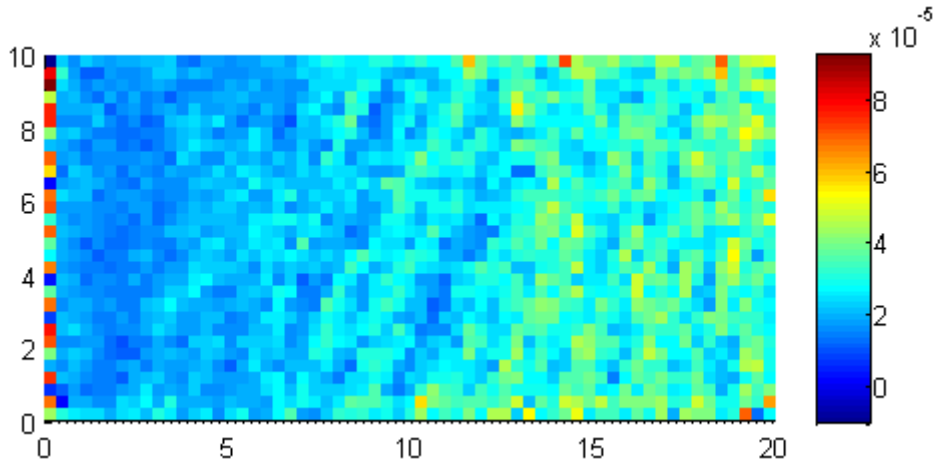
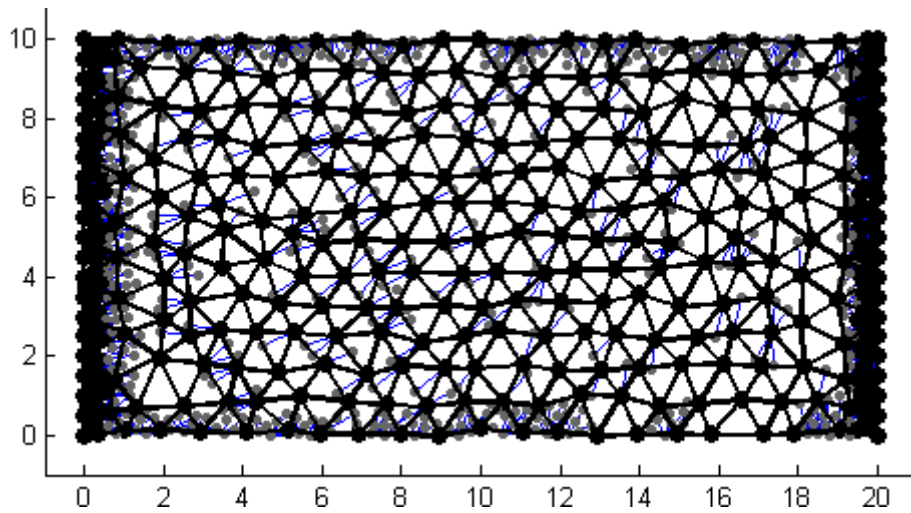*Fig. 49 Strain distribution in anisotropic material computed with M1.*

Fig. 50 Interpolation mesh with added repnodes.

The main features of individual models for anisotropic material can be summarized as follows:

Model **M2** is the most accurate because the stiffness is represented by the real geometry of links.

The models **M3** and **M4iso** with isotropic stiffness matrixes are not able to capture anisotropic phenomena. The inapplicability of these models is more significant if the error is measured in terms of the displacement. For M4iso the addition of repnodes leads to the   elimination of error and isotropic properties of material can be captured by the repnodes in the regions of high interest because the stiffness of all elements is assembled individually. Hence, M4iso can be eventually used for only locally anisotropic examples if the repnodes are used in the whole area of anisotropy. This is not true for

M3 where the stiffness is the same for all elements. Even if the repnodes represent the exact isotropic material, the constant stiffness of elements leads to the stiffer response. The elimination of the strain error for M3 along the left boundary is probably only a lucky effect of this example because the added repnodes even up the missing constant stiffness in the direction of loading. But this is not true in general. For example along the right boundary, the area of high interest does not eliminate the strain error; see *Fig. 52*.

Model **M4aniso** reaches very good accuracy and seems to be convenient for the continuous description of this type of materials. Also the addition of repnodes leads to the error reduction.

Unfortunately the total time effort of M4 is approximately twice as high as for the exact model M1 in this example. But most of the time is consumed in the process of stiffness assignment which is not optimized. For example, the parallelization of this process is possible because the contributions to the individual elements can be evaluated independently for all link connections. The time of the computation only, i.e., the solving time of the model M4 is approximately three times lower than M1; see *Table 10*. Therefore the results are still promising for both large examples in 3D where the influence of the computation demand is expected to be substantial and for nonlinear problems where the process of the stiffness assignment is done just once at the beginning and then several iterations are computed.

	Total time effort (s)					Computational time (s)				
	M1	M2	M3	M4iso	M4aniso	M1	M2	M3	M4iso	M4aniso
(a)	40.45	149.87	13.03	82.60	83.26	39.46	148.85	11.93	11.83	12.81
(b)	41.06	150.53	12.67	85.73	86.19	40.02	149.46	11.64	11.72	11.93
(c)	41.16	178.79	23.87	97.25	97.96	40.13	177.79	22.87	22.88	23.37
(d)	77.50	219.90	13.35	155.31	155.98	75.46	217.80	11.39	11.50	11.93
Avg	**50.04**	**174.77**	**15.73**	**105.22**	**105.85**	**48.77**	**173.48**	**14.46**	**14.48**	**15.01**

Table 10. Comparison of computational time and total time effort.
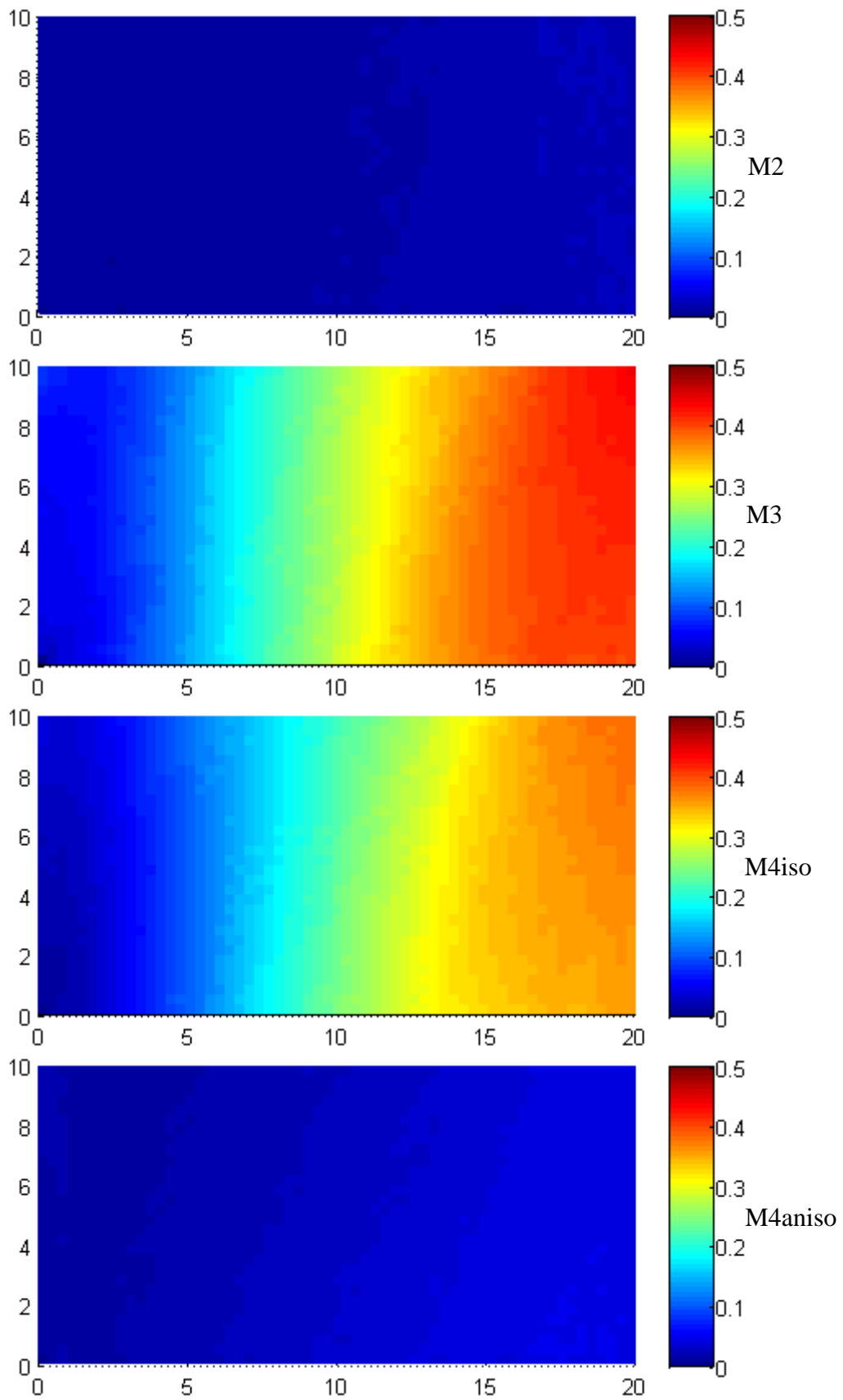
Fig. 51 Absolute displacement error divided by value of prescribed displacement for M2, M3, M4iso and M4aniso subsequently.
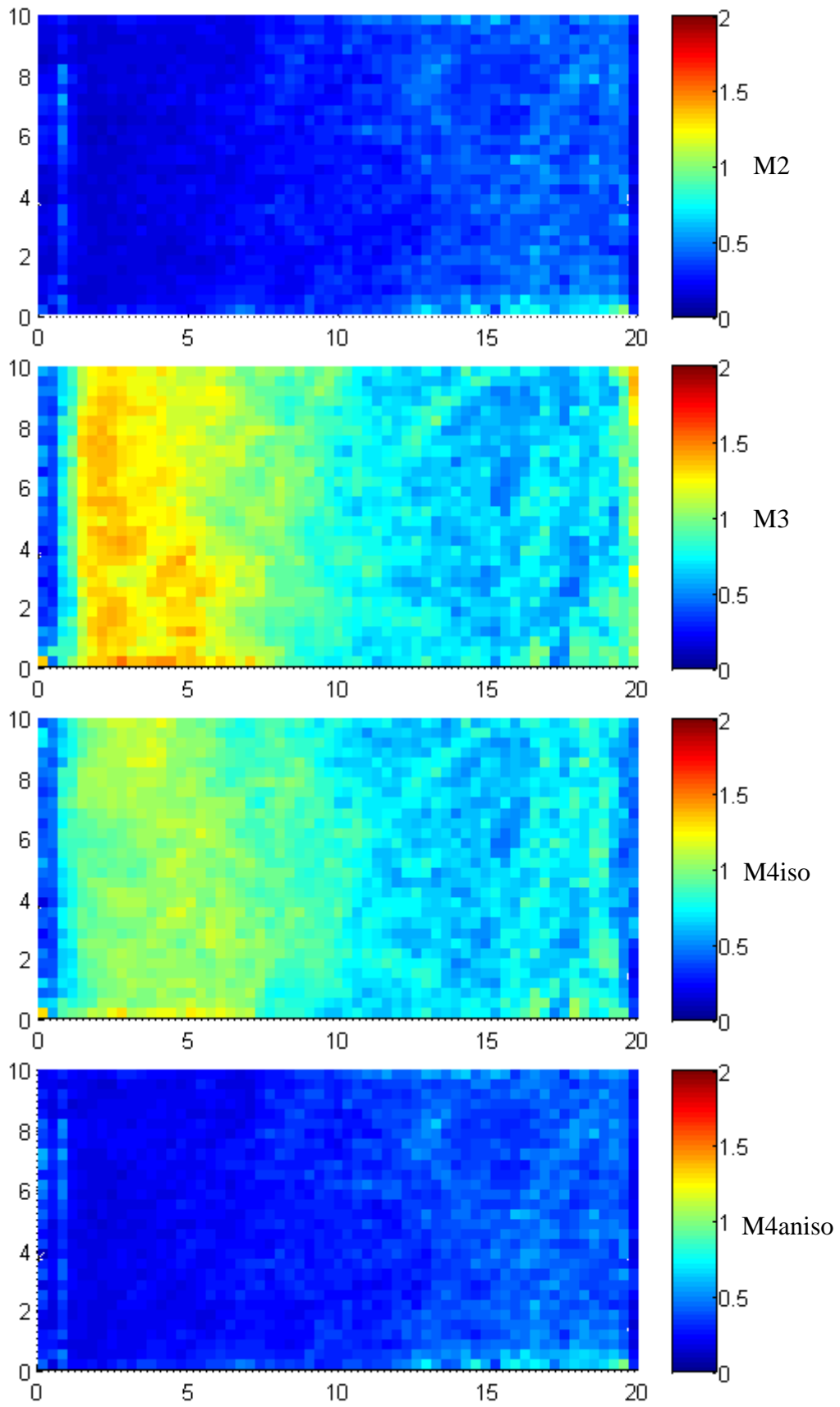
Fig. 52 Absolute strain error divided by characteristic value computed for M2, M3, M4iso and M4aniso subsequently.

74

	Strain error indicator (10^{-3})				Displacement error indicator (10^{-3})			
	M2	M3	M4iso	M4aniso	M2	M3	M4iso	M4aniso
(a)	1.55	4.02	3.54	1.59	1.58	26.10	23.18	2.54
(b)	1.60	4.04	3.62	1.64	1.48	26.28	22.27	3.20
(c)	1.68	4.02	3.67	1.72	1.33	27.16	24.39	2.84
(d)	1.66	4.20	3.62	1.70	1.74	27.90	23.01	3.09
Avg	**1.62**	**4.07**	**3.61**	**1.67**	**1.53**	**26.86**	**23.21**	**2.92**

Table 11. Comparison of error indicator in terms of strain and displacement.

7.6 Uniform tension test of plastic material

This example is formed by randomly generated particles with $R_\mathrm{P} = 0.5$ connected by plastic truss elements with $R_t = 1.9R_\mathrm{P}$ described in section 6.2.1 and submitted to the uniform tension test. The geometry of this example is depicted in *Fig. 54*. A significant narrow region is realized in the middle to avoid a high number of truss elements in plastic state starting from the loaded particles along the vertical boundaries.

The microplane model defined in 6.2.3 is used for 2D elements in simplified model using the idea of quasicontinuum. Formulas from section 6.2.6 and algorithm similar as for the elastic model M4 are used to fit the parameters of microplanes model to be equivalent to the particle model. Two computations of simplified model are realized. At the first (MP1), only the microplane elements are used in the central area and repnodes are added only along the boundaries. In the second computation (MP1 with RN), the same mesh is used and extra repnodes are added in the narrow region, where the plastic mechanism is expected; see *Fig. 55*.

Results of both quasicontinuum computations are compared with exact model M1 and summarized in *Table 12*. All three computations run until the plastic mechanism occurs. The plastic mechanism can be visible in the deformed particles of exact model M1; see *Fig. 54*. And it is also visible that some truss elements are in plastic state even if they are located outside the middle narrow area. The force-displacement diagrams are plotted in *Fig. 53*. And the strain error of simplified model is in *Fig. 56*.

The microplane model without repnodes is approximately four-times faster than the exact particle model M1. But the microplane elements in the narrow area are not

able to capture the exact plastic mechanism that is formed by some plastic bars for lower loading level. Therefore this model predicts higher value of maximal yield stress; see *Fig. 53*. And the strain error in the area of plastic mechanism is also unacceptable; see *Fig. 56*.

On the other hand, the added repnodes turn out to be able to capture the plastic mechanism exactly. And the microplane elements are sufficiently accurate to deal with some plastic bars outside the narrow area even if there are no repnodes. Therefore the results of MP1 with repnodes are in very good agreement with exact model M1; see *Fig. 53*. and *Fig. 56*. The reduction of total time effort is more than 20% and it not negligible save because the time effort of M1 is more than 10 minutes.

Finally, we can summarize that, the microplane elements are suitable to describe the particle model with plastic links but the final plastic mechanism must be captured by repnodes.
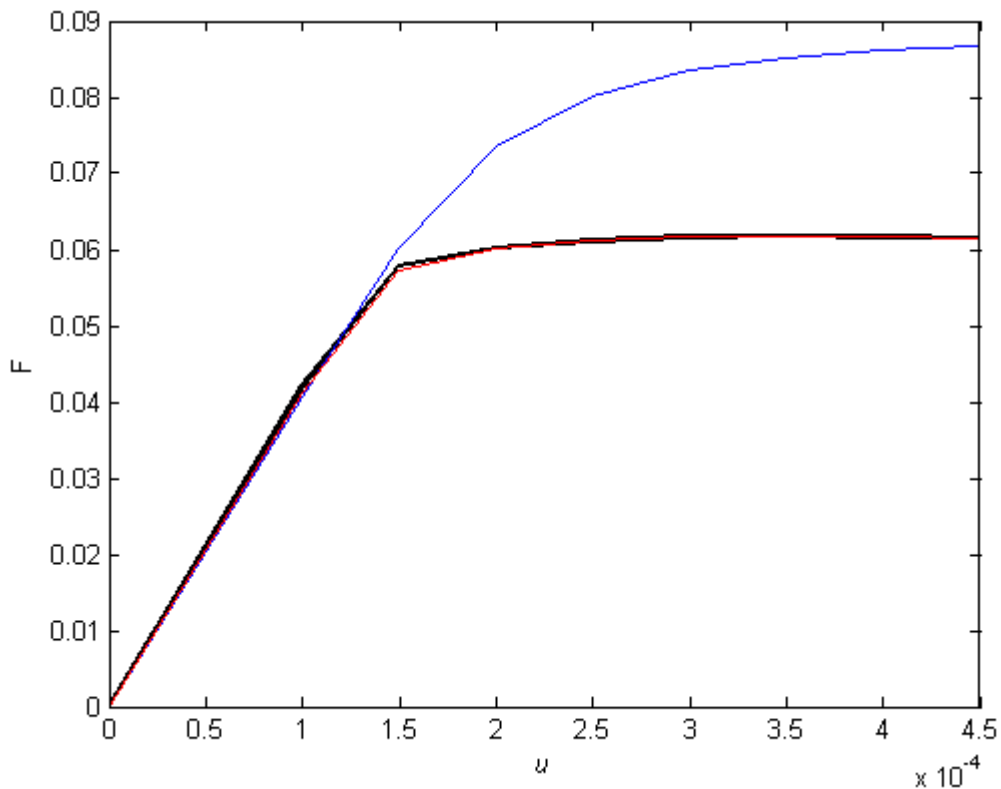
Fig. 53 Force- displacement diagram for particle model M1 (black), microplane model without extra repnodes (blue) and with repnodes in the narrow region (red).
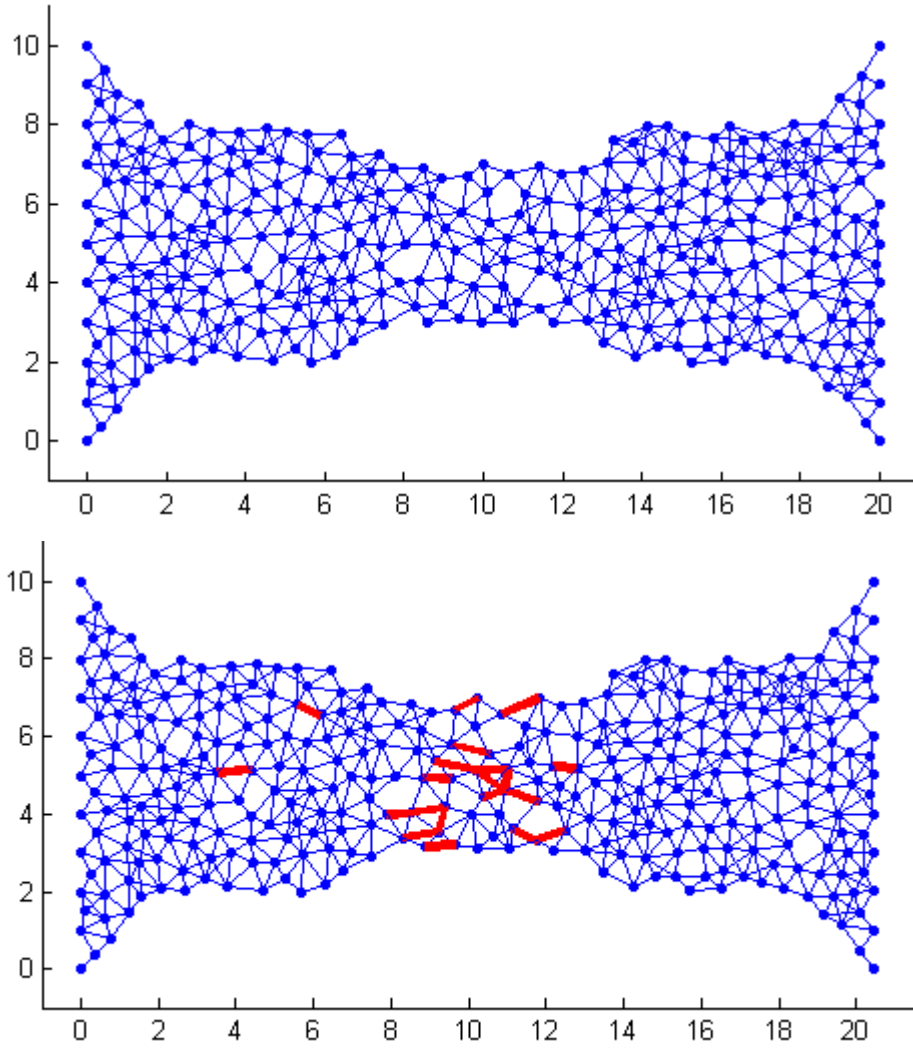
Fig. 54 Particles connected by links before (top) and after deformation (bottom). Bars in plastic state (red).

	Time effort (-)			Strain error indicator (10^{-5})	
	M1	MP1	MP1 with RN	MP1	MP1 with RN
Avg	**1.0**	**0.278**	**0.785**	**72.53**	**4.64**

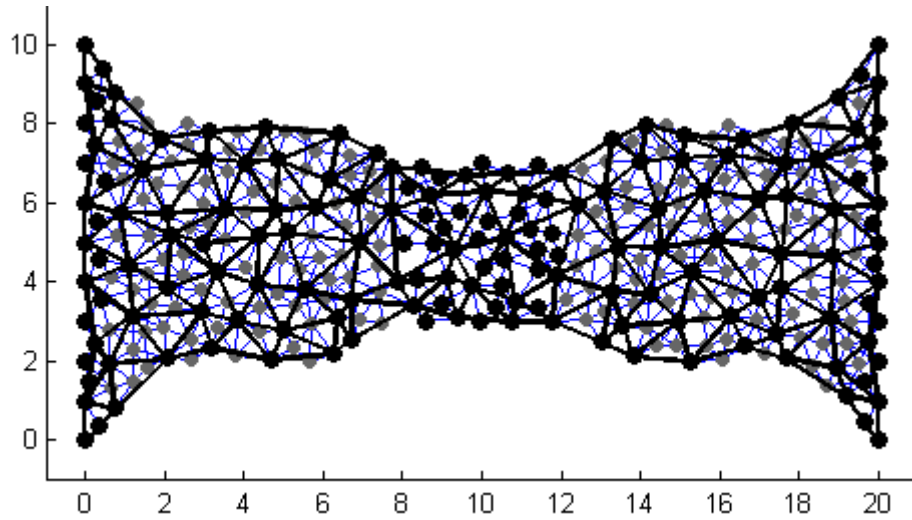*Table 12. Comparison of time effort and error indicator of an example with plastic material.*

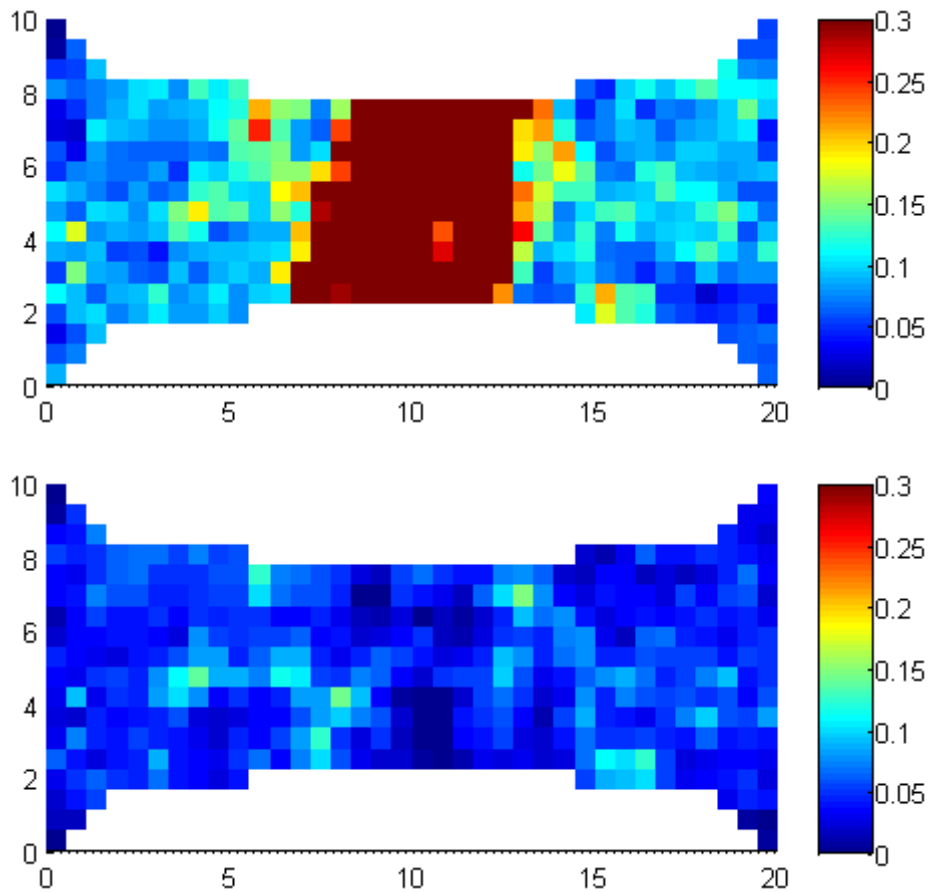*Fig. 55 Interpolation mesh with added repnodes.*

Fig. 56 Absolute strain error divided by characteristic value computed for microplane model without extra repnodes (top) and with repnodes in the narrow region (bottom).

8 Conclusions and outlook

8.1 Summary

For elastic materials, three simplified models M2-M4 based on the idea of QC have been presented and compared with exact particle model M1. Advantages and disadvantages of individual models and their numerical implementation have been discussed in chapter 7 for isotropic materials (sections 7.1 - 7.3), orthotropic material (section 7.4) and anisotropic material (section 7.5).

For plastic materials, the QC model originates from the microplane model. The microplane model has been proposed and studied in detail in section 6.2. The application of QC microplane model has been presented in section 7.6. It turned out that microplane provides a very good description of particle model with plastic links if the final plastic mechanism is captured by repnodes.

For both types of materials, the presented examples have shown that the QC-based method leads to a substantial reduction of unknown DOF. The error caused by this reduction can be effectively reduced by suitably setting the region of high interest. Finally, a significant simplification of the problem can be reached at the price of an acceptable error.

8.2 Future research

Future work will be, at the first, focused on an extension of all presented methods to 3D. It seems to be only a technical question to extend 2D to 3D because main theoretical features are the same and only the different types of elements must be used. But it takes some effort to modify corresponding algorithms, e.g. the stiffness assignment.

Another option of future research is a development of a suitable adaptive algorithm for repnodes addition during plastic simulation. This algorithm will be useful because the final plastic mechanism must be realized by repnodes and its position in not always known at the beginning of loading. The criterion used in this algorithm can be based for example on the value of plastic strain or the number of truss elements resp. microplanes in plastic state in a given microplane element.

Also, addition of other nonlinear material phenomena such as plastic softening, hardening, damage etc. can be realized on the level of microplanes and truss elements.

Acknowledgement

References

[1] Z. P. Bažant. Can multiscale-multiphysics methods predict softening damage and structural failure? *International Journal for Multiscale Computational Engineering*, 8(1), 2010.

[2] Z. P. Bažant and B. H. Oh. Microplane model for progressive fracture of concrete and rock. *Journal of Engineering Mechanics*, 111(4):559–582, 1985.

[3] Z. P. Bažant, M. R. Tabbara, M. T. Kazemi, and G. Pijaudier-Cabot. Random particle model for fracture of aggregate or fiber composites. *Journal of Engineering Mechanics*, 116(8):1686–1705, 1990.

[4] L. Beex, R. Peerlings, and M. Geers. Central summation in the quasicontinuum method. *Journal of the Mechanics and Physics of Solids*, 70:242 – 261, 2014.

[5] L. Beex, R. Peerlings, and M. Geers. A multiscale quasicontinuum method for dissipative lattice models and discrete networks. *Journal of the Mechanics and Physics of Solids*, 64(0):154 – 169, 2014.

[6] L. Beex, R. Peerlings, and M. Geers. A multiscale quasicontinuum method for lattice models with bond failure and fiber sliding. *Computer Methods in Applied Mechanics and Engineering*, 269(0):108 – 122, 2014.

[7] L. Beex, C. Verberne, and R. Peerlings. Experimental identification of a lattice model for woven fabrics: Application to electronic textile. *Composites Part A: Applied Science and Manufacturing*, 48(0):82 – 92, 2013.

[8] K. Crombecq and T. Dhaene. Generating sequential space-filling designs using genetic algorithms and monte carlo methods. In *Simulated Evolution and Learning*, volume 6457 of *Lecture Notes in Computer Science*, pages 80–84. Springer Berlin Heidelberg, 2010.

[9] W. A. Curtin and R. E. Miller. Atomistic/continuum coupling in computational materials science. *Modelling and simulation in materials science and engineering*, 11(3):R33, 2003.

[10] G. Cusatis, D. Pelessone, and A. Mencarelli. Lattice discrete particle model (ldpm) for failure behavior of concrete. i: Theory. *Cement and Concrete Composites*, 33(9):881 – 890, 2011.

[11] B. Eidel and A. Stukowski. A variational formulation of the quasicontinuum method based on energy sampling in clusters. *Journal of the Mechanics and Physics of Solids*, 57(1):87 – 108, 2009.

[12] M. Jirásek and Z. P. Bažant. *Inelastic analysis of structures*. John Wiley & Sons, 2002.

[13] M. E. Kersh, P. K. Zysset, D. H. Pahr, U. Wolfram, D. Larsson, and M. G. Pandy. Measurement of structural anisotropy in femoral trabecular bone using clinical-resolution CT images. *Journal of Biomechanics*, 46(15):2659 – 2666, 2013.

[14] I. Klicmanová. Analysis of microscopic structure of polymer nanotextiles. Master's thesis, Czech Technical University in Prague, 2015.

[15] J. Knap and M. Ortiz. An analysis of the quasicontinuum method. *Journal of the Mechanics and Physics of Solids*, 49(9):1899 – 1923, 2001.

[16] G. Lilliu and J. van Mier. 3d lattice type fracture model for concrete. *Engineering Fracture Mechanics*, 70(7-8):927 – 941, 2003.

[17] J. Liu, Z. Chen, and K. Li. A 2-d lattice model for simulating the failure of paper. *Theoretical and Applied Fracture Mechanics*, 54(1):1 – 10, 2010.

[18] J. Liu, S. Deng, J. Zhang, and N. Liang. Lattice type of fracture model for concrete. *Theoretical and Applied Fracture Mechanics*, 48(3):269 – 284, 2007.

[19] Mathworks. Matlab documentarion. [online]. [cit. 2014-10-30]. Available at: http://www.mathworks.com/help/optim/ug/fmincon.html.

[20] R. E. Miller and E. Tadmor. A unified framework and performance benchmark of fourteen multiscale atomistic/continuum coupling methods. *Modelling and Simulation in Materials Science and Engineering*, 17(5):053001, 2009.

[21] R. E. Miller and E. B. Tadmor. The quasicontinuum method: Overview, applications and current directions. *Journal of Computer-Aided Materials Design*, 9(3):203–239, 2002.

[22] E. Myšáková, A. Kučerová, and M. Lepš. Sequential space-filling design strategies. *The Proceedings of the 3rd European Seminar on Computing*, page 95, 2012.

[23] B. Patzák. OOFEM project home page - documentation. [online]. [cit. 2014-10-30]. Available at: http://www.oofem.org/cz/documentation/manual.html.

[24] B. Patzák. OOFEM - an object-oriented simulation tool for advanced modeling of materials and structures. *Acta Polytechnica*, 52(6):59–66, 2012.

[25] D. Rypl. T3D mesh generator. [online]. [cit. 2014-10-30]. Available at: http://ksm.fsv.cvut.cz/ dr/t3d.html.

[26] W. Sambaer, M. Zatloukal, and D. Kimmer. 3d air filtration modeling for nanofiber based filters in the ultrafine particle size range. *Chemical Engineering Science*, 82(0):299 – 311, 2012.

[27] E. Schlangen and E. Garboczi. Fracture simulations of concrete using lattice models: Computational aspects. *Engineering Fracture Mechanics*, 57(2–3):319 – 332, 1997.

[28] E. Schlangen and J. van Mier. Simple lattice model for numerical simulation of fracture of concrete materials and structures. *Materials and Structures*, 25(9):534–542, 1992.

[29] V. Shenoy, R. Miller, E. Tadmor, D. Rodney, R. Phillips, and M. Ortiz. An adaptive finite element approach to atomic-scale mechanics—the quasicontinuum method. *Journal of the Mechanics and Physics of Solids*, 47(3):611 – 642, 1999.

[30] J. Stránský, M. Jirásek, and V. Šmilauer. Macroscopic elastic properties of particle models. In *Proceedings of the International Conference on Modelling and Simulation 2010, Prague*, 2010.

[31] E. Tadmor and R. Miller. The theory and implementation of the quasicontinuum method. In S. Yip, editor, *Handbook of Materials Modeling*, pages 663–682. Springer Netherlands, 2005.

[32] E. Tadmor, R. Phillips, and M. Ortiz. Mixed atomistic and continuum models of deformation in solids. *Langmuir*, 12(19):4529–4534, 1996.

[33] E. B. Tadmor and R. E. Miller. QuasiContinuum Method. [online]. [cit. 2014-10-30]. Available at: http://qcmethod.org/.

[34] E. B. Tadmor and R. E. Miller. *Modeling materials: continuum, atomistic and multiscale techniques*. Cambridge University Press, 2011.

[35] E. B. Tadmor, M. Ortiz, and R. Phillips. Quasicontinuum analysis of defects in solids. *Philosophical Magazine A*, 73(6):1529–1563, 1996.

[36] D. Wilbrink, L. Beex, and R. Peerlings. A discrete network model for bond failure and frictional sliding in fibrous materials. *International Journal of Solids and Structures*, 50(9):1354 – 1363, 2013.